

# **Dissertation**

Submitted to the  
Combined Faculty of Natural Sciences and Mathematics  
of the Ruperto Carola University Heidelberg, Germany  
for the degree of  
Doctor of Natural Sciences

**Presented by**

**Msc. Daniel Rangel Rojas**

**Born in: Lorica, Colombia**

**Oral examination: 30.11.2020**

# Molecular and metabolic mechanisms underlying diabetic neuropathy

## **Referees:**

**Prof. Dr. Marc Freichel**

**Prof. Dr. Rohini Kuner**

**Jun-Prof. Dr. Daniela Mauceri**

**Dr. Ana Oliveira**

## TABLE OF CONTENTS

Table of contents.....	I
List of figures.....	VI
List of tables.....	IX
List of abbreviations.....	X
Summary.....	XII
Zusammenfassung.....	XIII
Acknowledgment.....	XV
Official declaration.....	XVI
<b>1.Introduction</b> .....	1
1.1 Diabetic peripheral neuropathy.....	2
1.2 DPN and oxidative stress.....	3
1.3 Role of HIF1 alpha during hyperglycaemia.....	8
1.4 Diabetes-induced damage to peripheral nerves.....	9
1.5 Myelination process in the peripheral nervous system.....	10
1.6 Role of Schwann cells in Myelination.....	11
1.7 Role of Periaxin in Schwann cells .....	12
1.8 Periaxin role in peripheral neuropathy.....	14
1.9 Protein function regulation.....	16
1.10 Sumoylation pathway of protein regulation.....	17
1.10.1 Components of the Sumoylation pathway.....	17
1.10.2 Desumoylating enzymes.....	19
1.11 Aims of the thesis work.....	20
<b>2. Materials and Methods</b> .....	21
2.1 Reagents.....	21
2.2 Antibodies.....	23
2.3 Protein and nucleic acid markers.....	25

2.4 Kits.....	25
2.5 Buffers.....	25
2.6 Primers.....	28
2.7 Molecular biology techniques.....	28
2.7.1 Isolation of DNA from E. coli DH5 $\alpha$ cells.....	28
2.7.2 Polymerase chain rection (PCR).....	29
2.7.3 DNA-agarose gel electrophoresis.....	30
2.7.4 DNA Purification from agarose gel.....	30
2.7.5 Determination of DNA concentration.....	30
2.7.6 Cloning .....	30
2.7.7 Site-directed mutagenesis.....	31
2.7.8 Transfection.....	32
2.7.9 Protein purification from HEK cells.....	33
2.7.9.1 GFP-Immunoprecipitation.....	33
2.7.9.2 Sumo1 and Prx-Immunoprecipitation.....	33
2.7.10 SDS-polyacrylamide gel electrophoresis.....	34
2.7.11 Western blotting.....	35
2.8 Cell culture techniques.....	36
2.8.1 Media for HEK cells, Schwann and DRG culture.....	36
2.8.2 Preparing coated cover slips and petri dishes.....	36
2.8.3 Enzymatic dissociation of sciatic nerve.....	37
2.8.4 <i>In vitro</i> myelination assay.....	37
2.9 Animal experiments.....	38
2.9.1 Housing conditions.....	38
2.9.2 Generation of SNS-HIF1 $\alpha$ <sup>-/-</sup> mice.....	38
2.9.3 Induction of Diabetes mellitus Type I.....	39
2.9.4 Blood glucose measurements.....	39

2.9.5 Generation of PLP-cre <sup>ERT2+/+</sup> Ubc9 <sup>fl/fl</sup> mice.....	40
2.9.6 Conditional deletion of Ubc9 in PLP-cre <sup>ERT2+/+</sup> Ubc9 <sup>fl/fl</sup> mice.....	40
2.10 Behavioural testing.....	41
2.9.10.1 Von Frey test.....	41
2.10.2 Hargreaves test.....	41
2.10.3 Hole-board .....	41
2.10.4 Elevated plus-maze.....	42
2.10.5 Home cage monitoring.....	42
2.10.6 Running wheel test.....	42
2.10.7 Cat-walk test.....	42
2.11 Analytical chemistry methods.....	44
2.11.1 Quantification of ROS.....	44
2.11.2 Quantification of hydrogen peroxide in tissue.....	44
2.11.3 Plasma collection.....	45
2.11.4 Tissue extraction.....	45
2.11.5 Determination of amino acid levels from serum.....	45
2.11.6 Determination of metabolites by gas chromatography/mass spectrometry from sciatic nerve tissue.....	46
2.11.6.1 Extraction.....	46
2.11.6.2 Derivatization.....	46
2.11.6.3 GC/MS analysis.....	46
2.12 Immunohistochemistry methods.....	47
2.12.1 Tissue preparation.....	47
2.12.2 Immunohistochemistry.....	47
2.12.3 Immunofluorescence on co-culture DRGs and Schwann cells.....	47
2.13 Data analysis.....	48
<b>3. Results.....</b>	<b>49</b>
3.1 Metabolomic screening in diabetes type I model.....	49

3.1.1 Induction of diabetic neuropathy in mice.....	49
3.1.2 Changes in amino acid levels during the onset and development of DPN.....	51
3.1.3 Changes in TCA cycle intermediates in sciatic nerve of diabetic mice.....	54
3.2 HIF1 $\alpha$ in Diabetic neuropathy.....	56
3.2.1 Regulation of nociception by HIF1 $\alpha$ in the STZ diabetic model.....	56
3.2.2 SNS-HIF1 $\alpha^{-/-}$ mice develop DPN post-STZ treatment.....	59
3.2.3 HIF1 $\alpha$ regulates ROS levels in DRGs of diabetic mice.....	59
3.2.4 Regulation of HIF1 $\alpha$ and its downstream target genes under DPN.....	63
3.3. Sumoylation in protein activity regulation in diabetic neuropathy.....	65
3.3.1 Analysis of Periaxin as a potential target of sumoylation.....	65
3.3.2 Analysis of Periaxin sumoylation <i>in vitro</i> .....	66
3.3.3 Co-transfection of HEK cells with Periaxin and SENP-1.....	67
3.3.4 Site-directed mutagenesis of Periaxin.....	69
3.3.5 Conditional deletion of Ubc9 in Schwann cells. ....	71
3.3.6 Behaviour experiments.....	74
3.3.6.1 Hole-board.....	74
3.3.6.2 Elevated plus-maze.....	75
3.3.6.3 Home cage monitoring.....	76
3.3.6.4 Running wheel.....	78
3.3.6.5 Cat-walk.....	79
3.3.7 <i>In vitro</i> myelination assay.....	80
<b>4. Discussion.....</b>	<b>83</b>
4.1 Metabolomic screening in diabetes type I model.....	83
4.2 HIF1 $\alpha$ in Diabetic neuropathy .....	87
4.3 Sumoylation in the regulation of protein activity in diabetic neuropathy.....	89
4.4. Conclusion.....	92
<b>5. References.....</b>	<b>93</b>

**6. Publications.....115**

## LIST OF FIGURES

Figure 1. Schematic representation of regulation of HIF-1 $\alpha$ stability under normoxia or hypoxia conditions.....	9
Figure 2. Graphical representation of the molecular structure of Dystroglycan-DRP2-Periaxin complex.....	12
Figure 3. Schematic representation of the structure of Periaxin.....	14
Figure 4. Schematic representation of the Sumoylation pathway.....	18
Figure 5. Map of the pcMV6-AC-GFP vector used for cloning Periaxin gene.....	31
Figure 6. Schematic representation of topo cloning and site-directed mutagenesis strategy used for introducing mutations in target lysines of pCMV6-Prx-GFP.....	32
Figure 7. Schematic representation of the generation of SNS-HIF1 $\alpha^{-/-}$ mouse line....	38
Figure 8. Schematic representation of the generation of PLP-cre <sup>ERT2+/+</sup> Ubc9 <sup>fl/fl</sup> mouse line.....	40
Figure 9. Course of DPN and behavioural analyses performed in STZ-injected C57BL6/j mice and control mice.....	50
Figure 10. Quantitative morphological analysis of DPN-pathology of peripheral nerves in STZ-injected C57BL6/j mice and control mice.....	52
Figure 11. Quantitative analysis of amino acid levels in serum of STZ-injected C57BL6/j mice and control mice.....	53
Figure 12. Mass spectrometry-based quantitative analysis of citric acid metabolites in sciatic nerve of STZ-injected C57BL6/j mice.....	55
Figure 13. Longitudinal analysis of hyperglycaemia in STZ-injected SNS-HIF1 $\alpha^{-/-}$ and HIF1 $\alpha^{fl/fl}$ mice.....	57
Figure 14. Analysis of sensory dysfunction in STZ-injected SNS-HIF1 $\alpha^{-/-}$ and HIF1 $\alpha^{fl/fl}$ mice.....	58
Figure 15. Immunostaining for CGRP and PGP 9.5 in the paw skin of STZ-injected SNS-HIF1 $\alpha^{-/-}$ and HIF1 $\alpha^{fl/fl}$ mice.....	60
Figure 16. Quantitative analysis of ROS measurement an H <sub>2</sub> O <sub>2</sub> levels in DRG and sciatic nerve in STZ-injected SNS-HIF1 $\alpha^{-/-}$ and HIF1 $\alpha^{fl/fl}$ mice.....	61
Figure 17. Quantitative analysis of PKG1 $\alpha$ expression in peripheral nerves in STZ-injected SNS-HIF1 $\alpha^{-/-}$ and HIF1 $\alpha^{fl/fl}$ mice.....	62
Figure 18. Quantitative analysis of HIF1 $\alpha$ and VEGF expression in peripheral nerves in STZ-injected SNS-HIF1 $\alpha^{-/-}$ and HIF1 $\alpha^{fl/fl}$ mice.....	64

Figure 19. Sumoylation of periaxin <i>in vivo</i> .....	66
Figure 20. Sumoylation of periaxin <i>in vitro</i> .....	67
Figure 21. Co-transfection of HEK cells with periaxin and SENP-1.....	68
Figure 22. <i>In vitro</i> desumoylation of periaxin.....	69
Figure 23. Identification of potential sumoylation sites in periaxin.....	70
Figure 24. Site-directed mutagenesis: multiple lysine mutations in Periaxin.....	71
Figure 25. Immunostaining for Ubc9 and S100 in DRGs of vehicle and tamoxifen-injected PLP-Cre <sup>ERT2</sup> +/+Ubc9 <sup>fl/fl</sup> mice.....	72
Figure 26. Immunostaining for Ubc9 and S100 in sciatic nerve of vehicle and tamoxifen-injected PLP-Cre <sup>ERT2</sup> +/+Ubc9 <sup>fl/fl</sup> mice.....	73
Figure 27. Immunostaining for Ubc9 and S100 in Schwann cells from PLP-Cre <sup>ERT2</sup> +/+Ubc9 <sup>fl/fl</sup> mice cultured and treated with 4-hydroxytamoxifen.....	74
Figure 28. Change in frequency of head-dipping in PLP-Cre <sup>ERT2</sup> +/+Ubc9 <sup>fl/fl</sup> mice during Hole-board test after tamoxifen or vehicle injection.....	75
Figure 29. Visits and time spent by PLP-Cre <sup>ERT2</sup> +/+Ubc9 <sup>fl/fl</sup> mice during elevated plus-maze test after tamoxifen or vehicle injection.....	76
Figure 30. Home cage monitoring of PLP-Cre <sup>ERT2</sup> +/+Ubc9 <sup>fl/fl</sup> mice after tamoxifen or vehicle injection.....	77
Figure 31. Voluntary running wheel behaviour of PLP-Cre <sup>ERT2</sup> +/+Ubc9 <sup>fl/fl</sup> mice after tamoxifen or vehicle injection.....	78
Figure 32. Dynamic gait parameters of PLP-Cre <sup>ERT2</sup> +/+Ubc9 <sup>fl/fl</sup> mice after tamoxifen or vehicle injection.....	79
Figure 33. Immunostaining of Schwann cells with $\alpha$ -Prx, $\alpha$ -S100 $\beta$ and $\alpha$ -p75.....	80
Figure 34. Immunostaining of DRGs and Schwann cells with anti-myelin basic protein and anti-S100 .....	81
Figure 35. Immunostaining of DRGs and Schwann cells with anti- $\beta$ -Tubulin and anti-myelin associated glycoprotein.....	81

## LIST OF TABLES

Table 1. List of reagents.....	21
Table 2. List of Primary antibodies.....	23
Table 3. List of Secondary antibodies.....	24
Table 4. List of Protein and nucleic acid markers.....	25
Table 5. List of Kits.....	25
Table 6. List of Buffers.....	25
Table 7. List of Primers.....	28
Table 8. List of reagents used for PCR.....	29
Table 9. PCR running conditions.....	29
Table 10. Composition of separating gels.....	34
Table 11. Composition of stacking gel.....	35
Table 12. Composition of Media for HEK cells, Schwann and DRG.....	36
Table 13. Insulin dosage scale.....	39
Table 14. Parameters measured during Cat-walk test.....	43

## LIST OF ABBREVIATIONS

APS	Ammonium persulfate
ANOVA	Analysis of variance
ATP	Adenosine triphosphate
BES	Bis(2-hydroxyethyl)-2-aminoethanesulfonic acid
BDNF	Brain-derived neurotrophic factor
BSA	Bovine serum albumin
CGRP	Calcitonin gene related peptide
CNS	Central nervous system
Cre	Cyclization recombination
DNA	Deoxyribonucleic acid
DAPI	4',6-Diamidin-2-phenylindol
DMSO	Dimethyl sulfoxide
DPN	Diabetic peripheral neuropathy
DRG	Dorsal root ganglia
DTT	Dithiothreitol
EDTA	Ethylendiaminetetraacetic acid
GDNF	Glial cell line-derived neurotrophic factor
GFP	Green fluorescent protein
HIF1 $\alpha$	Hypoxia-inducible factor 1 $\alpha$
HRP	Horseradish peroxidase
Ig	Immunoglobulin
IP	Immunoprecipitation
KDa	Kilodalton
LB	Luria-Bertani medium
MAG	Myelin associated glycoprotein
MBP	Myelin basic protein

MS	Mass spectrometry
NCV	Nerve conduction velocity
NEM	N-ethylmaleimide
NGF	Nerve growth factor
NT3	Neurotrophin 3
PBS	Phosphate-buffered saline
PBST	Phosphate-buffered saline with Triton-X-100
PCR	Polymerase chain reaction
PFA	Paraformaldehyde
PGP 9.5	Protein gene product 9.5
PLP	Proteolipid protein
PMSF	p-methano-sulfonic acid
PNS	Peripheral nervous system
PRX	Periaxin
ROS	Reactive oxygen species
RPM	Revolutions per minute
SDS	Sodium dodecyl sulfate
SDS-PAGE	SDS-polyacrylamide gel electrophoresis
SN	Sciatic nerve
SNS	Sensory neuron-specific
STZ	Streptozotocin
TBS	Tris-buffered saline
TEMED	N,N,N,N-tetramethyl ethylenediamine
TRIS	Tris(hydroxymethyl)aminomethane
Ubc	Ubiquitin conjugating enzyme

## SUMMARY

Diabetes is a metabolic disease with increasing incidence worldwide and with important economic effects. The disease is characterized by hyperglycaemia, which may be caused by an alteration of insulin production secondary to degeneration of pancreatic beta cells (type-1 diabetes), or by an insulin resistance and insufficient secretion from the pancreas (type-2 diabetes). Diabetic neuropathy is the most frequent complication of diabetes mellitus and is characterised by demyelination of neurons accompanied by sensory loss. In addition, hyperglycaemia and local hypoxia can cause glucose oxidation, formation and accumulation of glycation end-products, which lead to oxidative stress. In this work, we investigated the sequence of event occurring in alteration of metabolic pathways in relation to nerve damage and sensory loss in C57BL6/j mice in the model of type 1 diabetes. We employed a mass spectrometry-based screen to study alterations in levels of metabolites in peripheral sciatic nerve and amino acids in serum over several months. Our results indicated that the impaired metabolites in peripheral nerve are the primary cause of shunting metabolic substrate to compensatory pathways, which leads to sensory nerve fibre loss in skin and contribute to onset and progression of peripheral neuropathy.

Furthermore, hyperglycaemia-induced mitochondrial dysfunction and the generation of reactive oxygen species (ROS) have gained attention as possible mechanisms of organ damage in diabetes. We analysed the regulation of transcription factor HIF1 $\alpha$  in response to prolonged hyperglycaemia in mutant mice, lacking HIF1 $\alpha$  in peripheral sensory neurons. Our results indicated that HIF1 $\alpha$  is an upstream modulator of ROS in peripheral sensory neurons and possess a protective function in suppressing hyperglycaemia-induced nerved damage by limiting ROS levels, therefore, HIF1 $\alpha$  stabilization may be thus a new strategy target for limiting sensory loss, a debilitating late complication of diabetes.

In peripheral nervous system, Schwann cells wrap and myelinate spirally around axons, which is indispensable for the efficient propagation of nerve impulses along axons by saltatory conduction. Periaxin protein is expressed in the membrane of myelinating Schwann cells and it is a scaffold protein for coupling peripheral proteins to elements of the Schwann cell cytoskeleton. Post-translational modification via sumoylation has emerged as a central regulatory mechanism of protein function in health and disease. We studied the role of sumoylation on Periaxin by generating conditional PLP-Cre<sup>ERT2/+</sup>Ubc9<sup>fl/fl</sup> mice lacking sumo conjugating enzyme (Ubc9), which is expected to delete sumoylation in Schwann cells and oligodendrocytes. The conditional deletion of Ubc9 in Schwann cells considerably reduced the walking and running behaviour of PLP-Cre<sup>ERT2/+</sup>Ubc9<sup>fl/fl</sup> mice, which can be considered as early symptoms of onset of peripheral neuropathy. Although our results cannot be generalised to other mouse genotypes, our conditional Ubc9-knock-out mice may be useful for assessing the cell-specific role of sumoylation in myelination and peripheral neuropathies.

## ZUSAMMENFASSUNG

Diabetes ist eine Stoffwechselstörung mit erhöhter Verbreitung Weltweit und mit relevanten wirtschaftlichen Wirkungen. Das Hauptmerkmal die Hyperglykämie ist, die durch eine Störung der Insulins Freisetzung verursacht wird aufgrund der Zerstörung der pankreatischen Beta Zellen (Typ-1 Diabetes), oder durch Insulins Resistenz oder geringere Freisetzung aus der Bauchspeicheldrüse (Typ-2 Diabetes). Diabetische Neuropathie ist die häufigste Komplikation des Diabetes mellitus und gekennzeichnet wird, durch Demyelinisierung von Neuronen und als Folge sensorischer Verlust. Außerdem, Hyperglykämie und lokale Hypoxie können zu Glukose Oxidierung, Bildung und Anreicherung von Glykation-Produkten induzieren, die letztendlich zu oxidativem Stress führen. Hier forschten wir über die Reihenfolge der Ereignisse, die während der Störung des Stoffwechselwegs in Bezug auf Nervenschäden und sensorischer Verlust in C57BL6/j Mäuse im Model des Typ-1 Diabetes, stattfanden. Wir verwendeten ein Massenspektrometrie-basiertes Verfahren um die Änderung in Metabolite Spiegel im peripherischen Ischiasnerv und Aminosäuren in Serum während mehrerer Monate zu untersuchen. Unsere Ergebnisse zeigten, dass die beeinträchtigten Metabolite im peripherischen Nerv, die Ursache für das Rangieren des metabolischen Substrats zu alternativen Stoffwechselwege ist, welche zu Verlust der sensorischen Nervenfasern in der Haut und Entstehung und Entwicklung der peripherischen Neuropathie führt.

Des Weiteren kann die Hyperglykämie zur Freisetzung von reaktiven Sauerstoffspezies (ROS) und mitochondriale Störungen führen, welche zur Schädigung von Organen führen können. Wir untersuchten die Regulierung des Transkriptionsfaktors HIF1 $\alpha$  als Abwehr gegen eine langanhaltende Hyperglykämie in Mutanten Mäuse, in welchen HIF1 $\alpha$  in peripherischen sensorischen Neuronen ausgeknockt und nicht mehr exprimiert wurde. Unsere Ergebnisse zeigen, dass HIF1 $\alpha$  als Modulator eine Schutzrolle vor ROS in peripherischen sensorischen Neuronen übernehmen kann. Durch das Begrenzen der Anzahl an ROS Molekülen kann die Hyperglykämie-induzierte Nervenschädigung begrenzt werden. Eine Stabilisierung von HIF1 $\alpha$  könnte eine mögliche neue Strategie sein um vor durch Diabetes bedingten sensorischen Schäden zu schützen und damit die Spätschäden zu begrenzen.

Axone des peripherischen Nervensystems werden von Schwann Zellen umwickelt und myelinisiert. Diese Myelenisierung ist wichtig für eine saltatorische Leitung von Nervenimpulsen entlang des Axons. Das Protein Periaxin wird in der Membran der myelinisierenden Schwann Zellen exprimiert und übernimmt eine unterstützende Rolle, es ist zudem wichtig für die Kopplung periphererer Proteine zu Bestandteilen des Schwann Zellen Zytoskeletts. Sumoylierung ist ein zentraler regulatorischer Mechanismus der eine wichtige Rolle in verschiedenen zellulären Prozessen spielt. Wir haben untersucht was für einen Einfluss die SUMOylierung des Proteins Periaxin hat. Hierfür haben wir eine konditionale PLP-Cre<sup>ERT2+/-</sup>Ubc9<sup>fl/fl</sup> Mauslinie generiert, in welcher das SUMO konjugierende Enzym Ubc9 in Schwann Zellen und Oligodendrozyten ausgeschaltet wird. Diese Mäuse zeigen nach einigen Wochen ein deutlich schlechteres Laufverhalten, was auch ein typisches Symptom für

peripherische Neuropathie ist. Unsere Ergebnisse deuten auf eine spezifische Rolle der Sumoylierung während der Myelinisierung hin und könnten in Zusammenhang mit der Neuropathie stehen.

## ACKNOWLEDGMENT

In this instance, I want to express my gratitude to Professor Dr. Rohini Kuner for the opportunity provided to write this Doctoral thesis at the Molecular Pharmacology Department and for her interest on the elaboration of this work.

I am especially thankful with my supervisor, i.e. Dr. Nitin Agarwal. Thank you very much for the guiding, support, discussions and excellent supervision during the entire course of this work.

Moreover, I want to say thanks to all the co-workers of the AG Kuner for the comments, discussion, advice and recommendations received. Indeed, I want to say thanks to:

Karin Mayer for the training in the laboratory and her assistance through these years, Tessa Frank for her unconditional support, encouragement and help with statistical analysis, Nicolas Mandel for troubleshooting at the end of this work, Hans-Joseph Wrede for performing genotyping, Manuela Simonetti and Francisco Taberner for scientific discussion, Dunja Baumgartl-Ahlert for her assistance during primary culture, Nadine Gehrig and Verena Buchert for her assistance in surgery and behaviour, Anke Tappe-Theodor for discussion about behavioural analysis, the members of the Interdisciplinary Neurobehavioural Core for assistance, the members of the Metabolomics Core Technology Platform for support with metabolite quantification and other colleagues for the pleasant time shared in the laboratory.

In particular, I want to say thanks to God, who gave me the enough strength, endurance and perseverance to accomplish this work in the required frame of time and that, through my lived experiences I realised that he has been supporting me all of the time.

On the same manner, I am thankful to my parents Daniel and Carmen, who have been a model to follow, their great love and patient are a strong motivation in my life, I will be always grateful for the spiritual and unconditional support that they have provided to me and my plans all of the time.

*“If thou canst believe, all things are possible to him that believeth”*

*(Holy Bible-Mark 9:23)*

## **OFFICIAL DECLARATION**

I hereby declare that I have written this doctoral thesis independently and without impermissible external help. I have not used other sources or means than those mentioned, and the passages taken from my own and other publications are indicated with their respective source. Furthermore, I declare that this doctoral thesis has not been presented in the same or similar form to any other examination office.

Heidelberg, 09<sup>th</sup> September 2020

Daniel Rangel Rojas

## 1 INTRODUCTION

Diabetes is a persistent metabolic disorder marked by hyperglycaemia that results from insulin secretion and action dysfunction. The World Health Organization estimates that the overall occurrence of diabetes among adults is 8.5% (Mathers and Loncar, 2006). Diabetic peripheral neuropathy (DPN) is a remarkably complicated and frequent diabetic complication that is observed in approximately half of the diabetic patients. DPN is characterised by a gradual injury of peripheral nerve axons and is divided into two types: painless DPN, characterised by loss of sensation and numbness and painful DPN, characterised by altered foot architecture, lancinating and burning pain, as well as electric and stabbing sensations (Said *et al.*, 1992; Bansal *et al.*, 2006; Edwards *et al.*, 2008). Despite a lot of efforts in research that aimed to delineate the pathophysiology of DPN, researchers are only recently starting to comprehend the molecular mechanisms responsible for the development of DPN.

Oxidative stress induced by hyperglycaemia is considered one of the main inducers of diabetic complications and organ malfunction (Giacco and Brownlee, 2010). Several studies have shown that hyperglycaemia causes mitochondrial dysfunction, ultimately leading to an overproduction of superoxides and free radicals (Rolo and Palmeria, 2006). Elevated levels of reactive oxygen species (ROS) trigger alterations in the function of transcriptional factors (Zhou *et al.*, 2005; Ma *et al.*, 2006) and the release of chemokines and cytokines involved in inflammation (Johnstone *et al.*, 1999; Mital *et al.*, 2014). Additionally, ROS can induce the release of cytochrome c (Kushnareva *et al.*, 2002), activate caspase 3 (Chen *et al.*, 1998) and endonuclease-G (Endo-G) (Zhao *et al.*, 2007), alter biogenesis and cause cell death (Brownlee, 2001). Hyperglycaemia-induced ROS production is associated with both enzymatic and non-enzymatic pathways; the enzymatic pathways involve nicotinamide adenine dinucleotide phosphate oxidase and the uncoupling of nitric oxide synthase (Pereira *et al.*, 2015), while the non-enzymatic pathways involve the aberrant function of complex I and complex III of the electron transport chain (ETS) (Munusamy *et al.*, 2009). The metabolic inflexibility of cells to change how nutrients are utilised, especially between glucose and fatty acid oxidation, is thought to be a primary driver of ROS formation. ROS overproduction leads to oxidative stress (Ha *et al.*, 2008), which has been related to the development of diabetic complications (Rösen *et al.*, 2001). Oxidative stress is known in itself to cause the development of diabetes as it can induce insulin resistance

(Tangvarasittichai, 2015),  $\beta$ -cell dysfunction (Drewe *et al.*, 2010) and impaired glucose tolerance (Song *et al.*, 2007). Oxidative stress also activates a series of stress pathways that implicate a family of serine/threonine kinases, thereby disrupting insulin signalling (Rains and Jain, 2011). For instance, oxidative phosphorylation of serine/threonine on the insulin receptor substrate decreases its potency to activate downstream signalling molecules and its interaction with the insulin receptor is impeded (Kim, 2006).

Studies have shown that changes in signalling molecules, mitochondrial enzymes and glycolytic flux are partly responsible for specific adaptations in metabolism that are related to tissue malfunction (Obrosova *et al.*, 2005; Marcinek, 2004; Price *et al.*, 2004; Newsholme *et al.*, 2007). Additionally, hyperglycaemia can cause an imbalance of redox homeostasis which leads to various molecular changes including post-translational protein modifications (Stadtman, 2001; Chakravarti and Chakravarti, 2007; Cai and Yan, 2013). Among these molecular modifications protein sumoylation is shown to be significant. Sumoylation is involved in oxidative stress (Sahin *et al.*, 2014), inflammation (Luciani *et al.*, 2009) and protein translocation (Zhao, 2007). However, the role of sumoylation in diabetic late complications remains to be elucidated.

### **1.1 Diabetic peripheral neuropathy**

DPN is one of the most important aggravations of diabetes. Patients usually show symptoms like numbness, tingling and severe pain. This later evolves to a total sensory loss and motor weakness (Allen *et al.*, 2013). Additional complications such as vascular damage, can compound with those aforementioned and lead to severe consequences such as foot amputation which is a common procedure among diabetic patients (Dubby *et al.*, 2004; Colloca *et al.*, 2017). Previous studies have shown that diabetic patients are 15 times more susceptible to develop paraesthesia and neuropathic pain as compared to non-diabetic patients (Margolis *et al.*, 2011). Together, these DPN symptoms negatively impact the patient's quality of life (Galer *et al.*, 2000) and their mental and physical health (Van Acker *et al.*, 2009). It is then unsurprising that diabetes significantly impacts the healthcare system with an estimated annual cost of 4.6 to 13.7 billion dollars in diabetic treatments in the United States alone (Gordois *et al.*, 2003).

Clinical research over the last two decades has shown that a strict glucose control reduces the incidence of DPN, which indicates that hyperglycaemia has a relevant effect on the development of DPN (Callaghan *et al.*, 2012). However, glucose control does not decrease dyslipidaemia or systemic inflammation. Additionally, glucose-mediated damage in DPN is irreversible. While it is known that chronic hyperglycaemia leads to oxidative stress, inflammation and cellular damage in diabetic patients, strict glucose control alone is not enough to halt disease progression (Maclsaac *et al.*, 2017). Moreover, pain is a typical symptom of DPN that is often undertreated. Pain management is an important aspect of DPN treatment. However, current therapies aim to mask pain without addressing the aetiology of it. Therefore, there is a need to develop targeted therapies for DPN which can aid both symptom and pain management.

### **1.1 DPN and oxidative stress**

Understanding the molecular mechanisms that underly DPN has proved to be a challenge which has impeded the development of targeted DPN therapies. Over the past decade, the role of hyperglycaemia-induced mitochondrial dysfunction and ROS production in DPN has received a lot of attention (Vincent *et al.*, 2011). Studies have shown that moderate ROS levels e.g. free radical oxygen and H<sub>2</sub>O<sub>2</sub> can activate a series of signals that regulate cellular responses to several chemical and physical factors (Ayrapetov *et al.*, 2011; Ray *et al.*, 2012). Chronic hyperglycaemia activates diverse metabolites, leading to an augment in the proportion of NADH/NAD<sup>+</sup> at the intracellular level (Williamson *et al.*, 1993). Under diabetic conditions, the NADH/NAD<sup>+</sup> balance is disrupted. Influxes of glycolysis and the Krebs cycle as well as activation of the polyol pathway caused by hyperglycaemia results in the overproduction of NADH (Yan, 2014). Additionally, the increased activity of enzymes that use NAD<sup>+</sup> as a substrate such as lactate dehydrogenase and complex I in the mitochondria, reduces the amount of NAD<sup>+</sup>. This NADH/NAD<sup>+</sup> imbalance leads to oxidative stress and damages macromolecules such as proteins, lipids and DNA (Wu *et al.*, 2016). The oxidative stress induced by diabetes is implicated in the pathology of various diabetic complications. The polyol pathway is the largest contributor to oxidative stress in the nerves of diabetic mice (Chung *et al.*, 2003). Aldose reductase (AR) is the first enzyme in the pathway and reduces glucose to sorbitol (Kawanashi *et al.*, 2003).

It is thought that AR contributes most to hyperglycaemia-induced oxidative stress in nerves (Chung *et al.*, 2003). Therefore, it is unsurprising that AR-induced oxidative stress is thought to be the cause of neuronal dysfunction (Chung *et al.*, 2003). Contrary to this Oates (2002) suggested that metabolic flux but not the concentration of sorbitol in nerves is the predominant polyol pathway contribution to DPN. It was thus suggested that in the peripheral nerves inhibiting metabolic flux through the polyol pathway could be a useful therapeutic target for DPN.

Hyperglycaemia resulting from diabetes causes several pathological changes in small vessels, arteries and peripheral nerves. One proposed mechanism by which hyperglycaemia can lead to diabetic complications, is the shunting of glucose into the hexosamine pathway, which is known to have an important role in fat- and hyperglycaemia-induced insulin resistance (Marshall *et al.*, 1991; Rossetti *et al.*, 1995). It is currently unknown how increased flux through the hexosamine pathway mediates hyperglycaemia-induced gene transcription. However, it has been reported that hyperglycaemia reduces glyceraldehyde-3-phosphate dehydrogenase (GAPDH) activity and increases the production of mitochondrial superoxide (Brownlee and Giacco, 2012). It also increases hexosamine pathway activity (Gabriely *et al.*, 2002) and glycosylation (Pantaleon *et al.*, 2010), thus inducing the expression of genes that are partly responsible for the pathology of several diabetic complications (Du *et al.*, 2000).

Protein kinase C (PKC) is a family of protein kinase enzymes that are activated by the binding of diacylglycerol (DAG) and phosphatidylserine (Shinomura *et al.*, 1991). PKC isoforms phosphorylate a variety of intracellular target proteins and have several roles in signal transduction-mediated cellular regulation. Changes in PKC activity are implicated in diabetic complications (Borghini *et al.*, 1994). Under diabetic conditions PKC activity decreases or does not change in peripheral nerves (Borghini *et al.*, 1994). However, in non-neuronal tissue, there are elevated DAG levels and activated isoforms of PKC (Shiba *et al.*, 1993). In a rat model of diabetes, inhibition of PKC $\beta$  mitigated the formerly reduced nerve blood flow and nerve conduction velocity (Eichberg, 2002). One explanation by which neuronal changes occur is through reduced phosphoinositide turnover which leads to decreased DAG availability and reduces PKC activity. This results in a deficit of Na<sup>+</sup> and K<sup>+</sup>-ATPase activity, decreased nerve conduction velocity (NCV) and degeneration of axons and Schwann cells (Greene *et al.*, 1992). The role of PKC in disrupted neural cell metabolism is still unclear. Further

research is required to fully comprehend all of the biochemical pathways in neurons that modulate PKC activity as well as their role in diabetic neuropathy.

As a consequence of hyperglycaemia, advanced glycation end products (AGE) concentrate excessively on proteins and consequently lead to the development of diabetic complications (Singh *et al.*, 2014). The accumulation of AGE in the sural nerves of diabetic patients has been examined to investigate their role in DPN. In diabetic patients with developed DPN, Misur *et al.* (2004) found that there is excessive AGEs formation in peripheral nerves and an elevated level of AGE-immune complexes. Miyauchi *et al.* (1996) found that in diabetic rats, there was a six-fold increase in AGE levels in the renal cortex as compared to non-diabetic rats. In addition, they found that the motor nerve conduction velocity was inversely related to the AGEs levels.

It has been postulated that hyperglycaemia-induced oxidative stress is the main driver of diabetic complications and organ dysfunction (Giacco and Brownlee, 2010). Previous studies have shown that hyperglycaemia causes mitochondrial dysfunction, inducing the overproduction of free radicals and superoxides (Rolo and Palmeira, 2006). Obrosova *et al.* (2005) found that alterations in glycolytic flux, signalling molecules and mitochondrial enzymes favour tissue-specific adaptations in fuel utilization, which are similar processes that occur in tissue dysfunction (2005). Some remarkable neuronal abnormalities that have been found during the development of DPN comprise the decrease of neurotrophic receptors, neuropeptides and structural proteins. Upregulation of stress and repair proteins, high nitric oxide synthesis and altered neuronal survival pathways also contribute to development of DPN. However, it is still unclear how these pathways interact and ultimately result in neuronal degeneration (Zochodne, 2014).

Both rodent and human studies have shown that electron transport chain protein expression and activity is downregulated in the heart (Lashin *et al.*, 2006; Yang *et al.*, 2009) and also in muscles of type 2 diabetic patients (Kelley *et al.*, 2002; Mogensen *et al.*, 2007). This mitochondrial electron transport chain deficiency can account for metabolic abnormalities that are related to insulin resistance and lead to elevated excretion of lactate as well as the accumulation of methylglyoxal, diacylglycerols, products of incomplete fatty acid oxidation and reactive oxygen species (West, 2000; Choi *et al.*, 2002; Itani *et al.*, 2002; Beisswenger *et al.*, 2003; Su *et al.*, 2005). Additionally, in DPN mouse models, downregulation of mitochondrial enzymes in the

nerves and dorsal root ganglion (DRGs) have been observed. However, this is not seen in DPN patients (Akude *et al.*, 2011). Previous studies (Nishikawa *et al.*, 2000) have demonstrated that the generation of mitochondrial superoxide is a critical component of diabetic complications onset. In cultured endothelial cells, hyperglycaemia enhances electron flux through the respiratory chain, which then induces mitochondrial hyperpolarization and increased ROS production (Du *et al.*, 2000). Furthermore, in the type 1 diabetes STZ model in rats, the mitochondrial membrane potential is depolarized in sensory neurons opposite to that observed in endothelial cells (Huang *et al.*, 2003; Srinivasan, 2000). These results are consistent with findings from diabetic hearts where reduced enzymatic activity and mitochondrial respiration were reported (Lashin *et al.*, 2006). Compared to liver mitochondria, the phosphorylation of proteins is repressed and respiratory activity is reduced in the heart (Bugger *et al.*, 2009). Therefore, the production of mitochondrial superoxide may have significantly different impacts on the various cells that are targets of diabetic complications.

Although alterations in metabolic pathway enzyme activity and expression in the DRGs, peripheral nerves and nerve fibres in the skin occur, it is still unknown if these events cause DPN development or occur after DPN is established. Several metabolic mechanisms that depend on hyperglycaemia and hyperinsulinemia have been considered to promote the development of diabetic complications, including DPN.

In nerves, researchers initially focused on the direct neuronal effects, including glycation of structural proteins, myo-inositol depletion, accumulation of sorbitol, oxidative damage to neuronal membranes and changes in fatty acid composition (Yagihashi, 1995; Sima and Sugimoto, 1999; Greene *et al.*, 1992). In diabetic Akita mice, it has been shown that DRG neurons became more susceptible to glucotoxicity (Tomlinson and Gardiner, 2008). Studies in rodents and humans have shown that all of these mechanisms have vascular targets related to neuropathy (Cameron and Cotter, 1994).

Nevertheless, thus far there have been no reports on the progressive changes of metabolic pathways that occur before and during DPN development. It has been reported that branched-chain (BCAA), glucogenic and ketogenic amino acids have a crucial role in metabolism. Cross-sectional studies in type 2 diabetic patients and rodents have revealed that high levels of BCAA in serum lead to the progression of insulin resistance. Former studies have shown that mice deficient in the branched-

chain aminotransferase (BCAT) enzyme have elevated BCAA levels in serum and are resistant to the development of diabetes (She *et al.*, 2007). Conversely, a large-scale epidemiological study revealed that patients with elevated serum BCAAs were more likely to develop type 2 DM (Wang *et al.*, 2011). Additionally, it has been found that in patients with chronic liver or kidney diseases, there is a reduction in the transfer of BCAAs from various organs into the bloodstream. Moreover, patients with liver failure have low BCAA levels in skeletal muscles (Montanari, 1998).

Previous studies conducted in Zucker rats and ob/ob mice have reported an association among reduced BCAA-metabolising enzyme activity, BCAT and branched alpha-keto acid dehydrogenase in adipose tissue (She *et al.*, 2007). In adipose tissue, it has also been reported that there is increased BCAA metabolism by peroxisome proliferator-activated receptor  $\gamma$  stimulation, though the mechanisms by which this occurs remains unclear (Hsiao *et al.*, 2011). Furthermore, a study (Wijekoon *et al.*, 2004) conducted in a rat model of DPN found that during the insulin-resistant stage, plasma concentrations of the gluconeogenic amino acids aspartate, serine, glutamine, glycine and histidine were reduced, while taurine,  $\alpha$ -aminoadipic acid, methionine, phenylalanine, tryptophan and BCAA were significantly elevated. Later, during the diabetic stage, there were lower plasma concentrations of a large number of gluconeogenic amino acids. In the skeletal muscles and liver, however, there were lower concentrations of several gluconeogenic amino acids and higher levels of BCAAs during both insulin-resistance and diabetes. However, given the severe lack of longitudinal studies, it is unclear if there are any associations between amino acids and DPN development. As such, comprehensive and unbiased amino acid screening by which a “signature” can be identified is necessary to track amino acid changes throughout the progression of DPN.

Further, it is likely that a reduction in the cellular antioxidant potential that leads to cellular damage is augmented throughout DPN progression (van der Vlies *et al.*, 2003). The formation of hyperglycaemia-induced ROS leads to a pseudohypoxic state, which can then control several signalling pathways, for instance, nuclear factor kappa B (NF- $\kappa$ B), activator protein 1 (AP-1), mitogen activation protein kinases (MAPKs) and principally, hypoxia-inducible factor-1 (HIF1) (Fiorentino *et al.*, 2013; Catrina *et al.*, 2004).

### **1.3 Role of HIF1 alpha during hyperglycaemia**

HIF1 is a heterodimeric transcriptional factor composed of  $\alpha$  and  $\beta$  subunits (HIF1 $\alpha$  and HIF1 $\beta$ , respectively) (Masoud and Li, 2015). HIF1 $\alpha$  is an oxygen-labile subunit whose activity is strictly modulated by the concentration of intracellular oxygen (Wang *et al.*, 1995), while HIF1 $\beta$  is expressed constitutively. Under normal oxygen conditions (normoxia), HIF1 $\alpha$  is subjected to oxygen-dependent hydroxylation at two prolyl residues, which facilitates its binding to the von Hippel-Lindau protein (VHL), leading first to polyubiquitination and later, to its degradation by a proteasome complex (Salceda and Caro, 1997; Iwai *et al.*, 1999). Conversely, under hypoxic conditions or iron depletion, acetylation and hydroxylation of HIF1 $\alpha$  are inhibited; as a result, VHL cannot bind to HIF1 $\alpha$  for ubiquitination, leading to an accumulation of HIF1 $\alpha$  (Bae *et al.*, 2002; Fig 1). Thereafter, HIF1 $\alpha$  migrates to the nucleus, where it dimerises with HIF1 $\beta$ . As a result, the now stabilized transcription factor HIF1 binds to hypoxia response elements (HREs) and promotes the expression of genes related to oxygen homeostasis, oxidative phosphorylation, cell proliferation, erythropoiesis, glucose transport (GLUT1, GLUT3), glycolytic enzymes (including aldolase-A (ALD-A), enolase-1, phosphofructokinase-L (PFK-L) and phosphoglycerate kinase-1) and growth factors (transforming growth factor  $\alpha$ , vascular endothelial growth factor (VEGF) and platelet-derived growth factor) (Firth *et al.*, 1994; Pugh and Racliffe, 2003; Mizukami *et al.*, 2007). This cluster of genes represents an adaptive response to hypoxic conditions at a cellular level. Therefore, HIF1 is critical for managing physiological responses (Semenza, 1998).

It is clear that hypoxia can modulate HIF1 $\alpha$  activity but the role of hyperglycaemia in the modulation of HIF1 $\alpha$  activity is still a topic of frequent debate. For example, hyperglycaemia stabilises HIF1 $\alpha$  in pancreatic cancer while it inhibits HIF1 $\alpha$  in primary dermal fibroblasts (Gough and Cotter 2011; Kim *et al.*, 2004). It is currently unknown how hyperglycaemia modulates the function of HIF1 $\alpha$  in peripheral sensory neurons and contribute to the onset and development of DPN. It has recently been shown that HIF1 $\alpha$  suppression results in elevated acute thermal and cold nociception (Kanggiesser *et al.*, 2014) in naive mice, suggesting that HIF1 $\alpha$  activity is relevant in peripheral nociceptive neurons. Thus far, however, the function of HIF1 $\alpha$  during pathogenesis in peripheral sensory neurons under diabetic conditions has not been investigated.

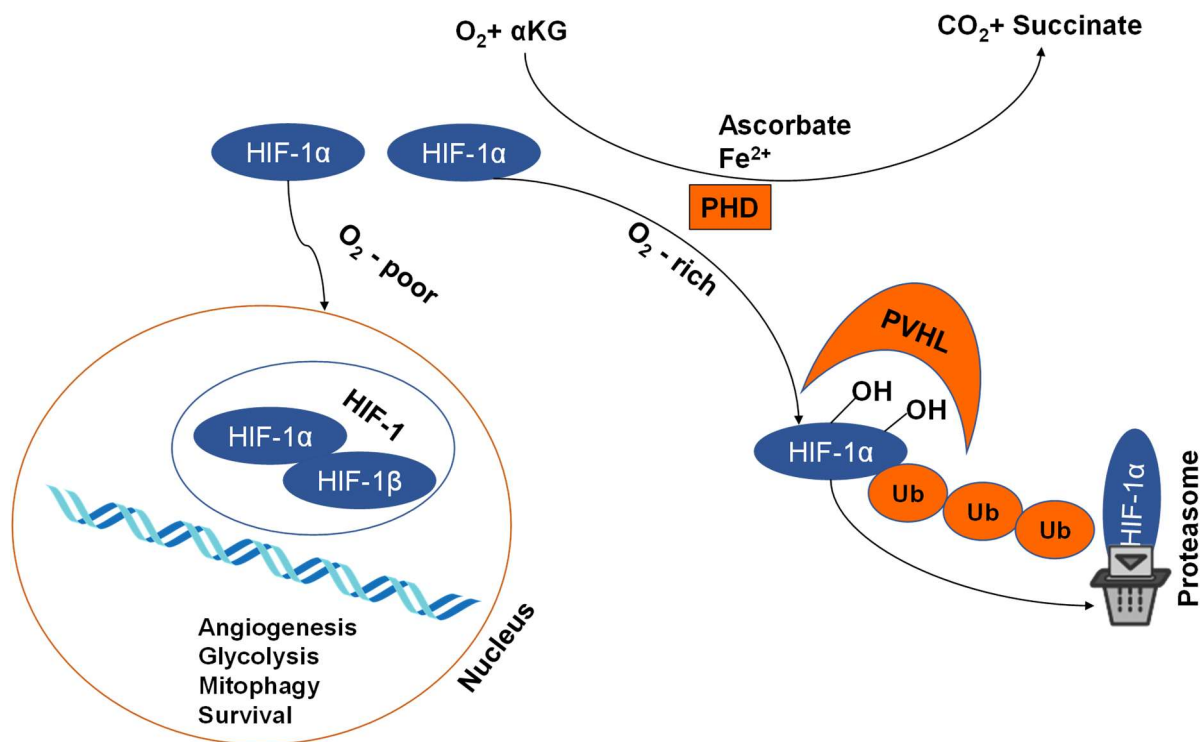


Figure 1. Schematic representation of the regulation of HIF-1 $\alpha$  stability under normoxia or hypoxia conditions (Adapted from Iommarini *et al.*, 2017). Hypoxia-inducible factor 1 $\alpha$  (HIF-1 $\alpha$ ), Ketoglutarate (KG), Proline hydroxylase (PHD), von Hippel-Lindau protein (PVHL) and Ubiquitin (Ub).

#### 1.4 Diabetes-induced damage to peripheral nerves

Diabetes can severely damage the peripheral nervous system (PNS). The most frequent types of damage are symmetric and bilateral damage to the nerves innervating the feet in a distal-to-proximal pattern (Callaghan *et al.*, 2012). Prediabetes, especially in individuals with numerous diabetic risk factors, is associated with the manifestation of peripheral neuropathy and more severe nerve dysfunction (Lee *et al.*, 2015). DPN is characterised by the gradual injury of peripheral nerve axons, leading to sensory loss and pain, which can ultimately result in amputation of the lower extremities (Vincent *et al.*, 2011; Feldman *et al.*, 2017). The loss of peripheral nerve fibres in the epidermis of the skin is used as a clinical diagnostic tool to detect DPN in diabetic patients. Small diameter nerve fibres are usually affected in early peripheral neuropathy and terminal sensory nerve endings are often damaged despite normal sural morphometry (Hanson *et al.*, 1992; Lacomis, 2002). Clinically, nerve conduction velocity tests are not sensitive enough to detect small fibre impairments. Conversely, a footpad skin biopsy, from which intraepidermal nerve fibre density (IENFD) can be quantified, is valuable for examining peripheral nerve fibres and is currently accepted

as a sensitive method to diagnose DPN (Kennedy *et al.*, 1996; McArthur *et al.*, 1998; Herrmann *et al.*, 1999; Periquet *et al.*, 1999).

Motor weakness and the loss of lower extremity sensation often results in balance loss, increased number of falls and a numb insensate foot (Pop-Busui *et al.*, 2017). It is unknown why sensory axons are so vulnerable to diabetes compared to motor axons, rendering it necessary to investigate the potential mechanisms responsible for this vulnerability (Feldman *et al.*, 2017). Despite decades of research defining the pathology of the disease, we are just commencing to comprehend the molecular mechanisms responsible for DPN, of which there is still a lack of understanding. Given the prevalence of DPN, lack of targeted treatment options and significant costs to global healthcare, it is necessary to understand why sensory axons are most affected by DPN such that better therapeutic options can be developed (Berger *et al.*, 2013; Stewart *et al.*, 2007).

### **1.5 Myelination process in the peripheral nervous system**

Myelin membranes are multilamellar structures derived from the spiral wrapping of glial plasma membrane around axons, forming Schwann cells in the PNS and oligodendrocytes in the central nervous system (CNS). Fibres must be myelinated for the effective transmission of nerve impulses along axons by saltatory conduction. In the PNS, axons and Schwann cells interact to form the myelin sheath, an essential complex structure. The significance of the myelin sheath is demonstrated by various neurological diseases that occur as a result of myelin sheath malformation or deterioration. For instance, multiple sclerosis and peripheral neuropathies are associated with myelin sheath dysfunction (Zalc *et al.*, 2008). Bidirectional communication between the axons and glial cells is fundamental for myelin development and maintenance as well as remyelination after tissue damage (Nave and Trapp, 2008). Axons provide the Schwann cells with trophic and mitogenic factors that participate in long-term axonal survival and in the arrangement and development of nodes of Ranvier (Monk *et al.*, 2015). Therefore, the ongoing communication between axons and Schwann cells is fundamental for the normal development of the nervous system, as it ensures efficient transmission of electrical impulses.

The utilization of myelin as an internodal insulator ensures that membrane depolarization only occurs at the nodes of Ranvier, which results in fast saltatory nerve

conduction. The myelin membrane is composed of a high percentage of lipids, of which cholesterol is the main component. Though the roles of myelin in the PNS and CNS seem to be the same, the myelination process differs between Schwann cells and oligodendrocytes. Schwann cells have tight associations with the axons they myelinate and line up along the axon to define a single internode whereas oligodendrocytes extend several processes, each of which myelinate distinct internodes that are usually on different axons (Sherman and Brophy, 2005).

### **1.6 Role of Schwann cells in Myelination**

Myelinating Schwann cells are very large cells that are longitudinally polarized and continuously interact with axons to ensure axonal function, repair and maintenance. A myelinating Schwann cell envelops an adjacent axon with a layer of cytoplasm that is bounded by an extension of the Schwann cell plasma membrane. Some Schwann cells ensheath A $\delta$  nociceptor fibres with a thin layer of compact myelin, while others create several spiral layers of compact myelin around sensory fibres (Arroyo and Scherer, 2007).

Previous studies have shown that axonal diameter is directly associated with the number of myelin compact lamella which then impacts saltatory conduction velocity. Myelinating Schwann cells also regulate the axonal cytoskeleton, transport and organelle content. When the myelinating Schwann cell is injured, as in the case of demyelinating diseases, it is unable to maintain its complex architecture nor support the axon (Jessen and Mirsky, 2005; Pereira *et al.*, 2012; Pollard and Armati, 2011).

Nevertheless, because the myelination process is so versatile, myelinating Schwann cells are very plastic. When the axon is injured and loses contact with Schwann cells, the Schwann cells will dedifferentiate to an immature-like stage, proliferate and serve as a support for axon regrowth, eventually remyelinating the axon (Mirsky *et al.*, 2008). The Schwann cell-axon unit is surrounded by a membrane that is essential for the differentiation and myelination of Schwann cells. However, in acquired and hereditary peripheral neuropathies, similar levels of demyelination occur but not followed by similar levels of remyelination (Dyck and Thomas, 2005; Suter and Scherer, 2003). Thus, Schwann cells are direct and indirect targets of diverse hereditary and acquired human peripheral myelin diseases, necessitating a greater understanding of their pathology and biology (Honkanen *et al.*, 2007).

## 1.7 Role of periaxin in Schwann cells

Periaxin protein (Prx) is expressed in the periaxonal membrane of the myelinating Schwann cells, which has a molecular size of 148 kDa (Yang and Shi, 2015; O55103 Uniprot). Periaxin is a scaffold and structural protein and relatively abundant in Schwann cells. It is implicated in the first stages of myelin deposition because it has been detected in the earliest layers of Schwann cell cytoplasm that wrap the axon (Gillespie *et al.*, 1994). Moreover, periaxin is a linker protein for joining proteins to elements of the Schwann cell cytoskeleton. For instance, periaxin interacts with the protein dystrophin-related protein 2 (Drp2) to assemble the periaxin-Drp2-dystroglycan (PDG) complex (Sherman *et al.*, 2001). This complex is located at regions between the plasma membrane of the Schwann cell and the abaxonal surface of peripheral myelin (Figure 2; Sherman *et al.*, 2001; Court *et al.*, 2004). During the development of the myelin sheath, periaxin become concentrated in the abaxonal (apposing the basal lamina) plasma membrane and can take part in the protein sorting and transmembrane signalling (Scherer *et al.*, 1995).

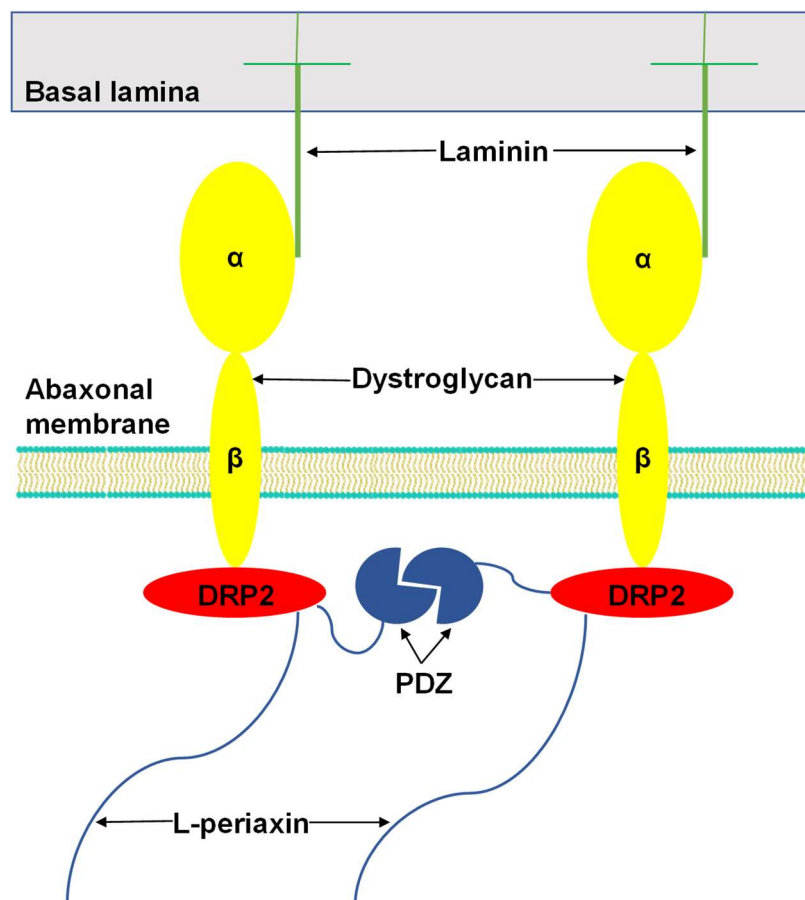


Figure 2. Graphical representation of the molecular structure of Dystroglycan-DRP2-Periaxin complex (adapted from Han and Kursula, 2014).

It has been shown that in periaxin-deficient mice compact myelin is assembled. However, the myelin sheath is inconsistent and unstable leading to demyelination and behavioural abnormalities which are related to the conditions observed under peripheral neuropathy (Gillespie *et al.*, 2000). Periaxin knock-out mice demonstrate a reduction in their peripheral nerve conduction velocity and behaviours associated with allodynia and hyperalgesia, revealing that periaxin plays an essential role in the formation of a stable Schwann cell-axon unit in myelinated fibres of the PNS.

Periaxin protein exists in nature in two isoforms produced by alternative mRNA splicing (Dytrych *et al.*, 1998). The two human isoforms of periaxin, S- and L-periaxin, have the first 127 amino acid-residues in common and are 147 and 1461 amino acid residues length in size, respectively (Boerkoel *et al.*, 2001; Figure 3). Both isoforms are expressed by myelinating Schwann cells. During myelination, L-periaxin is first found in the adaxonal membrane (apossing the axon) and later, in the abaxonal plasma membrane (Gillespie *et al.*, 1994; Scherer *et al.*, 1995). S- periaxin is distributed in the cytoplasm and the nucleus of the Schwann cell and it has been proposed that it is involved in the regulation of mRNA splicing (de Morrée *et al.*, 2012).

The common PDZ domain in S- and L-periaxin is capable to recognise and bind the carboxy terminus of its target proteins, which are either receptors or channels (Han and Kursula, 2014). Until now, apart from Drp2, the binding partners for periaxin have not been revealed and the ligand of the PDZ domain remains to be discovered (Dytrych *et al.*, 1998). In S-periaxin, the non-PDZ domain consists of approximately 50 amino acid residues, whereas L-periaxin consists of several non-PDZ domains mainly an acidic domain, a long repeat domain and a remarkably basic domain. The basic domain serves as a nuclear localisation signal (Sherman and Brophy, 2000; Fig. 3). The repeat region in Prx presents homology to the large repeat domain of the 700 kDa nucleoprotein AHNAK, also known as desmoyokin (Kursula, 2008). Besides, the formation of homodimers may play a crucial role in the scaffolding functions of AHNAK and Prx in large molecular complexes at the plasma membrane, joining the extracellular matrix to the cytoskeleton (de Morrée *et al.*, 2012). The functional relevance to these additional domains in L-periaxin is not known and further structural studies are required to reveal their contribution in periaxin function.

Several clinical studies have evidenced that mutations in the periaxin gene (*PRX*) results in the development of Charcot-Marie-Tooth 4F (CMT4F) disease, a serious

demyelinating neuropathy in humans, which is characterised by gradual muscle atrophy, absence of tendon reflexes and weakness (Boerkoel *et al.*, 2001; Guilbot *et al.*, 2001; Kijima *et al.*, 2004).

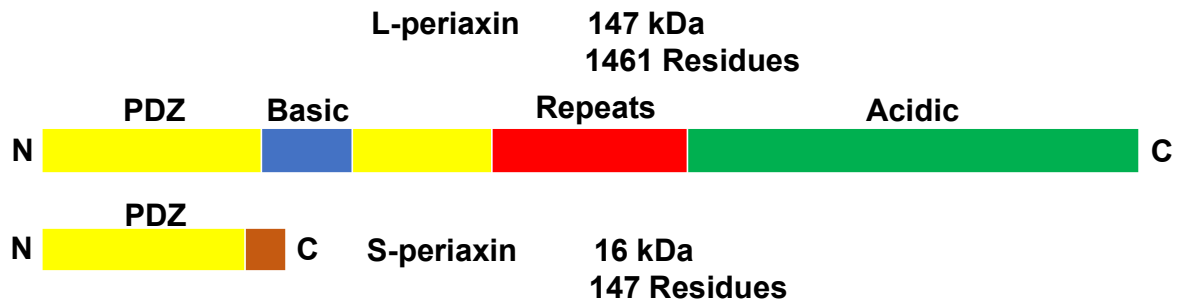


Figure 3. Schematic representation of the structure of Periaxin (adapted from Sherman, 1998).

### 1.8 Role of periaxin in peripheral neuropathy

Neurons and Schwann cells are affected by diverse hereditary neuropathies. In the CMT group, mutations in several different genes in Schwann cells result in similar disease phenotypes (Guilbot *et al.*, 2001). On the other hand, different mutations on the same gene can produce different CMT disease phenotypes (Boerkoel *et al.*, 2002). It is usually thought that in demyelinating neuropathies, the deficiency starts in Schwann cells resulting in demyelination and eventually length-dependent axonal loss. Furthermore, it has been shown that changes in or the absence of the myelin sheath have dramatic effects on the calibre of the axons, phosphorylation, packing of neurofilaments, axonal transport and the arrangement of ion channels in the axonal membranes (Martini, 2001).

Mutations in the *PRX* gene are recessively inherited and they are known to cause a broad range of demyelinating neuropathies with marked sensory implication (Takashima *et al.*, 2002). Mutations in periaxin also suggest persistent impairment of protein complexes associated with extracellular matrix signalling in several neuropathies (Feltri and Wrabetz, 2005). The main symptoms of CMT include constant muscular atrophy and debility, followed by sensory loss in the extremities of the limbs (Dyck, 2005). According to clinical and electrophysiological parameters, CMT disease has been classified into two main groups: CMT1 or demyelinating neuropathies and CMT2 or axonal neuropathies (Harding and Thomas, 1980). Several inheritance patterns for CMT disease have been found such as autosomal recessive, autosomal dominant and dominant X-linked. Data from the different studies on the recessive forms

of demyelinating CMT have demonstrated the significance and diversity of this group. Until now, eight loci have been involved in the progression of CMT4 (Ben Othmane *et al.*, 1993; Rogers *et al.*, 2000), one of these loci (CMT4F) was traced on human chromosome 19q13 in a large inbred family (Delague *et al.*, 2000). Guilbot *et al.*, (2001) sequenced *PRX* in a Lebanese patient and found a non-sense mutation that separated with CMT across the family. The mutation was identified as an early stop codon which results in the expression of a truncated form of L-periaxin. Additionally, Guilbot *et al.* performed immunohistochemistry and revealed that periaxin was absent in the sural nerve biopsy from a CMT4F patient. By using light and electron microscopy, it was possible to evidence that in periaxin knock-out mice and patients, the morphology of the myelinated fibres was pretty same which further confirmed the concept that the mutant mouse is a conclusive model for studying the human CMT4F disease (Gillespie *et al.*, 1997). Because the origin of neuropathic pain as an outcome of nerve damage and particularly in response to demyelination is unknown, further research on periaxin in the mouse model is required in order to provide new knowledge that will be of therapeutic use in diverse demyelinating diseases.

Dejerine-Sottas Neuropathy (DS) is a genetically divergent inherited peripheral myelinopathy. This disease belongs to a broad family of neuropathy phenotypes ranging in extent from hypomyelinating congenital neuropathy to neuropathy in adult stage with muscle shaking (Lupski and Garcia, 2001). Boerkoel *et al.*, (2001) reported that mutations in periaxin result in recessive DSN and therefore demonstrated the relevance of periaxin in preserving human myelin sheaths. Moreover, conforming with findings from the mouse model and comparison between phenotype and genotype support that patients impaired by recessive DSN present a more severe sensory involvement than patients with DSN.

It is thought that loss-of-function mutations in periaxin result in autosomal recessive DSN (Cohen and Campbell, 2000). These frameshift and non-sense mutations suppress the carboxyl region of L-periaxin, including the acidic domain, the function of which is not yet known in L-periaxin. However, acidic domains frequently modulate protein-protein interactions. Therefore, the deletion of this domain may interrupt the attachment of periaxin to the cytoskeleton or may hamper the communication between periaxin and other proteins. The fact that mutations in periaxin result in the development of many peripheral neuropathies not only indicates another genetic source for the broad range of myelinopathies but also comes up with clarity on the

molecular mechanisms behind these diseases. The interaction among periaxin, a membrane complex and the cytoskeleton indicate an interrelationship among the proteins of the dystrophin-sarcoglycan complex (Cohen and Campbell, 2000) and the signalling complexes structured by other PDZ domain proteins (Montell, 2000). Therefore, mutations originated in membrane and cytoskeletal proteins, which are associated with periaxin, may also end in the development of related neuropathies.

### **1.9 Protein function regulation**

Further than demyelination, during the unbalance of the redox homeostasis induced by hyperglycaemia, many molecular changes occur, including a variety of posttranslational protein modifications (PTM) (Stadman, 2001; Chakravarti and Chakravarti, 2007; Cai and Yan, 2013). PTMs are covalent modification processes that alter the function of proteins and their interactions. These modifications include glycation, nitration, carbonylation, succination, acetylation and sumoylation (Dmitriev and Dugin, 2007; Koeck *et al.*, 2009; Blanik *et al.*, 2008; Feligioni and Nistico, 2013). Among them, protein sumoylation constitutes a very crucial molecular modification pathway during oxidative stress (Li *et al.*, 2005). Namely, sumoylation is the reversible and covalent attachment of small ubiquitin-like modifier (SUMO) proteins, which are approximately 12 kDa in molecular size and are similar to the three-dimensional structure of ubiquitin, to specific lysine residues in target proteins (P63166 Uniprot). SUMOs comprise a highly conserved protein family fundamental for the viability of most eukaryotic cells, including yeast, flies and vertebrate cells. In multicellular organisms, SUMO conjugation occurs in all kind of tissues and at all stages of development (Chen *et al.*, 1998; Kamitani *et al.*, 1998; Shen *et al.*, 1996). Until now, there is evidence that SUMO covalently modifies proteins involved in nuclear transport, DNA repair, transcription, signal transduction and the cell cycle. Most of the SUMO-modified proteins identified in mammalian cells are implicated in transcription, which is modulated by SUMO conjugation. Furthermore, it is known that sumoylation is involved in translocation of proteins, inflammation and redox imbalance (Zhao, 2007; Le *et al.*, 2012). Commonly, SUMO has a modulatory effect on interactions at the protein level and supports the integration of diverse multi-protein complexes. Nonetheless, the effects of SUMO on interactions may vary across different substrates; for instance, SUMO can compete with ubiquitylation of a protein, by occupying the lysine residue where ubiquitin would usually attach (Desterro *et al.*, 1998; Lin *et al.*, 2003). Many

proteins that were studied for years have only recently been shown to be sumoylated. One plausible explanation for this is that if neither cleaving enzymes are inhibited nor cells are lysed under denaturing conditions, SUMO-cleaving enzymes rapidly deSUMOylate all conjugates. Moreover, only a small fraction of the substrate, frequently less than 1%, is sumoylated at a certain time point, therefore the elucidation of sumoylated proteins is challenging.

### **1.10 Sumoylation pathway of protein regulation**

The junction between SUMO and its target is formed by an isopeptide bond between the C-terminal carboxyl group of SUMO and the  $\epsilon$ -amino group of a lysine residue in the target protein. The linkage of SUMO to specific substrates is promoted by a three-step enzymatic pathway, while at the same time, other enzymes remove SUMO from its targets. The enzymes involved in the sumoylation pathway are exclusive for SUMO and do not participate in ubiquitylation or conjugating any of the other ubiquitin-like modifiers (Ubls).

#### **1.10.1 Components of the Sumoylation pathway**

The sumoylation pathway starts with the SUMO-activating enzyme (E1), in an ATP-consuming step, this enzyme activates the C terminus of SUMO and relocates the activated SUMO to the SUMO-conjugating enzyme (E2) also known as Ubc9 (Figure 4). Then, one SUMO-protein ligase (E3) transfers SUMO from Ubc9 to the substrate. Ubc9 and E3 enzymes cooperate to contribute specificity of the substrate. The lysine residues, where SUMO attaches, are usually found in the consensus sequence  $\Psi$ KXD/E, where  $\Psi$  is a large hydrophobic amino acid (leucine, isoleucine or valine), K is the target lysine, X is any amino acid residue, D is aspartic acid and E is a glutamic acid. Ubc9 binds directly to this motif. It is established that sumoylation is a reversible modification and deletion of SUMO is performed by enzymes of the SENPs family (Sentrin-specific protease), which precisely cleave at the C terminus of SUMO protein. SENPs are also needed for the formation of mature SUMO from the SUMO precursor, which possesses a small peptide hindering its C terminus (Johnson *et al.*, 1997; Okuma *et al.*, 1999).

Most organisms possess one SUMO-activating enzyme that is fundamental for the conjugation of SUMO forms to their targets. Although members of the SUMO pathway

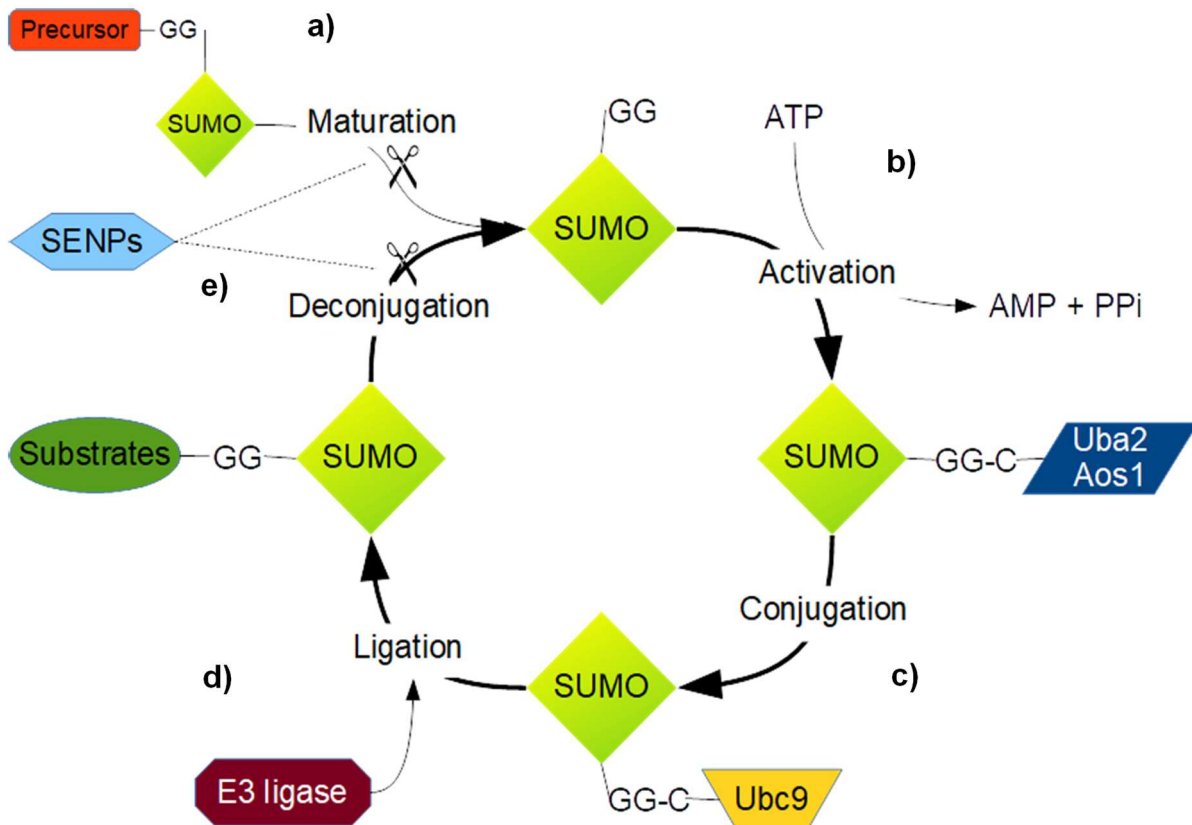


Figure 4. Schematic representation of the Sumoylation pathway: a) in order to conjugate synthesized SUMO to its targets, two glycine residues close to its carboxy terminus are displayed by the action of SENP proteases. b) The E1 enzyme Aos1-Uba2 activates mature SUMO in an ATP consuming step. c) SUMO is relocated to the E2 conjugating enzyme (Ubc9). d) E3 ligase enables the generation of an isopeptide bond between the  $\epsilon$ -amino group of a lysine residue in the target protein and the carboxyl group of the glycine residue at the SUMO carboxy terminus. e) The isopeptide bond between SUMO and its target is disrupted by SUMO-specific proteases (SENPs). (Adapted from Kumar and Zhang, 2015).

are analogous, SUMO E1 is a heterodimer, while the Ubiquitin E1 is a monomer. During the second step of the sumoylation pathway, SUMO is relocated from E1 to the active site of Ubc9. Until now, Ubc9 is the only SUMO-conjugating enzyme reported in yeast, invertebrates and vertebrates (Desterro *et al.*, 1997; Johnson and Blobel, 1997). Contrary to the ubiquitin pathway, where several E2s are involved in ubiquitylating different kinds of substrates, in the sumoylation pathway, there is only one SUMO-conjugating E2 enzyme. The protein sequence of Ubc9 is very similar to the sequence of ubiquitylation E2s and Ubc9 also adopts the identical folding pattern. However, Ubc9 displays a robust positive charge (Tong *et al.*, 1997). Furthermore, Ubc9 is expressed

primarily in the cell nucleus and barely in the cytoplasm and its levels may change depending on the organ or tissue. In addition, it is known that Ubc9 is commonly upregulated in solid tumours (McDoniels-Silvers *et al.*, 2002).

So far, three kinds of SUMO ligases (E3) have been reported. One involves members of the protein inhibitor of activated STAT (PIAS) family (Hochstrasser, 2001), the second includes a domain in the nuclear pore protein RanBP2/Nup358 (Pichler *et al.*, 2002) and the third is the polycomb group protein (Kagey *et al.*, 2003). These proteins bind E2 and the substrate and enhance the relocation of SUMO from E2 to the substrate. These SUMO E3s do not form covalent intermediates with SUMO, but they seem to play a role by binding the substrate and Ubc9. SUMO ligases E3s are certainly involved in most of the sumoylation reactions occurring in eukaryotic cells (Schmidt and Müller, 2002).

### **1.10.2 Desumoylating enzymes**

Sumoylation is a dynamic and reversible process. Then, the cellular abundance of specific SUMO-conjugated substrates is regulated by a balance between SUMO conjugation and deconjugation. SUMO deconjugating enzymes are also referred as isopeptidases which play two important roles. First, they make the modification reversible by removing SUMO from proteins and secondly, they provide a supply of free SUMO that can be used for conjugation to other proteins. During the SUMO pathway, SENPs catalyse three different reactions: processing, deconjugation and chain editing (Meluh and Koshland, 1995). SUMO precursor proteins possess a C-terminal peptide of variable length found after a conserved di-glycine motif. By the action of specific SENPs, this terminal motif is exposed in this way SUMO can be used for modification of target proteins (Jentsch and Pyrowolakis, 2000). SUMO deconjugating activity of SENPs is crucial for the disruption of the isopeptide bond between the  $\epsilon$ -amino group of the target lysine in the substrates and the C-terminus of SUMO. Both of these sources of free SUMO are fundamental for modulating normal levels of SUMO conjugation (Matunis *et al.*, 1996; Johnson *et al.*, 1997).

Until now, six human SENPs have been described and grouped into two classes. SENP1, SENP2, SENP3 and SENP5 are very closely related in sequence to Ulp1, while SENP6 and SENP7 are related to Ulp2. SENP6 and SENP7 include an additional sequence that splits the conserved catalytic domain; nevertheless, the role of this

inserted sequence remains to be identified (Hay, 2007; Mukhopadhyay and Dasso, 2007).

### **1.11 Aims of the thesis work**

As mentioned previously, modification or depletion of enzymes during hyperglycaemia can impair cellular mechanisms. Overproduction of ROS results in oxidative stress, which is one major factor in the progression of diabetic neuropathy. However, the alteration of metabolic pathways and the function of HIF1 $\alpha$  during the development of diabetic neuropathy remains unclear. Furthermore, it has been shown that deletion of periaxin leads to the development of severe demyelinating neuropathy. However, it is unknown if periaxin modification is essential for its stability or function and whether this is relevant to the course of DPN.

In order to address this topic, using a mouse model of type 1 diabetes, this thesis will concentrate on the following aims:

- 1) Analyse how metabolic pathways change related to nerve damage and sensory loss over the progression of DPN in peripheral sensory neurons of mice.
- 2) Address the function of transcription factor HIF1 $\alpha$  over the progression of DPN and ROS formation in peripheral sensory neurons of mice.
- 3) Identify whether periaxin undergoes PTM modification via sumoylation and investigate the potential relevance of such modification to protein function and the course of DPN in mouse models.

## 2 MATERIALS AND METHODS

### 2.1 Reagents

**Table 1. List of reagents**

<b>Name</b>	<b>Manufacturer</b>
Acetic acid	VWR Chemicals, DE
Acrylamide Rotiphorese	Carl Roth, DE
Agarose	Biozyme, DE
Ammonium persulfate	AppliChem, DE
Ascorbic acid	Sigma-Aldrich, DE
Bovine pituitary extract	Sigma-Aldrich, DE
Brain-derived neurotrophic factor	Biorbyt, UK
Bromophenol blue sodium	Sigma-Aldrich, DE
B-27 supplement	Gibco, UK
Calcium chloride	Merck, DE
Citric acid	Sigma-Aldrich, DE
Collagenase	Sigma-Aldrich, DE
Dimethyl sulphoxide	Fisher Scientific, US
Dithiothreitol	AppliChem, DE
Ethanol	Merck, DE
Ethidium bromide	Merck, DE
Ethylenediaminetetraacetic acid	Merck, DE
Fibroblast growth factor	Merck, DE
Foetal bovine serum	Gibco, UK
Forskolin	Sigma-Aldrich, DE
Glial cell line-derived neurotrophic factor	Sigma-Aldrich, DE
D-Glucose	Carl Roth, DE
Glutamine	Gibco, UK

Glycine	AppliChem, DE
Horse serum	Gibco, UK
Human heregulin $\beta$ 1	Sigma-Aldrich, DE
Isopropanol	Carl Roth, DE
Matrigel	Corning
$\beta$ -2-Mercaptoethanol	Merck, DE
Methanol	VWR Chemicals, DE
Mowiol-488	Merck, DE
Nerve growth factor	Sigma-Aldrich, DE
Neurotrophin 3	Sigma-Aldrich, DE
N-2 supplement	Gibco, UK
N-Ethylmaleimide	Sigma-Aldrich, DE
Paraformaldehyde	Sigma-Aldrich, DE
Penicillin/Streptomycin	Gibco, UK
Phosphate buffered saline	Gibco, UK
Poly-L-Lysine	Sigma-Aldrich, DE
Ponceau S	Applichem, DE
Potassium dihydrogen phosphate	Carl Roth, DE
Protein A/G Plus agarose	Santa Cruz Biotechnology, US
Protease inhibitor complete	Roche Diagnostics, DE
Sodium dodecyl sulphate	Sigma-Aldrich, DE
Sodium citrate	AppliChem, DE
Sodium deoxycholate	AppliChem, DE
Sodium dihydrogen phosphate	Carl Roth, DE
Streptozotocin	Sigma-Aldrich, DE
Tamoxifen	Sigma-Aldrich, DE
Tetramethylethylenediamine	Sigma-Aldrich, DE

Tris buffer	Carl Roth, DE
Triton-X-100	Merck, DE
Trypsin	Sigma-Aldrich, DE
Trypsin/EDTA	Gibco, UK
Tween 20	Carl Roth, DE

## 2.2 Antibodies

**Table 2. List of Primary antibodies**

Antigen	Species	Type	Producer	Catalog number	Dilution	Application
$\beta$ -III Tubulin	Rabbit	Polyclonal	Sigma-Aldrich	T2200	1:6000	WB
Calcitonin-gene related peptide (CGRP)	Rabbit	Polyclonal	Sigma-Aldrich	C8198	1:1000	IF
Calcium-binding protein (S100)	Rabbit	Polyclonal	Dako	Z0311	1:100	IF
Cyclic GMP-dependent protein kinase 1 (PKG1)	Rabbit	Polyclonal	Enzo Life Science	ADI-KAP- PK005	1:750	WB
Hypoxia-inducible factor 1 (HIF1 $\alpha$ )	Rabbit	Polyclonal	Novus Biologicals	NB100- 479	1:750	WB
Myelin associated glycoprotein	Mouse	Monoclonal	Sigma-Aldrich	SAB140 2258	1:100	IF

Myelin basic protein	Rat	Monoclonal	BIO-RAD	MCA 409S	1:100	IF
Periaxin	Rabbit	Polyclonal	Sigma-Aldrich	HPA001 868	1:750	WB
Protein gene product 9.5	Rabbit	Polyclonal	Dako	Z5116	1:1000	IF
SUMO-1	Mouse	Monoclonal	DSHB Iowa	21C7	1:750	WB
Vascular endothelial growth factor (VEGF)	Rabbit	Polyclonal	Merck-Millipore	ABS82	1:500	WB

**Table 3. List of Secondary antibodies**

Antigen	Species	Type	Producer	Catalog number	Dilution	Application
Mouse IgG	Sheep	Polyclonal- HRP	GE- Healthcare	NXA931V	1:4000	WB
Rabbit IgG	Goat	Polyclonal- HRP	Sigma- Aldrich	A6154	1:4000	WB
Mouse IgG	Donkey	Alexa Fluor-488	Invitrogen	A32766	1:700	IF
Mouse IgG	Donkey	Alexa Fluor-594	Invitrogen	A32744	1:700	IF
Rabbit IgG	Donkey	Alexa Fluor-488	Invitrogen	A32790	1:700	IF
Rabbit IgG	Donkey	Alexa Fluor-594	Invitrogen	A32754	1:700	IF

## 2.3 Protein and nucleic acid markers

**Table 4. List of Protein and nucleic acid markers**

<b>Name</b>	<b>Manufacturer</b>	<b>Catalog number</b>
PageRuler Protein Ladder	Thermo Scientific	26616
PageRuler Protein Ladder	Thermo Scientific	26619
Smart Ladder	Eurogentec	MW-1700-10

## 2.4 Kits

**Table 5. List of Kits**

<b>Name</b>	<b>Manufacturer</b>	<b>Catalog number</b>
Luminol Western blotting	Santa Cruz Biotechnology	SC-2048
Lumi-Light Western blotting	Roche Diagnostics	1205196001
QIAquick PCR Purification	Qiagen	28104
QIAquick Gel Extraction	Qiagen	28704
NucleoSpin Plasmid	Macherey-Nagel	74588.250
PureLink Plasmid Maxiprep	Thermo Scientific	K210007
GeneArt™ Site-directed Mutagenesis Plus	Invitrogen	A14604

## 2.5 Buffers

**Table 6. List of buffers**

Name	Concentration	Component	Comments
Blocking buffer (Staining)	1%	BSA	
	10%	Horse serum	
	1X	PBS	
	0.3%	Triton	
Citrate buffer (Staining)	10 mM	Tri-sodium citrate	pH 6.0

Citrate buffer (STZ injection)	0.05 M 0.05 M	Citric acid Sodium citrate	pH 4.5
Lämmolie (4x)	5% 0.04% 40% 8% 0.24 M	β-Mercaptoethanol Bromophenol blue Glycerol SDS Tris HCl	
Loading buffer (DNA electrophoresis)	0.025% 20%	Bromophenol blue Glycerol	
Mowiol	12% 4.3 M 0.1 M	Glycerol Mowiol 4-88 Tris pH 8.5	
PBS (10X)	27 mM 10.6 mM 1.5 M 29.6 mM	KCl KH <sub>2</sub> PO <sub>4</sub> NaCl Na <sub>2</sub> HPO <sub>4</sub> x 7H <sub>2</sub> O	pH 7.4
Ponceau S	1% 0.2%	Glacial acetic acid Ponceau S	
RIPA with 1% SDS	5 mM 5 mM 1X 1% 0.5% 1%	EDTA EGTA PBS SDS Sodium deoxycholate Triton	

	50 mM 1 mM 1 mM	DTT NEM PI	
RIPA without SDS	5 mM 5 mM 1X 0.5% 1% 1 mM 1 mM	EDTA EGTA PBS Sodium deoxycholate Triton NEM PI	
SDS-running buffer	1.92 M 1 M 0.25 M	Glycine SDS Tris-HCl	
TAE buffer (1X)	20 mM 2 mM 40 mM	Acetic acid EDTA Tris-HCl	pH 8.0
TBST (10X)	150 mM 0.25 M 150 mM	NaCl Tris-HCl pH 7.5 Tween	
Transfer buffer	1.92 mM 10% 0.01% 25 mM	Glycine Methanol SDS Tris	
Transfection buffer	50 mM 280 mM 1.5 mM	BES NaCl NaHPO	pH 6.9

## 2.6 Primers

Site-directed mutagenesis was performed on mouse periaxin gene using the following primers:

**Table 7. List of primers**

Primer's number	Primer's name	Sense strand	Anti-sense strand
P1	Prx K76R	5'AGATATGAGGATGCAC TTCGCCTG3'	5'GAAGTTCTCAAAGAACA CACGGGC3'
P2	Prx K171R	5'GGTCTCAGAGCCGAG GCTGTC 3'	5'GACAGCCTCGGCTCTGA GACC3'
P3	Prx K218R	5'CCAAGGAAGGCCAGA GCAGAA 3'	5'CTCAGCTTCTGCTCTGG CCTT3'
P4	Prx K893R	5'AAAGCTGTCAGAGGA GAGGTG3'	5'CACCTCTCCTCTGACAG CTTT3'
P5	Prx K1174R	5'GAAGCAGCCAGAAGT GAGGGT3'	5'ACCCTCACTTCTGGCTG CTTC3'

## 2.7 Molecular biology techniques

### 2.7.1 Isolation of DNA from *E. coli* DH5 $\alpha$ cells

Two mL of a saturated *E. coli* DH5 $\alpha$  overnight culture were used for the isolation of plasmid DNA. Cells were centrifuged at 11,000 g for 2 min and the supernatant was discarded. Following, 250  $\mu$ L of buffer A1 supplemented with RNase (Macherey Nagel) were added and the cell pellet was resuspended until complete dissolution of clumps. In order to induce complete cell lysis, 250  $\mu$ L of buffer A2 were added to the cells and mixed gently by inverting the tube, which was incubated at room temperature for 5 min. Subsequently, 300  $\mu$ L of buffer A3 were added and mixed by inverting the tube, which was later centrifuged at 11,000 g for 5 min at room temperature. The resulting supernatant was transferred onto a Nucleospin column (Macherey Nagel), which was centrifuged at 11,000 g for 1 min. The flow-through was discarded and the column was washed with 600  $\mu$ L of buffer A4 (supplemented with ethanol) for 1 min at 11,000 g; the flow-through was discarded and the column was dried for 2 min. The column was placed in a new 1.5 mL tube and 30  $\mu$ L of elution buffer AE were added to the column, which was incubated at room temperature for 2 min. The plasmid DNA was eluted by

centrifuging at 11,000 g for 2 min and stored at -20°C until further analysis.

### 2.7.2 Polymerase chain reaction (PCR)

The polymerase chain reaction (PCR) was used to amplify the purified DNA. The PCR mixture was prepared and run under the following conditions:

**Table 8. List of reagents used for PCR**

<b>Reagent</b>	<b>Amount</b>
Phusion GC buffer	10 µL
10 mM Primers (Section 2.6)	2.5 µL
10 mM dNTPs (dATP, dCTP, dGTP, dTTP)	2 µL
Phusion Taq polymerase	1 µL
Template DNA	100 ng
DMSO	1.5 µL
H <sub>2</sub> O	28.5 µL
Total volume	50 µL

**Table 9. PCR running conditions**

Initial denaturation	98°C/30s	Number of cycles
Denaturation	98°C/20s	
Annealing	65°C/30s	28 cycles
Extension	72°C/3 min	
Final extension	72°C/10 min	-
Store	4°C/α	-

The annealing temperature was chosen based on the melting temperature of the primers.

### **2.7.3 DNA-agarose gel electrophoresis**

In order to separate DNA fragments, it was used a 1% agarose gel prepared in 1X TAE buffer and containing Ethidium bromide 10 µg/mL. DNA samples were mixed with 4X loading buffer and electrophoresis was performed at 100 V. Subsequently, the gel was exposed to UV light and the image of the DNA bands was recorded using a Biometra Ti5 acquisition system and BioDocAnalyze software.

### **2.7.4 DNA Purification from agarose gel**

The amplified DNA band was identified, excised from the gel and collected in a 1.5 mL tube. Three volumes of Buffer QG (Qiagen) were added to one volume of gel and incubated at 50°C for 10 min. After the gel was dissolved, one volume of isopropanol was added and the mixture was transferred to a column which was centrifuged at 13,000 rpm for 1 min. The flow-through was discarded; the column was placed back into the original tube and 750 µL of buffer PE supplemented with ethanol was added and then centrifuged for 1 min. The column was placed into a new 1.5 mL tube, 30 µL of Elution buffer (10 mM Tris-Cl, pH8.5) were added to the centre of the column and incubated for 4 min at room temperature and centrifuged for 1 min at 13,000 rpm. Eluted DNA was stored at 4°C for further use.

### **2.7.5 Determination of DNA concentration**

To determine the DNA concentration in the samples, we used a Nanodrop spectrophotometer (ThermoScientific), which reported a value based on the absorbance at 260 nm ( $A_{260}$ ) and according to the formula:

$$\text{DNA concentration } (\mu\text{g/mL}) = A_{260} \times \text{dilution factor} \times 50 \mu\text{g/mL}$$

### **2.7.6 Cloning**

The cDNA encoding mouse periaxin (Prx, 4.5 kb) was cloned into the pcMV6-AC-GFP vector (6.6 kb, Origene; Fig. 5) using the restriction sites SgfI (1024bp) and MluI (1067bp). To identify cells that express Prx, the vector included a C-terminal GFP tag. The plasmid was propagated in *Escherichia coli* Stbl4 (Invitrogen) and purified using a Maxi-prep kit (Thermo Scientific).

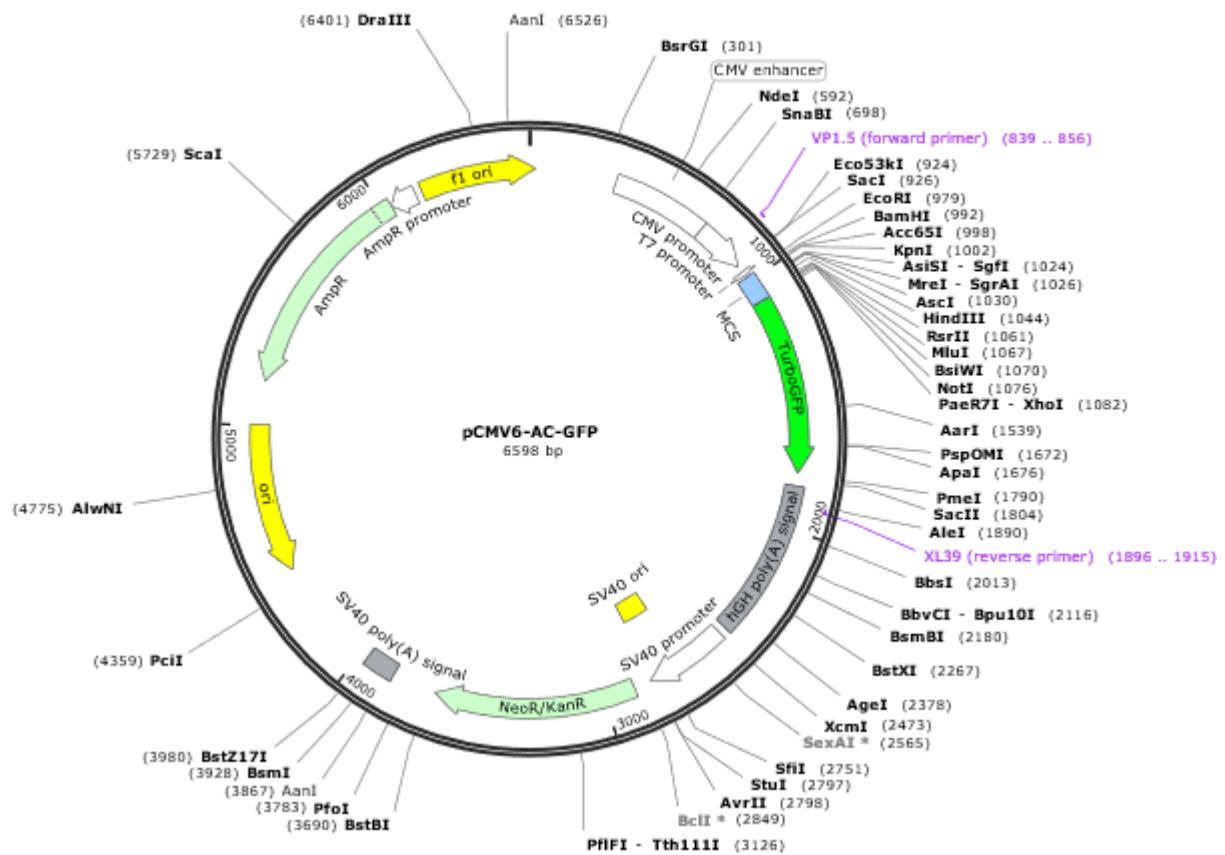


Figure 5. Map of the pcMV6-AC-GFP vector (Origene) used for the cloning of periaxin gene.

### 2.7.7 Site-directed mutagenesis

Sumo modification occurs at the lysine residue in the consensus sequence  $\Psi$ KXE/D, where  $\Psi$  is a hydrophobic amino acid residue (F, L, V, I or A), K is the target lysine, X is any amino acid and E/D is glutamic acid or aspartic acid. To identify the target lysine residue that is modified by sumoylation, we used SumoSP 2.0 software, which predicted five potential sumoylation sites in periaxin protein: K76, K171, K218, K893 and K1174. Based on the predicted sites, we designed primers (Section 2.6) for site-directed mutagenesis, in which the target lysine was mutated into arginine. Site-directed mutagenesis (Fig. 6) was performed using the following topo-cloning strategy: The Prx gene was cut-out from the pcMV6 vector using restriction enzymes (BamHI, HindIII, NotI) and subcloned into pCR-Blunt II-Topo Vector (Invitrogen). Mutations were introduced using the GeneArt™ Site-directed mutagenesis plus kit and the designed primers (Section 2.6). The mutant Prx gene was digested using the same restriction enzymes and ligated into the original vector (pcMV6). In this manner, it was possible to obtain plasmid constructs: Prx-B (K893R-K1174R), Prx-A (K76R-K171R-K218R)

and Prx-A+B (K76R-K171R-K218R-K893R-K1174R). Mutant constructs were successfully verified by sequencing, confirming the mutations in the targeted sites.

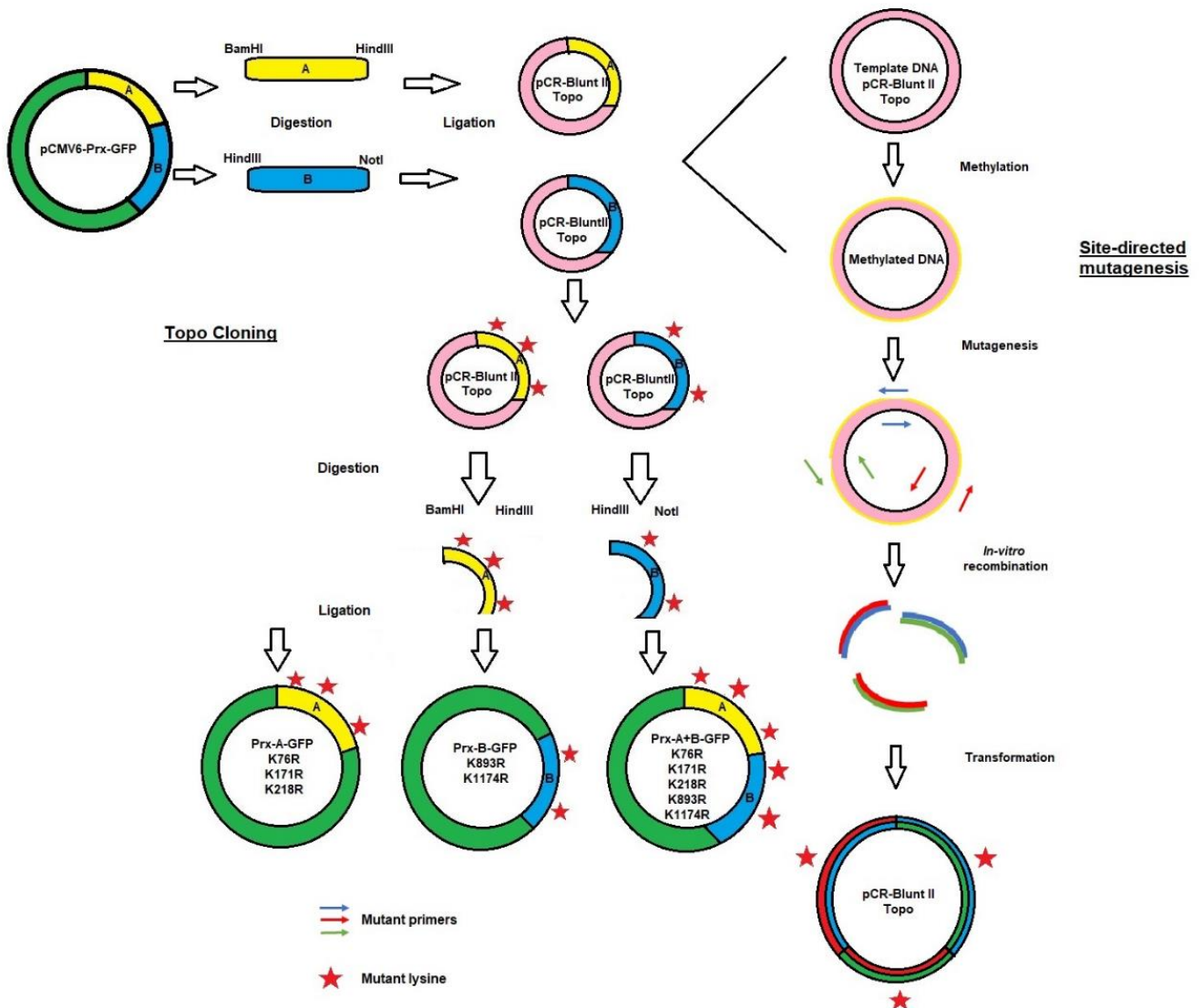


Figure 6. Schematic representation of topo cloning and site-directed mutagenesis strategy used for introducing mutations in target lysines of pCMV6-Prx-GFP.

### 2.7.8 Transfection

Human embryonic kidney cells (HEK 293) were maintained in Dulbecco's modified eagle's medium (DMEM, Gibco) supplemented with 4 mM L-Glutamine, 10% foetal bovine serum, 100 U/mL penicillin and 100 µg/mL streptomycin (Gibco) in a 37°C, 5% CO<sub>2</sub>, humidified incubator. Cells were split by trypsinization (0.25%, Gibco), centrifuged (800 rpm/ 5 min), resuspended in fresh culture medium (10 mL) and incubated at 37°C for 24h. HEK cells were transfected at 50% confluency with full-length mouse periaxin using a calcium phosphate protocol (20 µg DNA, 441 µL H<sub>2</sub>O,

48  $\mu\text{L}$   $\text{CaCl}_2$  and 510  $\mu\text{L}$  BBS buffer pH 6.9) and incubated for 10 min at 37°C. 6 mL of DMEM medium (without supplements) was added and the cells were incubated for 7 h at 37°C. Finally, the medium was removed and 10 mL DMEM supplemented with serum was added. The cells were incubated for 2 days at 37°C.

## **2.7.9 Protein Purification from HEK cells**

### **2.7.9.1 GFP-Immunoprecipitation**

For the immunoprecipitation reaction, approximately  $10^6$  HEK cells expressing GFP-tagged Prx protein were used. One mL of ice-cold PBS was added to the petri dish and adherent cells were harvested by scraping. Cells were centrifuged at 500 g for 3 min at 4°C. The supernatant was discarded and cells were washed twice with PBS. The cell pellet was resuspended in 300  $\mu\text{L}$  of lysis buffer (Ripa buffer containing 0.1% SDS, 50 mM DTT, 1x Protein inhibitor and 200 mM N-Ethylmaleimide) using a 25-gauge (0.5 x 25 mm) syringe. The tube containing the lysis buffer was placed on ice for 30 min and the cells were mixed every 10 min. After that the cell lysate was centrifuged at 20,000 g for 10 min at 4°C and 60  $\mu\text{L}$  of lysate were collected as lysate control for Western blot. The remaining lysate was transferred to a pre-cooled tube and 300  $\mu\text{L}$  of RIPA buffer without SDS (supplemented with 1 mM PMSF and 1X protease inhibitor) was added to achieve a concentration of 0.05% SDS; the cell pellet was discarded. 25  $\mu\text{L}$  of TurboGFP-Trap\_A beads were washed 3 times with 500  $\mu\text{L}$  of ice-cold RIPA buffer (without SDS) by centrifugation at 2500 g for 2 min at 4°C. The diluted lysate was added to the equilibrated TurboGFP-Trap\_A beads and incubated with rotary agitation for 1 h at 4°C. After incubation, the beads were centrifuged at 2500 g for 2 min at 4°C, the supernatant was discarded and the beads were washed 3 times with 500  $\mu\text{L}$  of ice-cold RIPA buffer without SDS. For protein elution, the beads were resuspended in 80  $\mu\text{L}$  of 2X Lämmli buffer and incubated at 90°C for 10 min to dissociate immunocomplexes from the beads. The beads were centrifuged at 2500 g for 2 min at room temperature and the supernatant was collected and stored at -20°C for further Western blot.

### **2.7.9.2 Sumo1 and Prx-Immunoprecipitation**

For the immunoprecipitation reaction, approximately  $10^6$  HEK cells expressing GFP-tagged Prx protein were used. The culture medium was removed from the petri dish and 300  $\mu\text{L}$  of lysis buffer (Ripa buffer containing 1% SDS, 50 mM DTT, 1x Protein

inhibitor and 200 mM N-Ethylmaleimide) were added. The cells were scraped and disrupted gently by sonication (6 micronsX5 pulses), followed by incubation at 60°C for 30 min. The cell lysate was centrifuged at 15,000 g for 10 min at room temperature and 60 µL of lysate were collected as lysate control for Western blot. The remaining lysate was transferred to a pre-cooled tube and diluted 10-fold with RIPA buffer without SDS (supplemented with 1X protease inhibitor and 200 mM N-Ethylmaleimide) to achieve a concentration of 0.1% SDS and 30 µL of anti-Sumo1 antibody or 15 µL of anti-periaxin antibody were added to the diluted lysate (as per requirement), which was incubated overnight at 4°C by mixing gently.

On the next day, 100 µL of the slurry of Protein G plus (for Sumo1) or Protein A/G plus (for periaxin) agarose beads (Santa Cruz) were washed 3 times with 500 µL of ice-cold RIPA buffer (without SDS). The beads were mixed in 100µL of RIPA buffer and added to the diluted lysate, which was incubated at 4°C for 3 h. The antibody-bead mixture was transferred to a Sigma-prep spin column, the beads were collected and the flow-through was discarded. The beads were washed 3 times with 500 µL of ice-cold RIPA buffer (without SDS) and the bottom of the column was closed with a cap. The beads were mixed in 80 µL of 2X Lämmli buffer and the column was incubated in a water bath at 60°C for 20 min, followed by centrifugation at 2500 g for 2 min at room temperature. The flow-through was collected in a new 1.5 mL tube and stored at -20°C for further Western blot.

### 2.7.10 SDS-polyacrylamide gel electrophoresis

Proteins were separated by SDS-polyacrylamide gel electrophoresis using a Mini-Protean 3 cell system (Biorad) with a 1.5 mm thickness gel. To separate efficiently proteins depending on their size, we used a 6% (60-250 kDa) or 10% (20-70 kDa) separating-gel, respectively:

**Table 10. Composition of separating gels**

<b>Separating gel</b>	<b>6%</b>	<b>10%</b>
H <sub>2</sub> O	5.3 mL	4.0 mL
30% acrylamide mixture	2.0 mL	3.3 mL
1.5 M Tris (pH 8.8)	2.5 mL	2.5 mL
10% SDS	0.1 mL	0.1 mL

10% APS	0.1 mL	0.1 mL
TEMED	8 $\mu$ L	4 $\mu$ L
Total volume	10 mL	10 mL

After mixing the components, the gel was allowed to polymerise at room temperature. To concentrate proteins, a 6% stacking-gel was poured on the top of the separating gel, set out as follows:

**Table 11. Composition of stacking gel**

<b>Stacking gel</b>	<b>6%</b>
H <sub>2</sub> O	2.1 mL
30% acrylamide mixture	0.5 mL
1.5 M Tris (pH 6.8)	0.38 mL
10% SDS	30 $\mu$ L
10% APS	30 $\mu$ L
TEMED	3 $\mu$ L
Total volume	3 mL

After polymerisation, gels were assembled in the vertical electrophoresis chamber. Samples (Lysates and IPs) were heated at 60°C for 20 min. Electrophoresis was performed in running buffer with 5  $\mu$ L of protein ladder, 30  $\mu$ L of lysate and 40  $\mu$ L of IP loaded into the gel wells. The samples were run at a constant voltage of 120 V for 3 h. Subsequently, the gel was subjected to western blotting.

### **2.7.11 Western blotting**

Proteins were transferred from the polyacrylamide gel to a nitrocellulose membrane (GE Healthcare) by blotting the gel at a constant current of 200 mA for 100 min, using a Mini-Trans-Blot system (Bio-Rad). To check the proper transfer of proteins, the blotted membranes were stained with Ponceau solution for a few seconds. To avoid unspecific binding of antibodies, membranes were then blocked with 5% bovine serum albumin (BSA) in Tris-buffered saline containing Tween (TBST) for 1 h at room temperature. The membranes were then incubated overnight at 4°C with the primary

antibodies diluted in TBST (5% BSA). The next day, the membranes were washed 3 times with TBST for 10 min each and incubated with horseradish peroxidase-linked secondary antibodies (anti-rabbit IgG or anti-mouse IgG; 1:4000 in TBST) for 1 h at room temperature and then washed 3 times in TBST. For visualization of reactive bands, Luminol reagent (Santa Cruz) or Lumi-light blotting substrate (Roche Diagnostics) was used and blots were exposed on X-ray films (Fujifilm). Afterwards, the films were developed and fixed using an X-ray film processor (Optimax).

## 2.8 Cell culture techniques

### 2.8.1 Media for HEK cells, Schwann and DRG culture

**Table 12. Composition of Media for HEK cells, Schwann and DRG**

Name	Composition
DMEM	4.5 g/L D-Glucose, 0.11 g/L Sodium pyruvate, 10% HS, 1% pen-strep, 1% glutamine
DRG growth medium	DMEM, 5 ng/mL NGF, 10 ng/mL BDNF, 10 ng/mL GDNF, 10 ng/mL NT3, 10 $\mu$ M Uridine, 10 $\mu$ M Deoxyuridine, 10 $\mu$ M 5-Fluorouracil
DRG myelination medium	DMEM, 1X B27, 1X N2, 5ng/mL NGF, 10 ng/mL GDNF, 10 ng/mL BDNF, 10 ng/mL NT3, 0.5 $\mu$ M Forskolin, 50 $\mu$ g/mL ascorbic acid, 20 $\mu$ g/mL bovine pituitary extract
Schwann cell growth medium	DMEM, 50 $\mu$ g/mL Forskolin, 2 ng/mL Heregulin $\beta$ 1, 10 ng/mL fibroblast growth factor, 20 $\mu$ g/mL bovine pituitary extract
Hanks balanced solution	Inorganic salts, glucose
L15 Medium	Amino acids, vitamins, inorganic salts, phenol red, sodium pyruvate

### 2.8.2 Preparing coated coverslips and petri dishes

Coverslips and petri dishes (35 mm diameter) were coated with 0.1 mg/mL poly-L-Lysine solution (Sigma-Aldrich P6407) and incubated overnight at room temperature. The next day, the poly-L-Lysine solution was removed and the surface was washed twice with sterile distilled water and left to dry for 2 h at room temperature before use.

### **2.8.3 Enzymatic dissociation of sciatic nerve**

Sciatic nerves were obtained from an adult PLP<sup>cre</sup><sup>ERT2</sup>Ubc9<sup>fl/fl</sup> mouse. Nerves were dissected under aseptic conditions and rinsed in ice-cold Leibovitz 15 medium containing penicillin and streptomycin. Under a stereo dissecting microscope (Leica MZFLIII), excess fat and the epineurium were carefully removed and the fibres were teased until they were separated from each other. The nerve fascicles were teased until getting individual fibres. The nerve fibres were placed into a 35 mm petri dish containing 2 mL of enzymatic solution (25 mg/ml Trypsin and 10 mg/ml Collagenase dissolved in F12 medium) and incubated at 37°C, 5% CO<sub>2</sub> for two hours.

Afterwards, digestion was stopped by the addition of 40% FBS in Hanks balanced solution and the mixture was centrifuged at 188 g for 10 min at 4°C. The pellet was resuspended in DMEM+10% FBS using a polished glass pipet and cells were centrifuged under the same conditions. The supernatant was discarded and the cells were resuspended in 1 mL of DMEM+10% FBS (supplemented with 10 nM Heregulin  $\beta$ 1 and 2  $\mu$ M Forskolin). Schwann cells were plated in 100  $\mu$ L drops in a 35 mm petri dish and incubated at 37°C, 5% CO<sub>2</sub>. The culture medium was replaced every 3 days. After 1 week in culture, the cells were immunostained with Schwann cell markers like Prx, S100 and p75.

### **2.8.4 *In vitro* myelination assay**

DRGs were isolated from E14 C57BL/6JRj mouse embryos and placed in 20  $\mu$ L drops of DRG growth medium. Subsequently, DRGs were mixed with Schwann cells (previously isolated) and seeded in 40  $\mu$ L drops on coated coverslips and covered with a layer of Matrigel (Corning, 100  $\mu$ L/well) prepared in a 1:1 dilution in DRG growth medium. The plate was incubated at 37°C for 30 min and afterwards, 500  $\mu$ L of basic growth medium was pipetted in each well. The explant DRGs and Schwann cells were cultured in basic medium containing growth factors including NGF, BDNF, GDNF and NT3, which support axonal growth from the cell body in the DRGs, as well as growth of Schwann cells. After three days, the culture medium was changed to myelination medium, which was supplemented with growth factors and forskolin to stimulate Schwann cell growth. The DRG-SC cocultures were continued for 3 weeks, changing the medium every 3 days.

## 2.9 Animal experiments

### 2.9.1 Housing conditions

Age-matched 7-8-week-old male mice were maintained in a humidity and temperature-controlled environment. Four littermates were housed in a socially stable and well-nested individually ventilated cage-rack system (Techniplast, Italy). Mice had free access to water and food and were housed in rooms with a 12-h light-dark cycle. All experiments were done following guidelines and approved by Regierungspräsidium Karlsruhe, Germany.

### 2.9.2 Generation of SNS-HIF1 $\alpha$ <sup>-/-</sup> mice

For animal experiments, SNS-HIF1 $\alpha$ <sup>-/-</sup> mice were used, in which the transcription factor HIF1 $\alpha$  is conditionally deleted in peripheral nociceptive neurons of the dorsal root ganglion (DRGs). Mice were kindly provided by Professor Irmgard Tegeder. For the generation of SNS-HIF1 $\alpha$ <sup>-/-</sup> mice, mice carrying the HIF1 $\alpha$  flox allele (HIF1 $\alpha$ <sup>fl/fl</sup>) were mated with SNS-Cre mice, which selectively express cre-recombinase in nociceptors under the control of the sodium channel 1.8 promoter (Kangiesser *et al.*, 2014) to obtain homozygous SNS-HIF1 $\alpha$ <sup>-/-</sup> mice (Fig. 7). Male and female 8-week-old SNS-HIF1 $\alpha$ <sup>-/-</sup> and their HIF1 $\alpha$ <sup>fl/fl</sup> littermates were used for experiments.

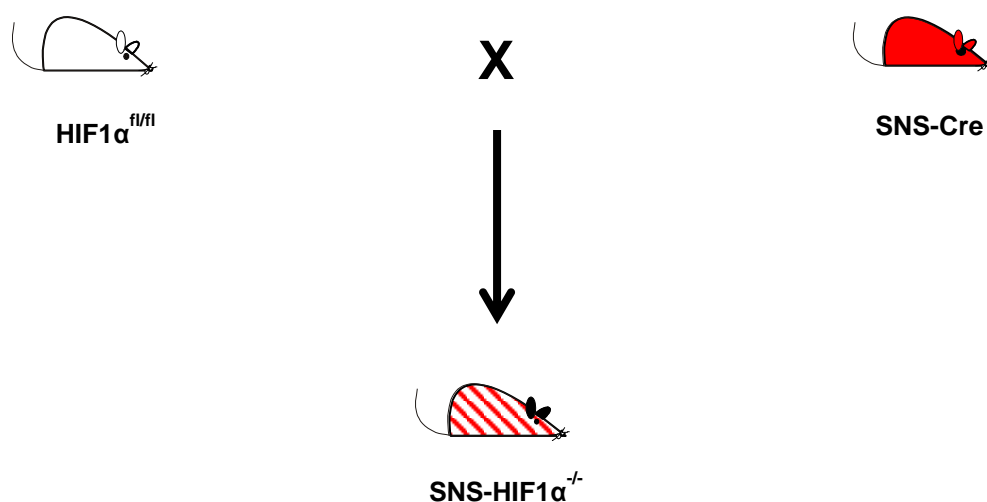


Figure 7. Schematic representation of the generation of SNS-HIF1 $\alpha$ <sup>-/-</sup> mouse line (Kangiesser *et al.* 2014)

### 2.9.3 Induction of Diabetes mellitus Type I

Diabetes type I was induced by multiple low-dose injections of Streptozotocin in citrate buffer (STZ, 60 mg/Kg body weight), which induce selective destruction of pancreatic beta cells and increases blood glucose levels. STZ was injected intraperitoneally in SNS-HIF1 $\alpha$ <sup>-/-</sup> or HIF1 $\alpha$ <sup>fl/fl</sup> mice for 5 consecutive days. Control mice received citrate buffer injections alone. Blood glucose levels were measured weekly along the entire course of the experiment. Mice with glucose level above 350 mg/dL were considered to be diabetic. Mice were analysed over a period of 5 to 24 weeks post-STZ injection.

### 2.9.4 Blood glucose measurements

After induction of diabetes by STZ injection, blood glucose levels were measured by taking a blood drop from the cheek vein with a needle (0.4 mm x 19 mm, 27-gauge). The blood sample was collected and glucose was measured using an Accu-Chek Aviva glucometer (Roche Diagnostics). Blood glucose levels were maintained in a range between 380 and 480 mg/dL by weekly subcutaneous administration of insulin (as required) over the course of the experiment to ensure uniformity and consistency. Depending on the blood glucose level, mice were injected with insulin in accordance with the following reference values:

**Table 13. Insulin dosage scale**

Glucose level (mg/dL)	Insulin units
300-375	1
375-425	2
425-500	3
500-600	4
>600	5

Mice were analysed over a period of 2 to 24 weeks post-STZ injection. In order to avoid inadvertent effects of insulin on experimental results, behavioural analyses and tissue extraction were performed at least three days after insulin administration.

### 2.9.5 Generation of PLP-Cre<sup>ERT2+/+</sup>Ubc9<sup>fl/fl</sup> mice

The generation of conditional mouse lines is a valuable approach to study genes and proteins in a physiological background. This is relevant specifically in analysing disease mechanisms of late-onset degenerative disorders and regeneration processes in mouse models. The approach using the Cre recombinase for deleting DNA fragments between loxP sites to generate mutations in a temporally controlled manner has demonstrated to be effective (Lewandosky, 2001). Based on this, we designed an experiment to investigate the effect of SUMO modification on periaxin function *in vivo*, using a mouse model. To address this, the mouse line PLP-Cre<sup>ERT2+/+</sup>Ubc9<sup>fl/fl</sup> was created in our laboratory as following: mice carrying homozygous flox alleles of the Ubc9 gene (Ubc9<sup>fl/fl</sup>) were mated with PLP-Cre<sup>ERT2</sup> mice in which, upon tamoxifen injection, the Cre-recombinase is expressed under the control of the proteolipid protein promoter selectively in Schwann cells and oligodendrocytes (Fig. 8). In these mutant mouse line, Ubc9 (SUMO-conjugating enzyme) can be conditionally deleted by Tamoxifen injection.

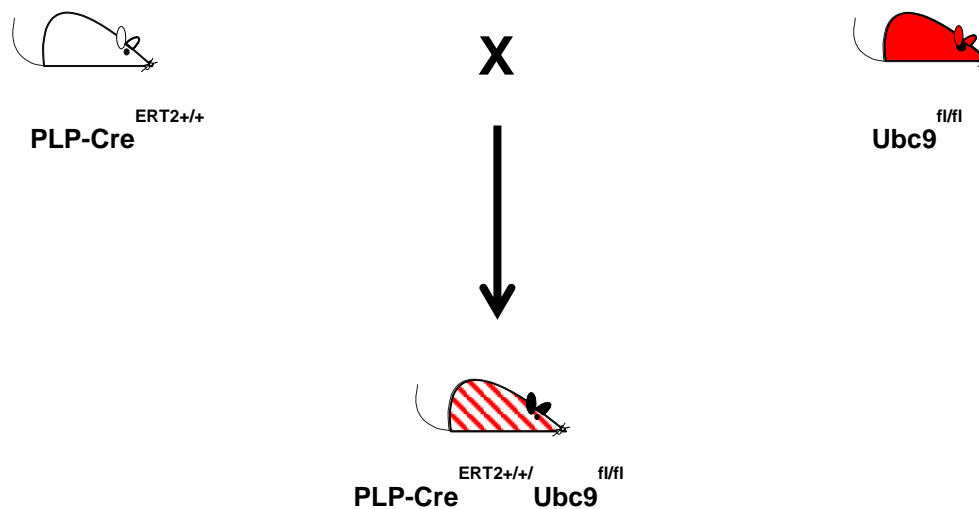


Figure 8. Schematic representation of the generation of PLP-Cre<sup>ERT2+/+</sup>-Ubc9<sup>fl/fl</sup> mouse line.

### 2.9.6 Conditional deletion of Ubc9 in PLP-Cre<sup>ERT2+/+</sup>Ubc9<sup>fl/fl</sup> mice

Tamoxifen (Sigma-Aldrich) was dissolved 20 mg/mL in corn oil (vehicle) by rotary agitation overnight at room temperature. Female and male 8-9 week-old PLPcre<sup>ERT2+/+</sup>Ubc9<sup>fl/fl</sup> mice were injected with 100  $\mu$ L of tamoxifen solution (75 mg/kg body weight) intraperitoneally for 5 consecutive days, twice a day. A control group was

injected only with the vehicle following the same protocol. All behavioural tests were performed over a period of 2 to 16 weeks post-Tamoxifen or vehicle injection.

## **2.10 Behavioural testing**

### **2.10.1 Von Frey test**

All behavioural experiments were done in awake, unrestrained, acclimatized and age-matched adult mice. All experimental groups included equal numbers of male and female mice. Mice were habituated to the experimental setup twice a day for 4 days before behavioural testing. The experimenter was blinded to both the genotype and group (Bourquin *et al.*, 2006). After habituation, mechanical sensitivity was assessed with graded strength Von Frey filaments exerting a specific force (0.07, 0.16, 0.4, 0.6, 1.0, 1.4, 2.0 and 4.0 g). Five stimuli of each filament were applied to the hind paw, keeping a time interval of 5 min between filaments of different force and the number of paw withdrawals was counted. Sixty percent response frequency was set as threshold.

### **2.10.2 Hargreaves test**

Thermal sensitivity was assessed by the Hargreaves Test (Plantar Test Ugo Basile). An infrared (IR) heat source was placed under a plexiglass surface upon which the experimenter deposited the mouse into a plexiglass box. The IR source emitted a high-intensity light beam until the hind paw was withdrawn, at this point the IR source automatically stopped and recorded the time the mouse took for paw withdrawal (Cheah *et al.*, 2017). A maximum cut-off of 20 seconds was set to avoid burning tissue. The mean paw withdrawal latency (PWL) of three applications with at least 5 min intervals was used for statistical analyses.

### **2.10.3 Hole-board**

We used the hole-board test as a measure of neophilia in mice, which is the attraction that an animal displays towards a novel object or place (Brown and Nemes, 2008). The hole-board apparatus is comprised of 16 equally-spaced holes that are 3 cm in diameter and the entire apparatus was raised to a height of 18 cm above floor level. For the experiment, each mouse was placed in the centre of the apparatus and allowed to freely explore for 10 min and the number of head dips was recorded. A head dip was scored when the head was introduced at a minimum of eye-level into a hole. All

trials were carried out between 08:00 and 10:00 am. Each trial lasted 10 min, at the end of which, the mouse was immediately returned to the home cage.

#### **2.10.4 Elevated plus-maze**

The elevated plus-maze is a behavioural repertoire used to detect anxiety in mice (Espejo, 1997). The elevated plus-maze is comprised of 2 open arms and 2 enclosed arms that extend from a common central platform. The apparatus is elevated to a height of 70 cm above the floor level. For the test, the mouse is placed in the centre of the cross of the maze and allowed to explore for 10 min. The percentage of visits and time spent in both the open and closed arms are recorded.

#### **2.10.5 Home cage monitoring**

The assessment of daily activity was carried out employing the automated system Laboras home cage observation (Metris B.V.), which uses small sensors to detect mouse movement and transmits the signals to a recording computer with processing software (Laboras version 2.6; Quinn *et al.*, 2003). Animals were placed individually in the calibrated cage with free access to food and water during the entire recording period. Climbing, locomotion, grooming and distance were all recorded each hour for 24 h.

#### **2.10.6 Running wheel test**

The voluntary running wheel test is used as a measure of motor activity (Fredriksson *et al.*, 2011). Animals were housed individually and a running wheel was mounted in each cage. The running wheel was interfaced with a magnetic sensor that counted the total wheel revolutions and time spent by each mouse. The measure started in the morning for a total duration of 24 hours. The total distance and total exercise time were recorded every hour for each mouse.

#### **2.10.7 Cat-walk test**

We used the Cat-walk gait analysis system (Noldus, The Netherlands) to analyse gait changes. The Cat-walk instrument consists of an enclosed walk-way, a high-speed colour camera and recording and analysis software to assess the locomotor performance of rodents (Gabriel *et al.*, 2007). All experiments were performed between 8:00 and 11:00 am. Mice were trained for 1 week to cross the cat-walk before testing

began by placing the mice on one end of the glass plate and allowing them to cross it freely. On the testing day, mice were allowed to cross the walk-way 3 times before the test ended and mice were returned to their cages.

**Table 14. Parameters measured during Cat-walk test**

<b>Parameter</b>	<b>Description</b>
Body speed	Calculated by dividing the distance that the animal's body travelled from one initial contact of one paw to the next by the time to travel that distance
Duty cycle	expresses Stand as a percentage of the Step cycle. Duty cycle = (Stand/Stand+Swing) *100%
Maximum contact area	It is the maximum area of a paw that comes into contact with the glass plate
Maximum intensity	It is the maximum intensity of a complete paw on the glass plate
Minimum intensity	It is the minimum intensity of a complete paw on the glass plate
Mean intensity	It is the mean intensity of a complete paw on the glass plate
Print length	It is the length (horizontal direction) of a complete print. The complete print is the sum of all contacts with the glass plate
Print width	It is the width (vertical direction) of a complete paw print on the glass plate
Print area	It is the surface area of a complete print. The print area is by definition at least as large as the maximum contact area.
Stand	It is the duration in seconds of contact of a paw with the glass plate
Step cycle	It is the time in seconds between two consecutive initial contacts of the same paw. Step cycle= Stand + Swing
Stride length	It is the distance (distance units) between successive placements of the same paw
Swing	It is the duration in seconds of no contact of a paw with the glass plate
Swing speed	It is the speed (distance unit/ second) of the paw during the swing. Swing speed= Stride length/ swing

Behavioural tests were applied over a period of 2 to 30 weeks post-Tamoxifen or vehicle injection.

## **2.11 Analytical chemistry methods**

### **2.11.1 Quantification of ROS**

To detect the production of ROS and superoxide in DRGs of SNS-HIF1 $\alpha^{-/-}$  and HIF1 $\alpha^{fl/fl}$  mice, we intrathecally injected MitoTrackerRedCM-H<sub>2</sub>XROS (100 nM, 10  $\mu$ l, Life Technologies). The dye, which is in a reduced form and non-fluorescent in the basal state diffuses across the plasma membrane, it is oxidized and sequestered into the mitochondria, where it reacts with thiols and becomes fluorescent upon oxidation (Poot *et al.*, 1996; Keij *et al.*, 2000). After 24 h, mice were perfused with 1x PBS and 4% PFA; DRGs were extracted and cut on a cryotome as 16  $\mu$ m sections (Leica Biosystems). In order to detect the increase or decrease of ROS levels, the presence of MitoTrackerRedCM-H<sub>2</sub>XROS fluorescence was analysed at different time points after STZ injection using a laser-scanning spectral confocal microscope (Leica TCS SP8). A total of 110 cells per tissue section were counted. In total, 10 sections per mouse and 6 mice per group were included for the quantification of fluorescence intensity. The DRG sections were stained with DAPI to differentiate neuronal cells from satellite cells. The number of DRG cells positive for MitoTracker Red was quantified.

### **2.11.2 Quantification of hydrogen peroxide in tissue**

The Amplex red hydrogen peroxide (H<sub>2</sub>O<sub>2</sub>) assay (Life Technologies) was used to quantify the levels of H<sub>2</sub>O<sub>2</sub> in the DRGs and sciatic nerves of diabetic and non-diabetic HIF1 $\alpha^{fl/fl}$  and SNS-HIF1 $\alpha^{-/-}$  mice prior to and at 24 weeks post-STZ. In the presence of peroxidase, the Amplex red reacts with H<sub>2</sub>O<sub>2</sub> and produces the red-fluorescent oxidation product resorufin, which possesses a maximum excitation and emission wavelength of 571 nm and 585 nm, respectively (Zhou *et al.*, 1997). By using this assay, it is possible to detect until 10 picomols of H<sub>2</sub>O<sub>2</sub> in a volume of 100  $\mu$ l. Fresh tissue samples were lysed in 250  $\mu$ l of ice-cold PBS. Tissue was homogenized and incubated for 20 min with shaking at 4°C. Lysates were centrifuged at 1200 rpm for 10 min at 4°C. 50  $\mu$ l of tissue lysate was mixed with 50  $\mu$ l of Amplex red substrate and incubated in the dark at room temperature for 10, 20, 30 and 60 min. Fluorescence was measured at 540/595 nm excitation/emission. The amount of H<sub>2</sub>O<sub>2</sub> in tissue was quantified and normalized over tubulin. The fold changes in levels of H<sub>2</sub>O<sub>2</sub> in the

diabetic tissue over basal (non-diabetic) were calculated to determine changes in levels of H<sub>2</sub>O<sub>2</sub> upon induction of diabetes.

### **2.11.3 Plasma collection**

Blood samples were collected before and at different time points post-STZ injection. Age-matched citrate buffer-injected, non-diabetic mice were used as controls. Blood samples were drawn from the venous sinus using the retro-orbital bleeding method. Blood samples were collected at basal, 8, 12 and 22 weeks post-STZ injection in EDTA-treated tubes and plasma was separated by centrifugation and stored at -80°C,

### **2.11.4 Tissue extraction**

Sciatic nerve tissue was extracted from basal, 12 and 22 weeks post-STZ injected diabetic mice. Citrate buffer-injected, non-diabetic mice were used as controls. The extracted sciatic nerves were snap-frozen using liquid nitrogen and stored at -80°C until analysis.

### **2.11.5 Determination of amino acid levels from serum**

The determination of amino acids and metabolites was done in collaboration with the Metabolomics Core Technology Platform of the Centre for Organismal Studies Heidelberg. Amino acids from mice serum were quantified after specific labelling with the fluorescence dye AccQ-Tag<sup>TM</sup> (Waters), according to the manufacturer's protocol. The resulting derivatives were separated by reversed-phase chromatography on an Acquity BEH C18 column (150 mm x 2.1 mm, 1.7 µm, Waters) connected to an Acquity H-class UPLC system and quantified by fluorescence detection (Acquity FLR detector, Waters, excitation 250 nm, emission 395 nm) using ultrapure standards (Sigma). The column was heated to 42°C and equilibrated with 5 column volumes of buffer A (140 nM sodium acetate pH 6.3, 7 mM triethanolamine) at a flow rate of 0.45 mL/min. Baseline separation of amino acid derivatives was achieved by increasing the concentration of acetonitrile (B) in buffer A as follows: 1-min 8% B, 16-min 18% B, 23-min 40% B, 26.3-min 80% B, hold for 5 min and return to 8% B in 3 min. Data acquisition and processing were performed with the Empower3 software suite (Waters).

## **2.11.6 Determination of metabolites by gas chromatography/mass spectrometry from sciatic nerve tissue**

### **2.11.6.1 Extraction**

Frozen material was extracted in 180  $\mu\text{L}$  of 100% MeOH for 15 min at 70°C with vigorous shaking. 5  $\mu\text{L}$  ribitol (0.2 mg/mL) was added as an internal standard, followed by an additional 100  $\mu\text{L}$  chloroform to each sample. All samples were shaken at 37°C for 5 min. Subsequently, 200  $\mu\text{L}$  of water was added to each sample and centrifuged at 11,000 g for 10 min. 300  $\mu\text{L}$  of the polar (upper) phase was transferred to a fresh tube and dried in a speed-vac (Eppendorf vacuum concentrator) without heating and used for derivatization.

### **2.11.6.2 Derivatization**

Pellets were re-dissolved in 20  $\mu\text{L}$  of methoximation reagent containing 20 mg/mL methoxyamine hydrochloride (Sigma 226904) in pyridine (Sigma 270970) and incubated for 2 h at 37°C with shaking. For silylation, 32.2  $\mu\text{L}$  N-methyl-N-(trimethylsilyl)-trifluoroacetamide (MSTFA; Sigma M7891) and 2.8  $\mu\text{L}$  alkane standard mixture (50 mg/mL C<sub>10</sub>-C<sub>40</sub>; Fluka 68281) were added to each sample. After incubating for 30 min at 50°C, samples were transferred to glass vials for gas chromatography/mass spectrometry (GC/MS) analysis.

### **2.11.6.3 GC/MS analysis**

GC/MS-QP2010 Plus (Shimadzu®) fitted with a Zebron ZB 5 MS column (Phenomenex®; 30 m x 0.25 mm x 0.25  $\mu\text{m}$ ) was used for GC/MS analysis. The GC was operated at an injection temperature of 230°C and 1  $\mu\text{L}$  sample was injected with split mode (1:10). The GC temperature program started with a 1 min hold at 40°C followed by a 6°C/min ramp to 210°C, a 20°C/min ramp to 330°C and a bake-out for 5 min at 330°C using helium as the carrier gas with constant linear velocity. The MS was operated with ion source and interface temperatures of 250°C, a solvent cut time of 8 min and a scan range (m/z) of 40-700 with an event time of 0.2 s. The GCMS solution software (Shimadzu®) was used for data processing.

## **2.12 Immunohistochemistry methods**

### **2.12.1 Tissue preparation**

Tissue samples were collected at different time points pre- and post-Tamoxifen injection. Age-matched vehicle-injected PLPcre<sup>ERT2</sup>Ubc9<sup>fl/fl</sup> mice were used as controls for tissue collection. For paw punches biopsies, the mice at 30 weeks post-Tamoxifen were perfused with phosphate-buffered saline (1X PBS) and fixed with 4% PFA. The punch biopsies of the plantar skin of the hind paws, sciatic nerves and DRGs were prepared and post-fixed in 4% PFA for 24 h at 4°C. The tissue was transferred into 30% sucrose in PBS for overnight incubation at 4°C. The tissue was embedded in freezing medium (Leica Biosystems) and cut at 16-µm cryosections for immunohistochemical analysis.

### **2.12.2 Immunohistochemistry**

Immunohistochemistry was performed on punch biopsies from the plantar surface of the hindpaws in diabetic and non-diabetic SNS-HIF1 $\alpha$ <sup>-/-</sup> and HIF1 $\alpha$ <sup>fl/fl</sup> and C57BL6/j mice prior to and at different time points post-STZ. Sections were permeabilised in 1X PBS with Triton-X-100 (0.2% PBST), washed and blocked with 7% horse serum in 1X PBS. The sections were incubated overnight with anti-CGRP (1:1000, Sigma-Aldrich) or Protein Gene Product 9.5 (Dako) primary antibody in 7% horse serum at 4°C. The next day, sections were washed and incubated with Alexa Fluor-594 or Alexa Fluor-488 conjugated secondary antibody (1:700, Invitrogen). Finally, sections were washed and embedded in Mowiol. Fluorescent images were obtained using a Leica TCS SP8 confocal microscope and maximum projections were created using Leica SP8 software (Leica TCS SP8 Biosystems). All tissues were imaged using the same settings irrespective of group allocation. The acquired images were analysed using ImageJ software. Each image was converted to 8-bit and the epidermal area was marked using the region of interest (ROI) tool. Fluorescence density was calculated over the marked epidermal area after background subtraction. The experimenter was blinded to the identity of the sections during the acquisition and quantification of images.

### **2.12.3 Immunofluorescence on co-culture DRGs and Schwann cells**

The DRG-Schwann cell cocultures were fixed with 4% PFA for 20 min at room temperature. The cocultures were washed 3 times with 1x PBS for 5 min each and incubated with 50 mM Glycine for 20 min. The cultures were washed with 0.3% Triton

for 15 min. To avoid any non-specific binding, the co-cultures were blocked with 0.3% Triton, 10% horse serum and 1% bovine serum albumin (BSA) for 30 min. The primary antibodies used were: rat anti-myelin basic protein (MBP, Bio-Rad), mouse anti-myelin-associated glycoprotein (MAG, Sigma-Aldrich) and rabbit anti-S100 (Dako). Antibodies were diluted in a blocking solution containing 1% BSA to a final dilution of 1:50, 1:50 and 1:100, respectively and incubated for 3 days at 4°C. Subsequently, the cocultures were washed 3 times with 0.3% Triton for 5 min each and incubated with secondary antibodies. The secondary antibodies used were: donkey anti-rat IgG-Alexa Fluor 488 conjugated, donkey anti-rabbit IgG-Alexa Fluor 594 and donkey anti-mouse IgG-Alexa Fluor 647. Antibodies were mixed and diluted in a blocking solution containing 1% BSA, to a final dilution of 1:700. Finally, the immunolabeled co-cultures were embedded in Mowiol. Fluorescent images were obtained at 20x magnification using a Leica TCS SP8 confocal microscope. Maximum projections were created using Leica SP8 software (Leica TCS SP8 Biosystems).

### **2.13 Data analysis**

Data are presented as mean  $\pm$  SEM. Two-way repeated-measures ANOVAs with Bonferroni post-hoc tests for multiple comparisons were employed for analysis. Changes with  $p \leq 0.05$  were considered to be statistically significant.

### 3 RESULTS

The first section examines how nerve damage and altered metabolic pathways are related during the development of DPN in peripheral sensory neurons of mice. Second, the function of the transcription factor HIF1 $\alpha$  during the progression of DPN and generation of ROS in sensory neurons of mice was examined. Finally, we determined if periaxin could be a potential sumoylation target and we studied the functional consequences of this post-translational modification in Schwann cells.

#### 3.1 Metabolomic screening in diabetes type I model

##### 3.1.1 Induction of diabetic neuropathy in mice

Previous studies demonstrated the alterations occurring in the expression and activity of metabolic enzymes in peripheral nerves over the course of the progression of DPN (Kelley *et al.*, 2002; Mogensen *et al.*, 2007). However, it is not yet understood if these modifications take place after DPN is established or if they are the trigger for the onset and progression of DPN (Akude *et al.*, 2011).

Until now, no attempts were made to investigate the longitudinal changes occurring in metabolic pathways, which lead to onset and progression of DPN. In the current study we investigated the alterations in the amino acid profile in serum and the metabolic alterations in the sciatic nerve before the onset and during the progression of diabetic neuropathy.

We have used the low-dose STZ model to mimic type 1 diabetes, which does not show any adverse neurotoxic effects (Koulmanda *et al.*, 2003). This model is characterised by the infiltration of lymphocytes into the pancreatic islets, which induces cell death and therefore produces insulin deficiency and hyperglycaemia (Leiter, 1982). We have carried out a long-term study in mice injected with STZ and age-matched mice injected with citrate buffer, considered as control mice, in order to elucidate the function of hyperglycaemia-induced metabolic alterations at the beginning and during the progression of DPN. The stability of hyperglycaemia was determined by measuring the level of blood glucose. The mice injected with STZ continuously presented blood glucose levels of >400 mg/ dL from 2 weeks post-STZ injection over the entire period of analysis (Fig. 9a,  $p < 0.05$ , ANOVA). Mice injected with STZ neither lost weight nor gained any weight along the experiment, but the

citrate buffer-injected control mice gained weight during the period of analysis (Fig. 9b,  $p < 0.05$ , ANOVA). We studied the induced pain in STZ diabetic and control mice at basal state, as well as 12 and 22 weeks after STZ injection. Despite changes in behaviour reported in the past, which are related to the STZ model of diabetes type I (Rajashree *et al.*, 2011), it was relevant to evaluate the metabolic alterations and sensory anomalies in the same group of mice in order to find relevant relationships.

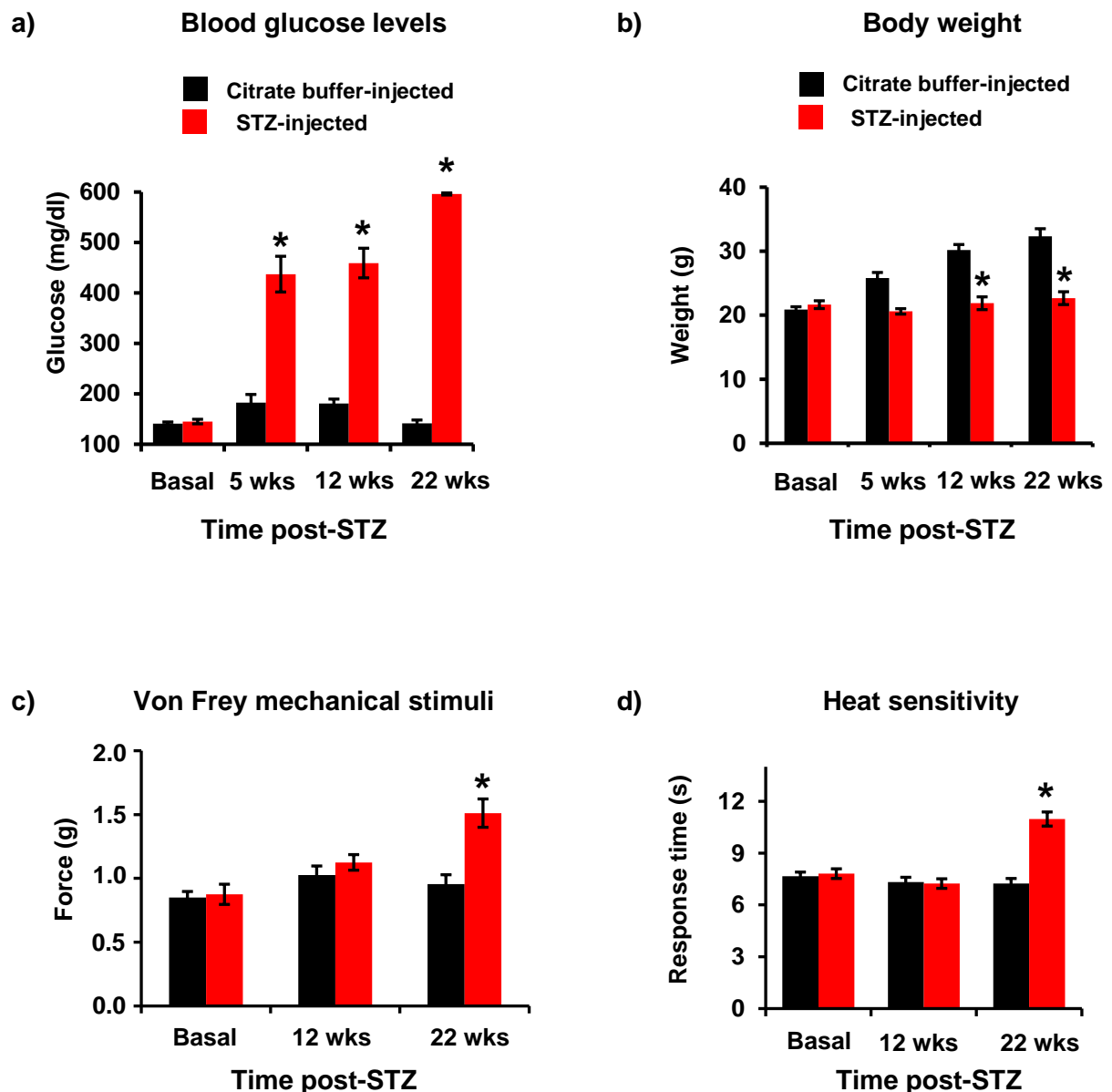


Figure 9. Behavioural recordings and development of DPN in diabetic C57BL6/j mice and age-matched control mice. a) Glucose levels in C57BL6/j mice post-STZ injection. b) Course of change in body weight post-STZ injection. Response thresholds to c) Von Frey mechanical stimuli and d) a heat ramp.  $n = 8$  mice per group. Data are represented as mean  $\pm$  S.E.M. \* $p < 0.05$  compared to baseline; # $p < 0.05$  compared to the control group two-way repeated measures ANOVA with Bonferroni multiple comparison test (Rangel Rojas *et al.*, 2019).

We chose the time points based on the rationale in order to focus on the onset and progression of DPN. In comparison to controls at 12 weeks post-STZ injection, the STZ-injected mice did not present alterations in response thresholds during the plantar application of von Frey filaments (Fig. 9c).

In the same manner, we did not observe any relevant difference in the Hargreaves test in withdrawal response between control mice and STZ injected mice at 12 weeks after STZ injection (Fig. 9d). However, 22 weeks post-STZ, we observed that diabetic mice showed mechanical and thermal hypoalgesia, confirming sensory loss (Fig. 9c, d,  $*p < 0.05$  two-way ANOVA). The control mice did not display any symptoms of neuropathy.

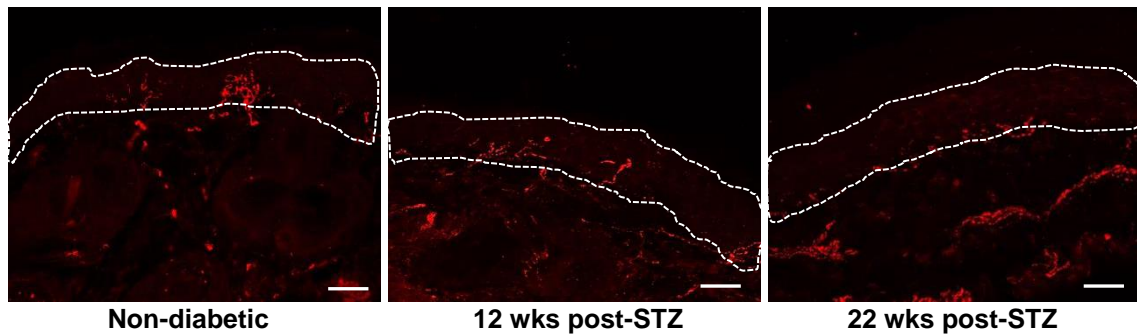
An important diagnostic tool to study the progression of DPN is the estimation of intra-epidermal nerve fibre density (IENFD) in skin biopsies (Yagihashi *et al.*, 2011). In order to correlate quantitative sensory testing with IENFD measurement, we performed immunostaining using Calcitonin Gene-Related Peptide (CGRP) (Fig.10a) or labelling with Protein Gene Product 9.5 (PGP 9.5) (Fig. 10b) on skin sections. We did not observe significant differences in IENFD at 12 weeks post-STZ, however, the IENFD was significantly reduced at 22 weeks post-STZ as compared to control mice (Fig. 10c,  $*p < 0.05$ , ANOVA).

### **3.1.2 Changes in amino acid levels during the onset and development of DPN**

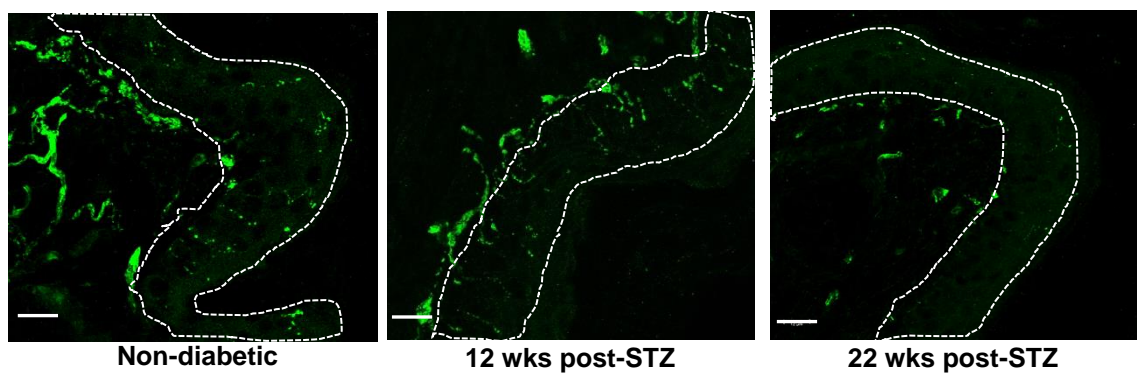
To identify the molecular signature of DPN progression in serum, we measured amino acid alterations in a longitudinal study involving early, middle and late time points. The levels of BCAA, ketogenic and glucogenic amino acids showed significant increase at 12 and 24 weeks post-STZ injection as compared to control mice (Fig. 11a, b, c  $*p < 0.05$ , repeated measures ANOVA). In STZ-injected mice, the level of leucine was almost three times higher as compared to the citrate buffer-injected control mice at 22 weeks. Diverse ketogenic and glucogenic amino acids remained invariable at 12 and 22 weeks in STZ-injected mice as compared to the control mice. For instance, glutamate (Glu), glutamine (Gln), methionine (Met), glycine (Gly), aspartate (Asp), phenylalanine (Phe) and threonine (Thr) were invariable at 12 and 22 weeks after-STZ injection, but serine (Ser), tyrosine (Tyr), asparagine (Asn), histidine (His), proline, (Pro) and alanine (Ala) (Fig. 11b, c,d,  $*p < 0.05$ , ANOVA) were found to be elevated in plasma at 12 weeks post-STZ. According to our results, it could be inferred that the plasma levels of BCAA and

ketogenic and gluconeogenic amino acids changed much earlier than manifestations of DPN symptoms.

**a) Immunostaining using  $\alpha$ -CGRP antibody**



**b) Immunostaining using  $\alpha$ -PGP 9.5 antibody**



**c) Quantification of IENFD**

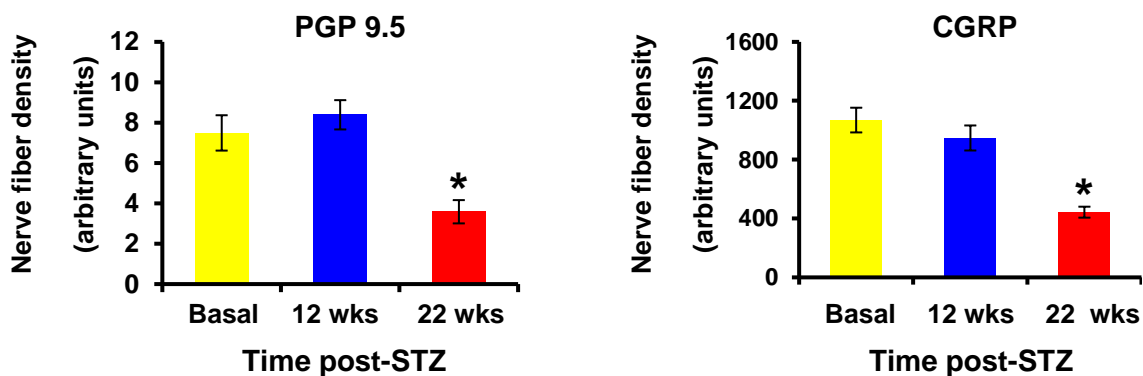


Figure 10. Morphological analysis of pathology associated with DPN in peripheral nerves of diabetic and age-matched control C57BL6/j mice. Intraepidermal nerve fibres of the paw skin were stained with (a) CGRP or (b) PGP 9.5. The dotted white lines represent the epidermal layer of the skin. Reduction in IENFD was quantified in c) STZ-injected and control mice.  $n = 8$  mice per group. Data are represented as mean  $\pm$  S.E.M. \* $p < 0.05$  compared to baseline; # $p < 0.05$  compared to the control group two-way repeated measures ANOVA with Bonferroni multiple comparison test. Scale bars represent 30  $\mu$ m (Rangel Rojas *et al.*, 2019).

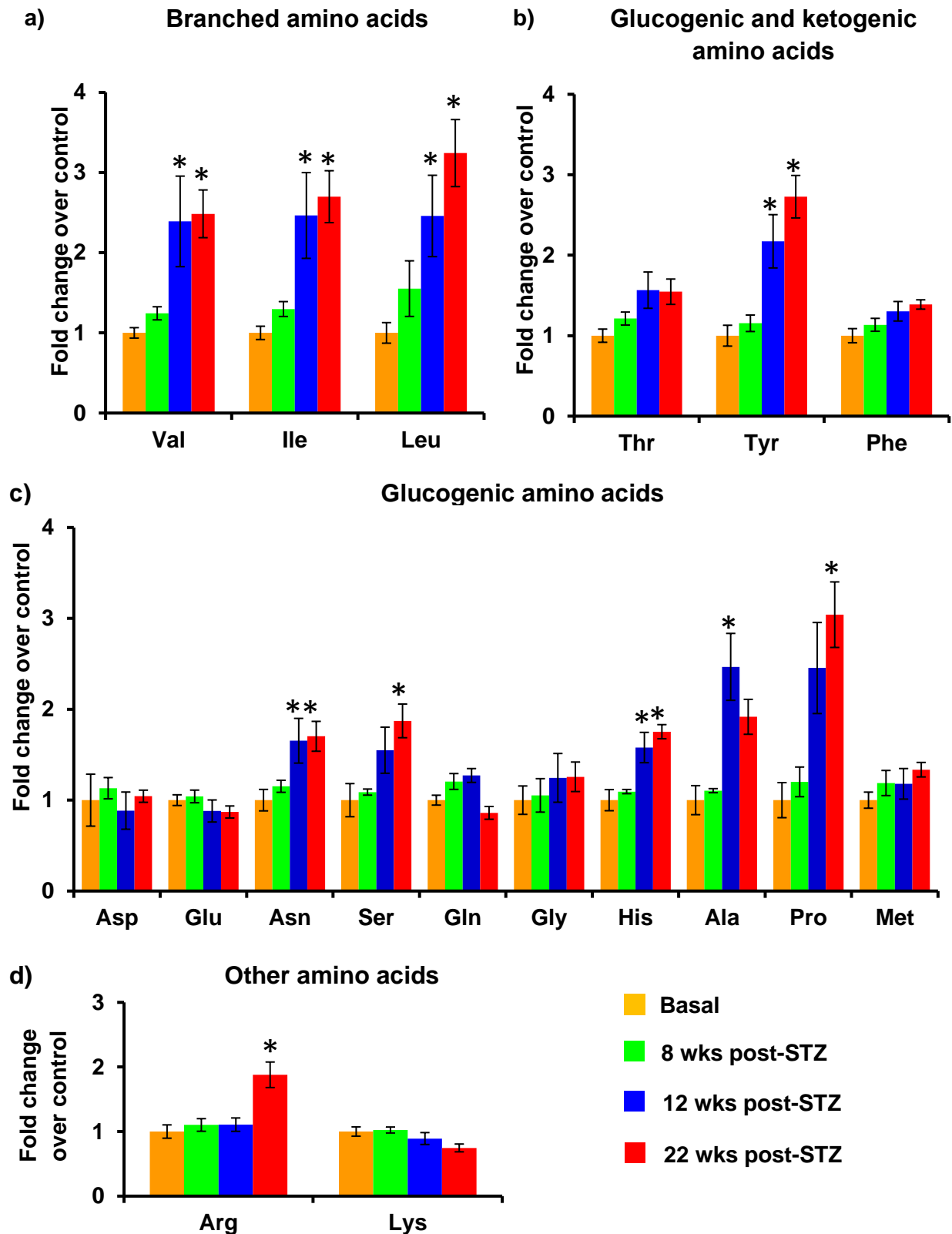


Figure 11. Analysis of amino acid levels in serum of diabetic and control C57BL6/j mice. a) Branched-chain amino acids. b) Glucogenic and ketogenic amino acids. c) Glucogenic amino acids. d) Levels of other amino acids at basal, 8, 12 and 22 wks after STZ and citrate buffer injection. Fold changes of amino acids were determined in relation to age-matched citrate injected controls.  $n = 5$  mice in each group. \* $p < 0.05$  compared to baseline; repeated measures ANOVA with Bonferroni multiple comparison tests (Rangel Rojas *et al.*, 2019).

### **3.1.3 Changes in TCA cycle intermediates, sorbitol and lactate in the sciatic nerve of diabetic mice**

We attempted to understand if glucose metabolic pathways show alterations prior to the onset of DPN symptom. Therefore, we carried out a targeted metabolomics screening based on LC/MS-MS. We aimed to determine the levels of glycolytic and TCA cycle intermediates in the sciatic nerve of mice at several time points, namely, basal (pre-STZ), 12 and 22 weeks post-STZ or citrate buffer-injection.

At 22 weeks post-STZ, the levels of ketoglutaric acid, fumaric acid, citric acid, malic acid and succinic acid were considerably decreased in the sciatic nerve in comparison to the control mice injected with citrate buffer (Fig. 12a,  $*p < 0.05$ , ANOVA). At 12 weeks post-STZ, we observed a decrease of some TCA metabolites, however, notable changes were found at 22 weeks post-STZ, which matched with nerve injury and loss of sensation. The gradual decrease in TCA metabolites induces a metabolic shift to alternative pathways in order to fulfil the energy requirements. At 12 and 22 weeks post-STZ, we also observed a gradual accumulation in the levels of sorbitol in the biopsies of the sciatic nerve as compared to controls (Fig. 12b,  $*p < 0.05$ , ANOVA).

The gradual augment in the concentration of sorbitol and the reduced kinetics of the TCA cycle in association with the extended diabetic state suggests that there is a switch in energy metabolism from the glycolytic pathway to the polyol pathway, which is related to tissue malfunction. In addition, at 22 weeks post-STZ injection, the levels of L-lactate in the sciatic nerve were also increased (Fig. 12c,  $*p < 0.05$ , ANOVA).

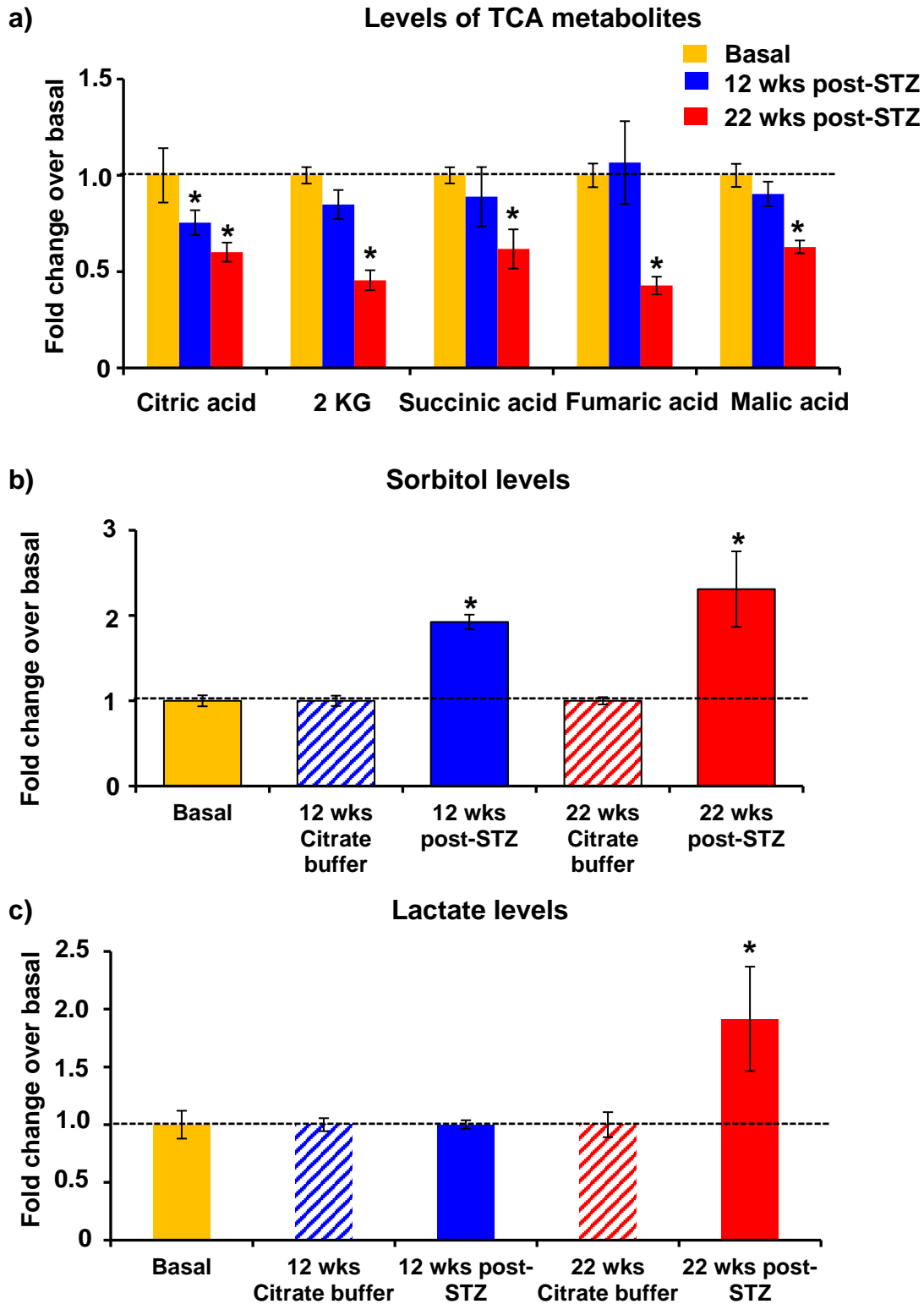


Figure 12. Levels of citric acid metabolites in the sciatic nerve of diabetic C57BL6/j mice based on a mass spectrometry analysis. a) Citric acid metabolites. b) Levels of sorbitol. c) Levels of L-lactate in sciatic nerve from diabetic and control mice at basal, 12 and 22 weeks post-STZ. Fold changes were determined in relation to citrate injected control mice. 2KG = ketoglutaric acid.  $n = 5$  mice in each group. \* $p < 0.05$  compared with baseline; repeated measures ANOVA with Bonferroni multiple comparison test (Rangel Rojas *et al.*, 2019).

The gradual augment in the concentration of sorbitol and the reduced kinetics of the TCA cycle in association with the extended diabetic state suggests that there is a switch in energy metabolism from the glycolytic pathway to the polyol pathway, which is related to tissue malfunction. In addition, at 22 weeks post-STZ injection, the levels of L-lactate in the sciatic nerve were also increased (Fig. 12c, \* $p < 0.05$ , ANOVA).

## 3.2 HIF1 $\alpha$ in Diabetic Neuropathy

### 3.2.1 Regulation of nociception by HIF1 $\alpha$ in the STZ diabetic model

Hyperglycaemia induces both mitochondrial dysfunction and the production of ROS, they have gained special attention as potential mechanisms of organ injury in diabetes (Vincent *et al.*, 2011).

Hypoxia, hyperglycaemia and ROS can activate the transcription factor HIF1 $\alpha$ , which suggests an important function in DPN sensitivity (Catrina *et al.*, 2004; Fiorentino *et al.*, 2013). In order to correlate the previously observed findings at the level of molecular pathways, we analysed the function of HIF1 $\alpha$  in the regulation of ROS levels in DRGs in diabetic and control mice. To study the possible function of HIF1 $\alpha$  in DPN, we generated a mouse line with conditional genetic loss of HIF1 $\alpha$  in a sensory neuron-specific manner (SNS-HIF1 $\alpha$ <sup>-/-</sup>). Employing *in situ* hybridization and using HIF1 $\alpha$ -specific riboprobes, we were able to confirm the Cre/loxP-mediated HIF1 $\alpha$  deletion selectively in small-diameter neurons of the DRG (red arrows, Fig. 13a), while HIF1 $\alpha$  was preserved in large-diameter neurons (blue arrows, Fig. 13a).

In order to investigate the role of HIF1 $\alpha$  in diabetes, we analysed this mouse line longitudinally over 6 months in the STZ model of type 1 diabetes (Agarwal *et al.*, 2004; Kanngiesser *et al.*, 2014). Both SNS-HIF1 $\alpha$ <sup>-/-</sup> and HIF1 $\alpha$ <sup>fl/fl</sup> mice showed similar blood glucose levels (Fig. 13b).

At 5 weeks after STZ, we found that SNS-HIF1 $\alpha$ <sup>-/-</sup> as well as HIF1 $\alpha$ <sup>fl/fl</sup> mice showed comparable levels of hypersensitivity in response to mechanical stimuli which comprised von Frey hairs applied to plantar surface of the hind paw. 40% response thresholds were calculated (Fig 14 a,b). However, we observed strong hypoalgesia in mutant mice at 13 and 24 weeks post-STZ in response to von Frey stimuli (Fig. 14a).

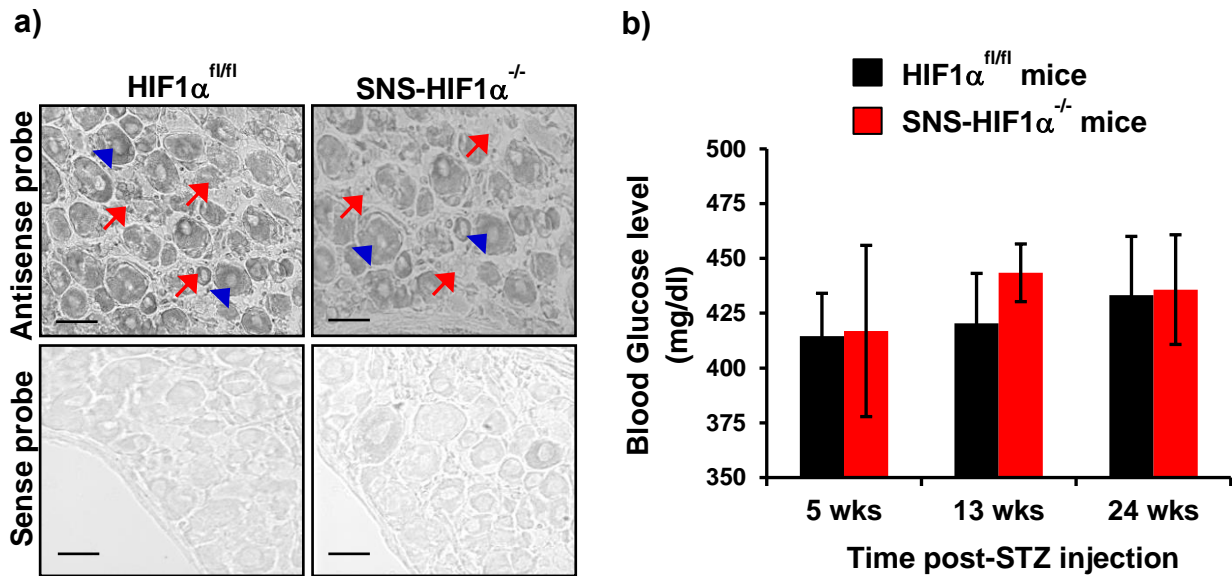


Figure 13. Analysis of hyperglycaemia in diabetic SNS-HIF1 $\alpha^{-/-}$  mice for 6 months. A) *In situ* hybridisation in DRG tissue of SNS-HIF1 $\alpha^{-/-}$  and HIF1 $\alpha^{fl/fl}$  mice using antisense or control probe. The blue arrowheads indicate large-diameter neurons where recombination did not occur; the red arrows indicate small-diameter neurons where HIF1 $\alpha$  is expressed in HIF1 $\alpha^{fl/fl}$  mice but deleted in SNS-HIF1 $\alpha^{-/-}$  mice. b) Glucose levels in SNS-HIF1 $\alpha^{-/-}$  and HIF1 $\alpha^{fl/fl}$  mice post-STZ.  $N = 10$  mice per group, data are represented as mean  $\pm$  SEM. Scale bar represents 30  $\mu$ m (Rangel Rojas *et al.*, 2018).

At 5 weeks post-STZ, SNS-HIF1 $\alpha^{-/-}$  and HIF1 $\alpha^{fl/fl}$  mice presented comparable levels of hyperalgesia to thermal stimuli, which was observed as a reduction in time response to an infrared heat lamp applied to the hind paw surface (Fig. 14a, b). However, at 13 and 24 weeks post-STZ, we observed that mutant mice became hypoalgesic as compared to control mice (Fig. 14b,  $*p < 0.05$ ,  $***p < 0.0001$ ,  $\#p < 0.01$ , ANOVA, Bonferroni's test). Furthermore, mice injected with citrate buffer did not show differences in behaviour (Fig. 14c). We did not observe any significant differences in thermal sensitivity in control mice injected with citrate buffer (Fig. 14d).

These results demonstrate that SNS-HIF1 $\alpha^{-/-}$  mice presented a faster onset of hypoalgesia as compared to control mice, indicating that they have in sensory neurons a stronger sensory loss compared to control mice. These findings show that HIF1 $\alpha$  is one of the key molecules involved in onset and progression of DPN.

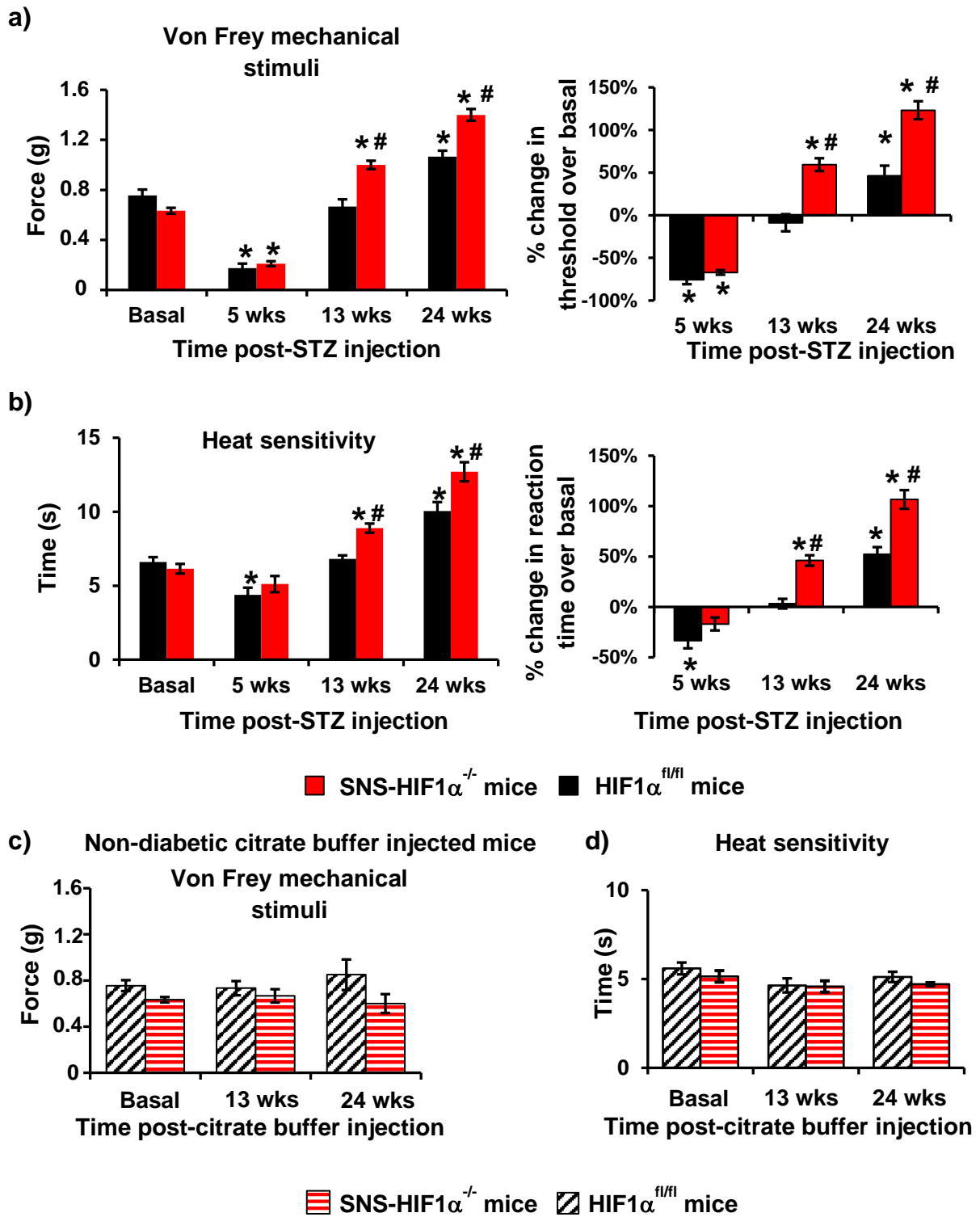


Figure 14. Analysis of sensory loss in diabetic SNS-HIF1 $\alpha^{-/-}$  and HIF1 $\alpha^{fl/fl}$  mice. a) Response thresholds to mechanical stimuli; the right panel represents the percent change in threshold from basal. b) Heat ramp at basal, 5, 13 and 24 weeks post-STZ in SNS-HIF1 $\alpha^{-/-}$  or HIF1 $\alpha^{fl/fl}$  mice. Response threshold to c) mechanical stimuli and d) thermal latency of non-diabetic SNS-HIF1 $\alpha^{-/-}$  or HIF1 $\alpha^{fl/fl}$  mice at basal, 13 and 24 weeks after citrate buffer injection.  $n = 10$  mice. 40% response thresholds were calculated. Data are represented as mean  $\pm$  SEM. \* $p < 0.05$  compared to baseline, # $p < 0.05$  compared to the control group; two-way repeated measures ANOVA with Bonferroni multiple comparisons test (Rangel Rojas *et al.*, 2018).

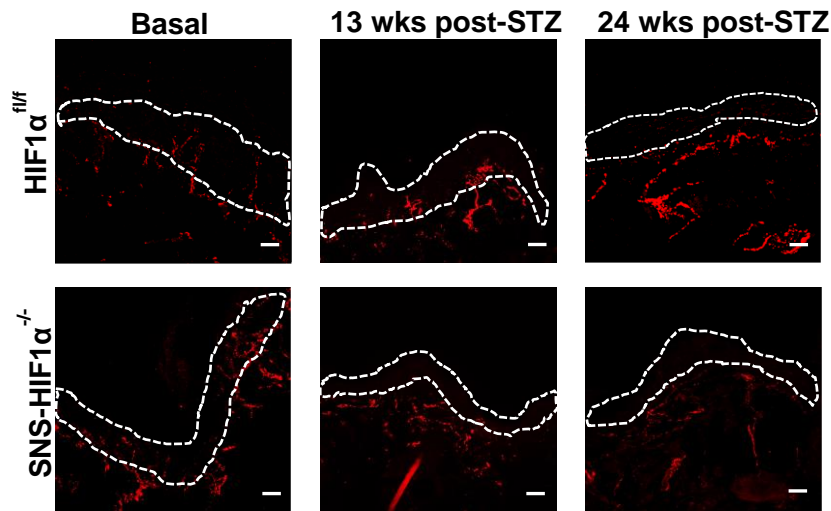
### 3.2.2 SNS-HIF1 $\alpha$ <sup>-/-</sup> mice develop DPN post-STZ treatment

We performed immunostaining for CGRP and PGP 9.5 on plantar skin sections, an analysis up to 24 weeks post-STZ. We have analysed the reduction in the density of epidermal innervation by measuring the intensity of PGP 9.5 and CGRP-positive fibres in the epidermal region of the paw skin. At 13 and 24 weeks after STZ injection, the loss of CGRP and PGP 9.5 immunoreactivity in the epidermis was higher in SNS-HIF1 $\alpha$ <sup>-/-</sup> mice as compared to HIF1 $\alpha$ <sup>fl/fl</sup> mice (Fig. 15a, d, b, e \* $p$  < 0.0001, # $p$  < 0.01, ANOVA, Bonferroni's test), which reveals an exacerbation of DPN manifestations upon HIF1 $\alpha$  deletion in sensory neurons.

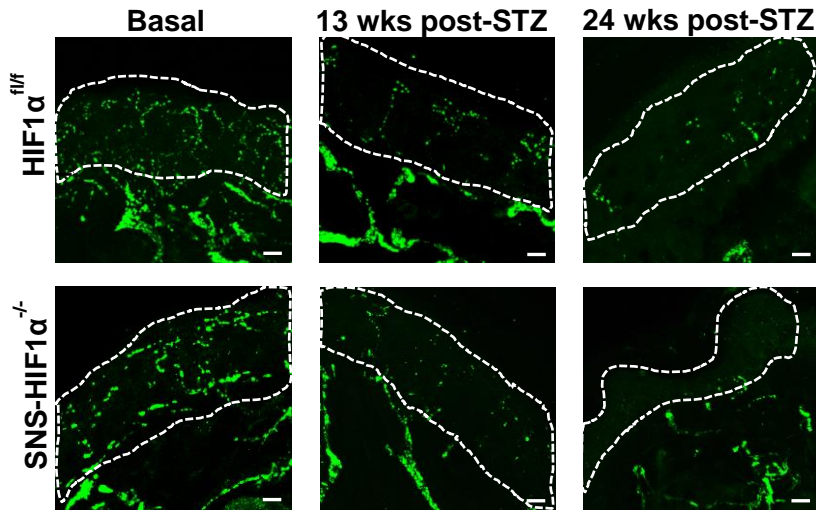
### 3.2.3 HIF1 $\alpha$ regulates ROS levels in DRGs of diabetic mice

Several studies demonstrate that ROS modulates HIF1 function (Salceda and Caro, 1997; Hirota and Semenza, 2001; Catrina *et al.*, 2004; Bullock *et al.*, 2009). However, no one has focused on the effect of HIF1 function on the regulation of ROS levels. We therefore investigated the impact of HIF1 $\alpha$  activation on ROS via measuring the levels of ROS *in vivo* in DRG neurons of SNS-HIF1 $\alpha$ <sup>-/-</sup> and control HIF1 $\alpha$ <sup>fl/fl</sup> mice at basal, 13 and 24 weeks post-STZ injection. For this, we have intrathecally injected MitoTracker Red CM-H<sub>2</sub>XROS (100 nm, 10  $\mu$ L), an indicator for ROS generation (Cottet-Rouselle *et al.*, 2011). MitoTracker Red CM-H<sub>2</sub>XROS is a dye originally found in reduced form, which passively diffuses across the plasma membrane and accumulates in the mitochondria, where it reacts with thiol groups on peptides and proteins to form a fluorescent aldehyde fixable conjugate. We found that STZ-induced DPN was associated with a remarkable increase in Mito Tracker Red CM-H<sub>2</sub>XROS fluorescence in DRG neurons, indicating the formation of ROS and superoxide (Fig. 16a, b \*, # $p$  < 0.0001, ANOVA, Bonferroni's test). Furthermore, at 13 and 24 weeks post-STZ injection, the accumulation of ROS and superoxide was considerably higher in SNS-HIF1 $\alpha$ <sup>-/-</sup> mice compared to HIF1 $\alpha$ <sup>fl/fl</sup> mice (Fig. 16a, b). In order to confirm these findings, we determined the levels of H<sub>2</sub>O<sub>2</sub> in the DRG neurons and sciatic nerve of SNS-HIF1 $\alpha$ <sup>-/-</sup> and control HIF1 $\alpha$ <sup>fl/fl</sup> mice at basal and 24 weeks post-STZ injection. We found that at 24 weeks post-STZ, the levels of H<sub>2</sub>O<sub>2</sub> were notably increased in DRG and sciatic nerve tissue of SNS-HIF1 $\alpha$ <sup>-/-</sup> in comparison to control HIF1 $\alpha$ <sup>fl/fl</sup> mice (Fig. 16c, \*, # $p$  < 0.01, ANOVA, Bonferroni's test).

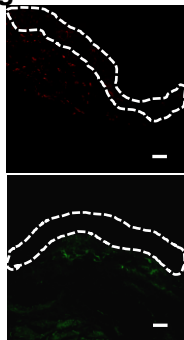
a) Immunostaining using  $\alpha$ -CGRP antibody



b) Immunostaining using  $\alpha$ -PGP 9.5 antibody

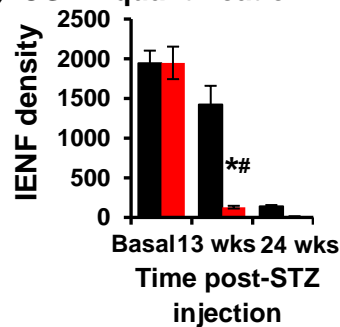


c) IgG control CGRP

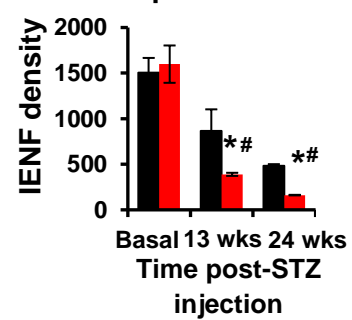


IgG control PGP9.5

d) CGRP quantification



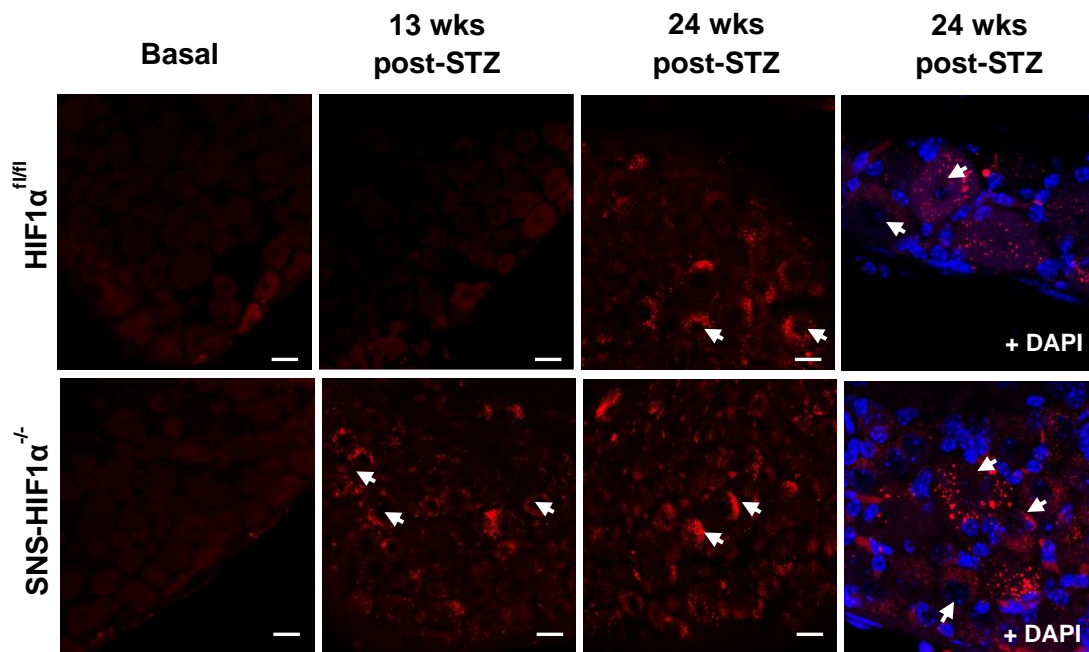
e) PGP 9.5 quantification



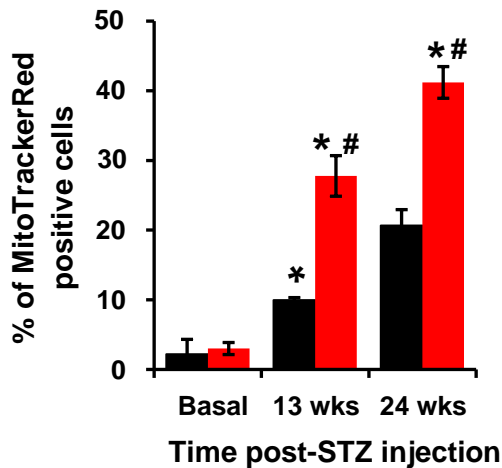
■ SNS-HIF1 $\alpha^{-/-}$  mice ■ HIF1 $\alpha^{fl/fl}$  mice

Figure 15. Morphological analysis of pathology associated with DPN in peripheral nerves of HIF1 $\alpha^{fl/fl}$  and SNS-HIF1 $\alpha^{-/-}$  mice. Intraepidermal nerve fibres of the paw skin were immunostained with a) CGRP and b) PGP 9.5 at basal and post-STZ injection. The dotted white lines indicate the epidermal layer of the skin. c) IgG control for CGRP and PGP 9.5 staining. Quantification of IENFD post-STZ for d) CGRP and e) PGP 9.5.  $n = 6-8$  mice. Data are represented as mean  $\pm$  SEM. \* $p < 0.05$  compared to baseline, # $p < 0.05$  compared to the control group; two-way repeated measures ANOVA with Bonferroni multiple comparisons test. Scale bar represents 30  $\mu$ m (Rangel *et al.*, 2018).

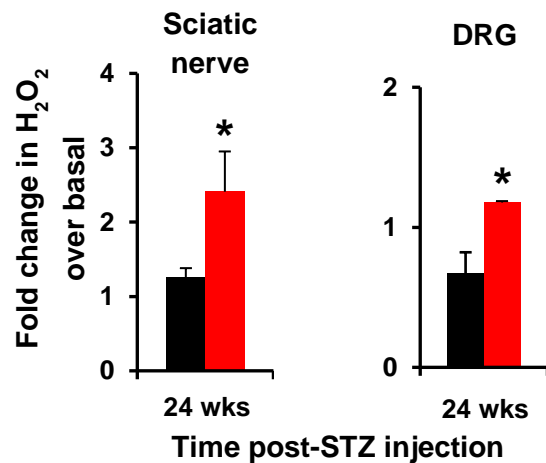
a) Measurement of ROS in DRG using MitoTrackerRedCM-H<sub>2</sub>XROS



b) Quantification of ROS in DRG



c) H<sub>2</sub>O<sub>2</sub> levels in 24 wks diabetic tissue



■ SNS-HIF1 $\alpha^{-/-}$  mice ■ HIF1 $\alpha^{fl/fl}$  mice

Figure 16. Analysis of ROS quantification in peripheral neurons during the progression of DPN in mice. a) MitoTracker Red staining and b) analysis in DRGs of diabetic SNS-HIF1 $\alpha^{-/-}$  and HIF1 $\alpha^{fl/fl}$  mice. White arrows hint at ROS-positive neurons;  $n = 6$  DRGs per group. c) Quantification of H<sub>2</sub>O<sub>2</sub> levels in DRG and sciatic nerve tissue in SNS-HIF1 $\alpha^{-/-}$  and HIF1 $\alpha^{fl/fl}$  at 24 weeks post-STZ. Data are represented as mean  $\pm$  SEM. \* $p < 0.05$  compared to baseline, # $p < 0.05$  compared to the control group; two-way repeated measures ANOVA with Bonferroni multiple comparisons test (Rangel Rojas *et al.*, 2018).

This evidenced that upon deletion of HIF1 $\alpha$ , ROS and superoxide accumulate in the sciatic nerve and DRG tissue. It is known that high levels of H<sub>2</sub>O<sub>2</sub> can modulate diverse signalling cascades, affecting genomic stability, cellular function and eventually resulting in cell death (Gough and Cotter, 2011).

Furthermore, peripheral nerve dysfunction has been associated with the regulation of cGMP-dependent protein kinase PKG1 and PKG2. Oxidative cysteine modification is mediated by ROS, which produces the dimerization and auto-activation of PKG1 $\alpha$  that is essential for the regulation of actin and myosin and the recovery of peripheral neurons after injury. For this reason, we studied the effect of ROS and superoxide levels on the dimerization of PKG1 $\alpha$ . We found comparable levels of PKG1 $\alpha$  in dimeric and monomeric form, in the sciatic nerve of SNS-HIF1 $\alpha$ <sup>-/-</sup> and control HIF1 $\alpha$ <sup>fl/fl</sup> at basal conditions. However, at 24 weeks post-STZ, SNS-HIF1 $\alpha$ <sup>-/-</sup> presented higher levels of dimerised PKG1 $\alpha$  compared to control HIF1 $\alpha$ <sup>fl/fl</sup> (Fig. 17a, b \*, #*p* < 0.01, ANOVA, Bonferroni's test).

**a) PKG1 $\alpha$  dimerization in diabetic mice    b) Quantification of dimerized PKG1 $\alpha$**

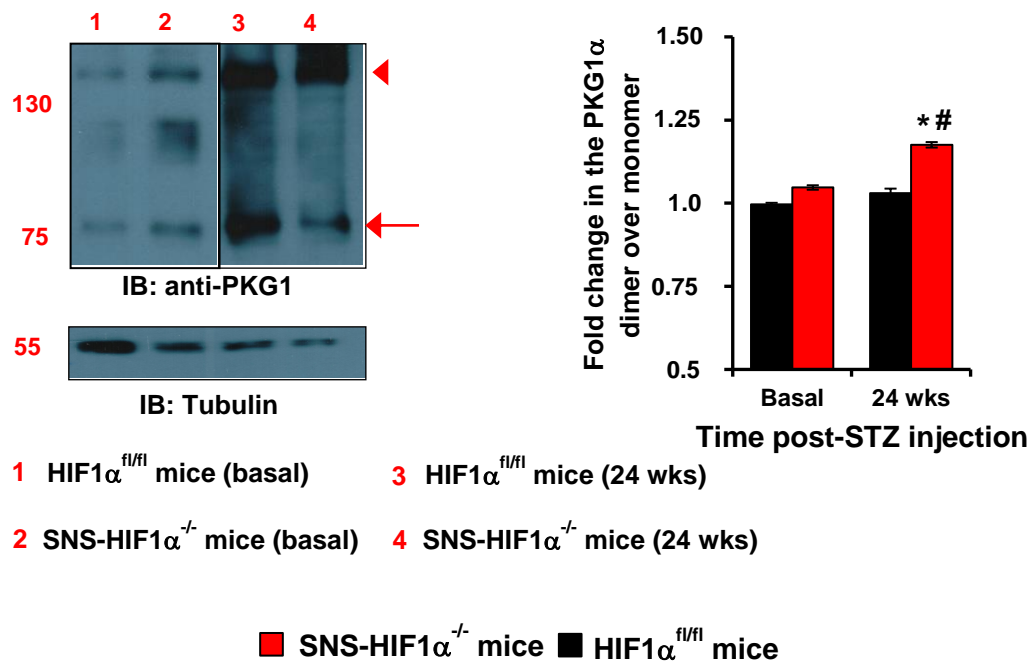


Figure 17. Analysis of PKG1 $\alpha$  expression in peripheral neurons during the progression of DPN in mice. a) PKG1 $\alpha$  expression in SNS-HIF1 $\alpha$ <sup>-/-</sup> and HIF1 $\alpha$ <sup>fl/fl</sup> at basal and 24 weeks post-STZ, analysed by western blot. b) Measurement of dimerised PKG1 $\alpha$  over monomeric PKG1 $\alpha$  at basal and 24 weeks post-STZ. Input amounts were normalized to tubulin. *n* = 4 mice. \**p* < 0.05 compared to baseline, #*p* < 0.05 compared to the control group; two-way ANOVA for repeated measurements with Bonferroni multiple comparison test (Rangel Rojas *et al.*, 2018).

Therefore, the selective deletion of HIF1 $\alpha$  led to elevated levels of ROS generation in peripheral sensory neurons at time points that spatially coincided with the aggravation of DPN in SNS-HIF1 $\alpha$ <sup>-/-</sup> mice.

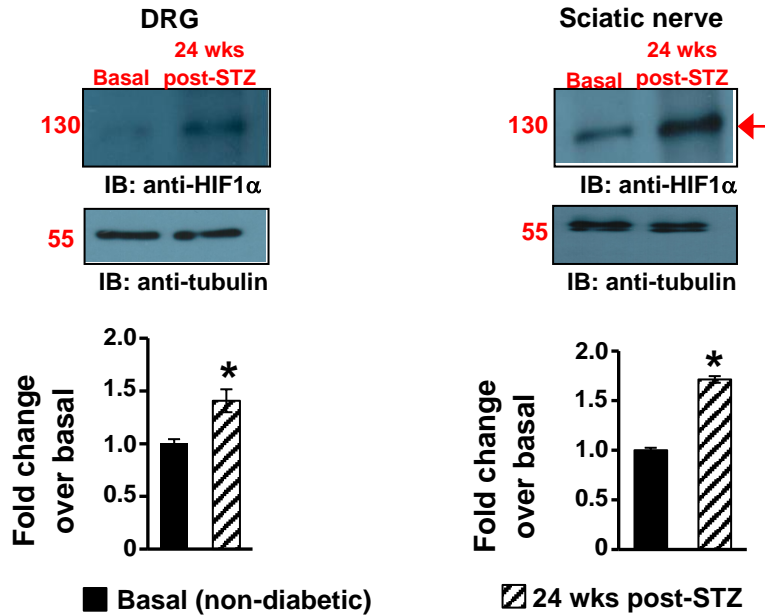
### **3.2.4 Regulation of HIF1 $\alpha$ and its downstream target genes under DPN**

Even though stabilisation of HIF1 $\alpha$  under low oxygen tension has previously been studied, the mechanisms responsible for the effect of hyperglycaemia on the regulation of HIF1 $\alpha$  are not fully known. Therefore, we attempted to investigate the impact of hyperglycaemia on the levels of HIF1 $\alpha$  in the sciatic nerve and DRGs neurons of SNS-HIF1 $\alpha$ <sup>-/-</sup> and control HIF1 $\alpha$ <sup>fl/fl</sup> mice at basal state and 24 weeks after STZ. We found that during prolonged hyperglycaemia, the HIF1 $\alpha$  levels also increased (Fig. 18a, \*, # $p < 0.01$ , ANOVA, Bonferroni's test).

From this, we could infer that hyperglycaemia induces the stabilisation and activation of signalling and the modulation of its downstream targets. To better comprehend the effect of HIF1 $\alpha$  activation on DPN, we analysed the levels of VEGF, one of the downstream targets of the transcriptional activity of HIF1 $\alpha$  (Dengler *et al.*, 2014).

At the basal state, we found that upon the deletion of HIF1 $\alpha$ , the expression of VEGF is reduced in SNS-HIF1 $\alpha$ <sup>-/-</sup> mice. At 24 weeks post-STZ, the levels of VEGF were substantially increased in control HIF1 $\alpha$ <sup>fl/fl</sup> mice, though in DRGs neurons of SNS-HIF1 $\alpha$ <sup>-/-</sup> mice, VEGF was diminished (Fig. 18b, \*, # $p < 0.01$ , ANOVA, Bonferroni's test), which indicates a reduction of VEGF expression upon deletion of HIF1 $\alpha$  in sensory neurons.

a) HIF1 $\alpha$  regulation in diabetes



b) VEGF expression in diabetes (sciatic nerve)

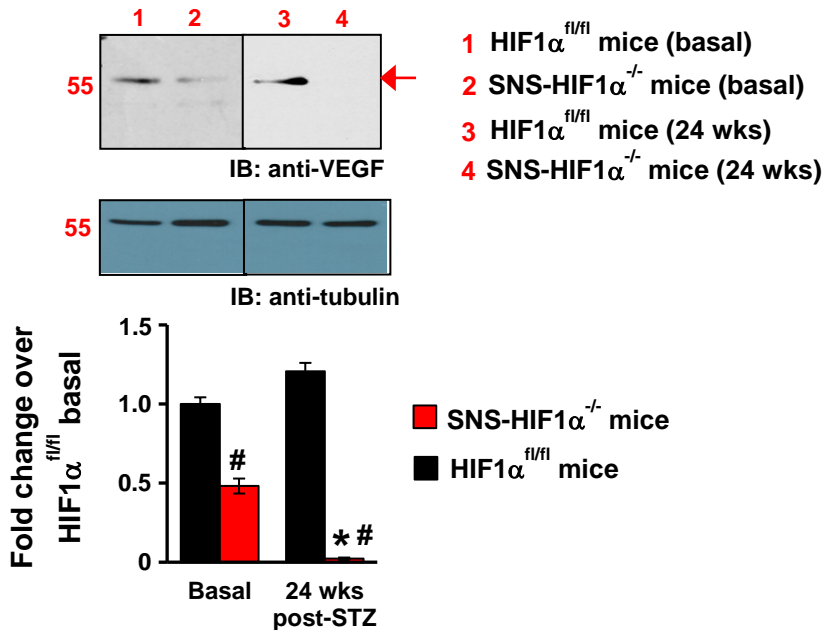


Figure 18. Analysis of HIF1 $\alpha$  and VEGF expression in peripheral neurons during the progression of DPN in mice. a) HIF1 $\alpha$  expression in sciatic nerve and DRG tissue of C57BL6/j mice at basal and 24 weeks post-STZ analysed by western blot;  $n = 4$  mice. b) VEGF expression in HIF1 $\alpha^{fl/fl}$  and SNS-HIF1 $\alpha^{-/-}$  mice at basal and 24 weeks post-STZ analysed by western blot. Lower panel indicates the quantification of VEGF over basal VEGF expression in HIF1 $\alpha^{fl/fl}$  mice. Input amounts were normalised to tubulin.  $n = 4$  mice. \* $p < 0.05$  compared to baseline, # $p < 0.05$  compared to the control group; two-way ANOVA for repeated measurements with Bonferroni multiple comparison test (Rangel Rojas *et al.*, 2018).

### 3.3 Sumoylation in protein activity regulation in diabetic neuropathy

#### 3.3.1 Analysis of periaxin as a potential target of sumoylation

Many molecular changes occur during the unbalance of the redox homeostasis, which is accompanied by a variety of posttranslational protein modifications (Stadtman, 2001; Cai and Yan, 2013). These posttranslational modifications include phosphorylation, ubiquitination, nitrosylation and sumoylation (Cereghetti *et al.*, 2008; Cho *et al.*, 2009; Han *et al.*, 2008; Wasiak *et al.*, 2007). Despite the fact that sumoylation exerts an important regulatory function, which has been well described for nuclear proteins (including transcription factors), cytosolic and membrane proteins (Hayashi *et al.*, 2006; Janssen *et al.*, 2006), the role of sumoylation in late complications of diabetes still remains to be determined.

For identification of the potentially sumoylated proteins in DRGs of mice, a mass spectrometry-based screening was performed. For this, DRGs from diabetic (5 wks) and non-diabetic mice were extracted and lysed. The pool of sumoylated proteins was immunoprecipitated using an anti-SUMO1 antibody and the eluted proteins were analysed using LC-MS/MS (Agarwal *et al.*, *Neuron* in press). The screening identified more than 180 proteins modified by sumoylation, periaxin occurred with very high probability. In order to examine if the sumoylation of periaxin takes place *in vivo*, we extracted dorsal root ganglion (DRG) and sciatic nerve (SN) tissue from C57BL6 mice. Kidney tissue was used as a control organ which does not express periaxin. We lysed the tissue and immunoblotted with anti-periaxin antibody. Our immunoblotting analyses revealed the presence of periaxin in DRG and sciatic nerve tissue, but not in kidney (Fig. 19a, b).

To further confirm the sumoylation of periaxin, we performed immunoprecipitation studies using either anti-SUMO1 or anti-periaxin. The precipitated proteins were immunoblotted with anti-periaxin. The sumoylated periaxin was detected in sciatic nerve, but not in kidney tissue (Fig. 19c, d). The theoretical molecular weight of periaxin is 148 kDa (O55103, Uniprot) and the expected molecular weight of a single sumoylated periaxin is at least ~165 kDa. We observed a band of ~180-200 kDa in our blots, indicating that periaxin possesses multiple sumoylation lysine residues. Altogether, our immunoblotting analyses revealed that periaxin is sumoylated *in vivo*.

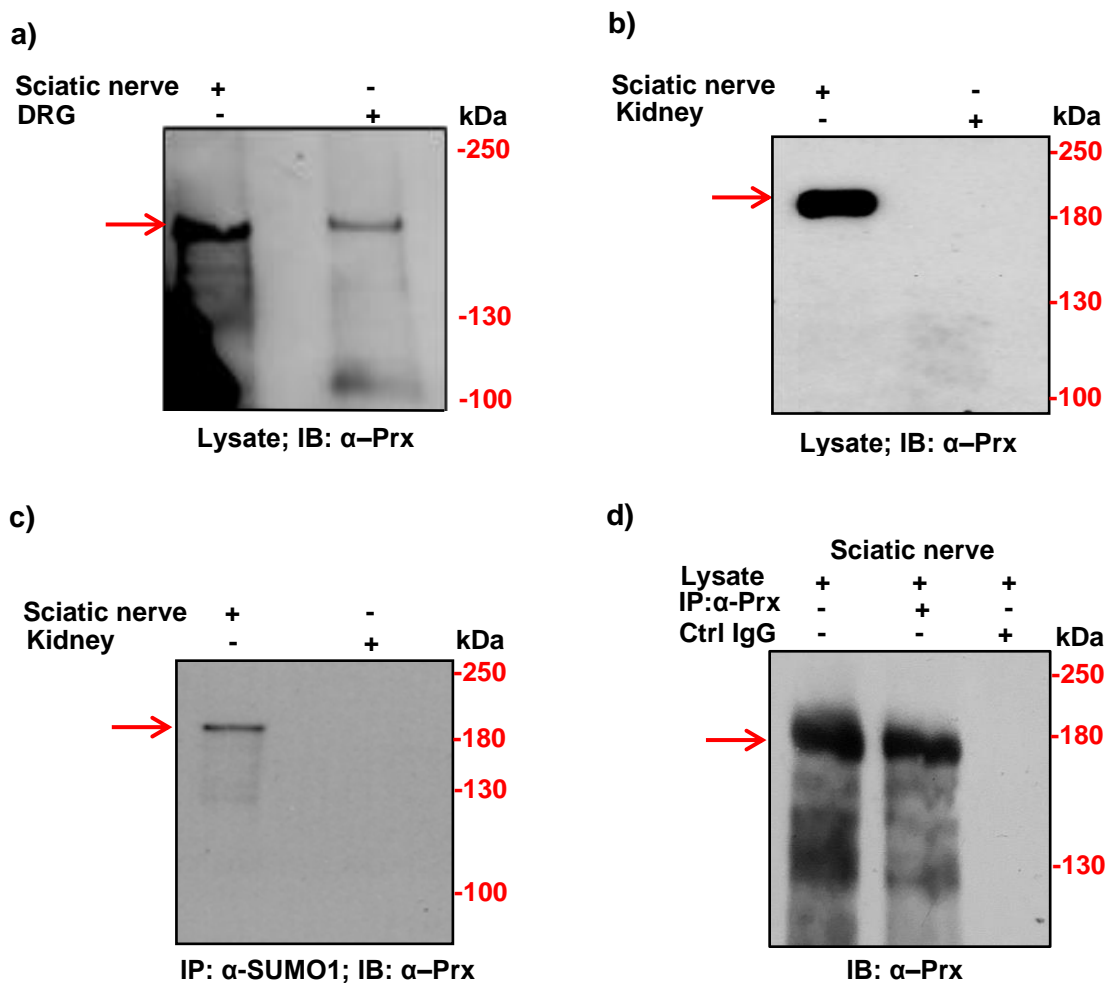


Figure 19. Sumoylation of periaxin *in vivo*. a) Lysates from the sciatic nerve and DRG tissue were immunoblotted with anti-periaxin antibody. b) Lysates from the sciatic nerve and kidney tissue (negative control) immunoblotted with anti-periaxin. c) Immunoprecipitated from the sciatic nerve and kidney tissue using anti-SUMO1 antibody and immunoblotted with anti-periaxin. d) Lysate, immunoprecipitated with anti-periaxin and IgG control from sciatic nerve tissue and immunoblotted with anti-periaxin. Arrow indicates sumoylated periaxin. DRG : dorsal root ganglia, IB : immunoblot, Ig : immunoglobulin, IP : immunoprecipitation, Prx : periaxin.

### 3.3.2 Analysis of Periaxin sumoylation *in vitro*

To further investigate the modification of periaxin by sumoylation, we expressed a C-terminal GFP-tagged mouse periaxin protein in HEK cells. Cells with a transfection efficiency of 80% or more were used for all experiments. We purified periaxin by immunoprecipitation using GFP-trap beads and immunoblotted with the anti-SUMO1 antibody.

The expected molecular weight of periaxin protein with the GFP tag is 175 kDa (O55103, P42212, Uniprot). However, we detected one protein band with a molecular weight around 210-230 kDa in the sample from Prx-transfected HEK cells,

but not in the plasmid control transfection sample, which corresponds to sumoylated periaxin protein (Fig. 20a). To further validate, we immunoprecipitated all sumoylated proteins using anti-SUMO1 antibody and detected the presence of periaxin via immunoblotting. As before, we observed a protein band with a molecular weight of approximately 220 kDa in the periaxin-transfected cells, but not in the samples from plasmid control (negative control; Fig. 20b).

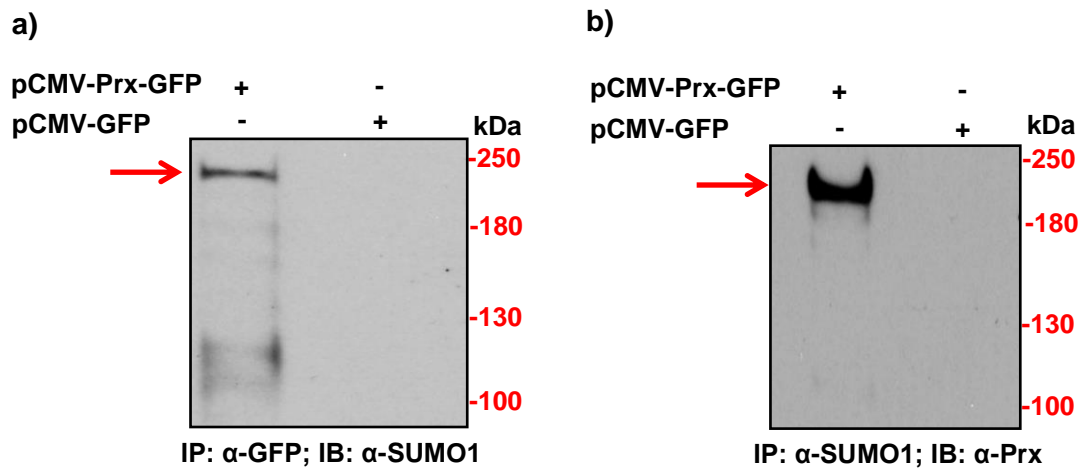


Figure 20. Sumoylation of periaxin in transfected HEK cells: a) Immunoprecipitation using anti-GFP and immunoblotted with anti-SUMO1. b) Immunoprecipitation using anti-SUMO1 and immunoblotted with anti-periaxin. Arrow indicates sumoylated periaxin. GFP : green fluorescent protein, IB : immunoblot, IP : immunoprecipitation, Prx : periaxin.

### 3.3.3 Co-transfection of HEK cells with periaxin and SENP-1

To further confirm the sumoylation of periaxin, we co-transfected HEK cells with plasmids encoding periaxin and Sentrin-specific protease 1 (SENP-1). SENP-1 is a cysteine isopeptidase, which possesses cleaving activity of SUMO1 from target proteins (Yu *et al.*, 2010). After co-transfection, we lysed HEK cells with buffer containing 0.1% SDS to promote the activity of the isopeptidase and immunoblotted using anti-periaxin antibody. We detected a protein band with a size ~220 kDa in the sample transfected with periaxin alone (Fig. 21). However, after co-transfection with SENP1, a protein band of lower molecular weight (~200 kDa) appeared (Fig. 21, lane Prx + SENP1), which could be due to partial desumoylation.

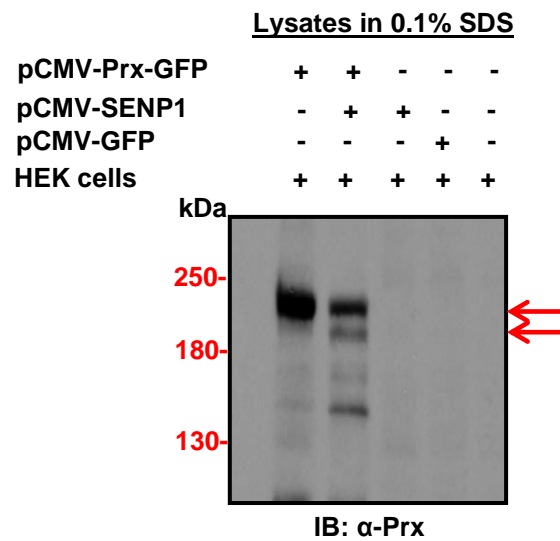


Figure 21. HEK cells transfected with Periaxin, SENP1 or GFP were lysed with buffer containing 0.1% SDS and immunoblotted by the anti-periaxin antibody. Red arrows indicate sumoylated periaxin. GFP : green fluorescent protein, IB : immunoblot, Prx : periaxin, SENP1 : sentrin-specific protease 1.

This indicates that periaxin is modified at multiple lysine residues by sumoylation. In the control samples included (Fig. 21, lanes SENP1, GFP, HEK cells), we did not detect any protein bands using the anti-periaxin antibody.

To further confirm that periaxin is modified by sumoylation, we transfected HEK cells with GFP-tagged periaxin and lysed with buffer containing 0.1% SDS and 1% SDS (denaturing condition). Proteins were precipitated using the anti-GFP antibody and immunoblotted by the anti-periaxin antibody. We detected a protein band with a size of approximately 220 kDa (Fig. 22).

However, after lysis with 0.1% SDS, we observed a reduction in molecular size of the band and the presence of two additional bands, which corresponds to partially desumoylated and non-sumoylated forms of periaxin (Fig. 22, lane 2). These findings confirm that periaxin is modified by sumoylation at multiple lysine residues.

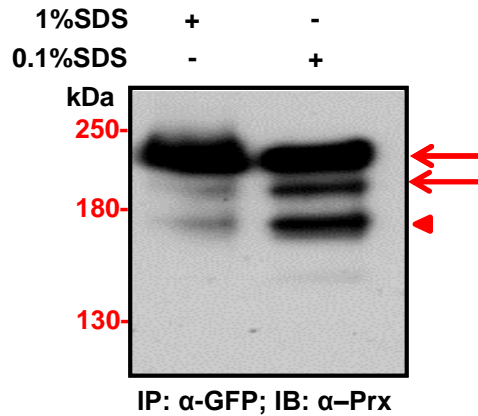


Figure 22. Western blot of HEK cells transfected with GFP-tagged periaxin: Cells were lysed and proteins were immunoprecipitated using anti-GFP antibody. The precipitated proteins were immunoblotted with anti-periaxin. Arrow indicates sumoylated periaxin and arrowhead indicates desumoylated periaxin. GFP : green fluorescent protein, IB : immunoblot, Prx : periaxin.

### 3.3.4 Site-directed mutagenesis of periaxin

We attempted to identify the target lysine residues that can be modified by sumoylation. We used SUMOSP 2.0 software to predict potential sumoylation sites in the periaxin protein. The software predicted the lysine residues K76, K171, K218, K893 and K1174 as potential sumoylation targets. Using site-directed mutagenesis, we introduced point mutations at the predicted lysine residues, which were mutated to alanine. The constructs were verified by DNA sequencing for the insertion of desired mutations. The verified constructs were transfected in HEK cells for expression and purification of mutant periaxin proteins and identification of the potential sumoylation sites. The transfected HEK cells were lysed and periaxin protein was immunoprecipitated using an anti-periaxin antibody. In the lysates of cells transfected with mutant-Prx, we observed two specific protein bands for periaxin, but not in the lysate of plasmid control and HEK cells alone. These bands corresponded to sumoylated forms of periaxin (red arrows, Fig. 23a).

Furthermore, to confirm the sumoylation of periaxin, we immunoprecipitated periaxin protein from transfected HEK cells using the anti-periaxin antibody and immunoblotted using the anti-SUMO1 antibody. We observed one protein band in the lanes of mutant periaxin with a molecular weight of ~221-230 kDa, but not in controls, indicating that mutation of individual lysines had no effect on the molecular size of the band (Fig. 23b). It suggests that there is no single lysine for sumoylation.

Although we could not identify the target lysines in the periaxin protein, it leads to a possibility that there are multiple lysine residues involved in modification by SUMO1.

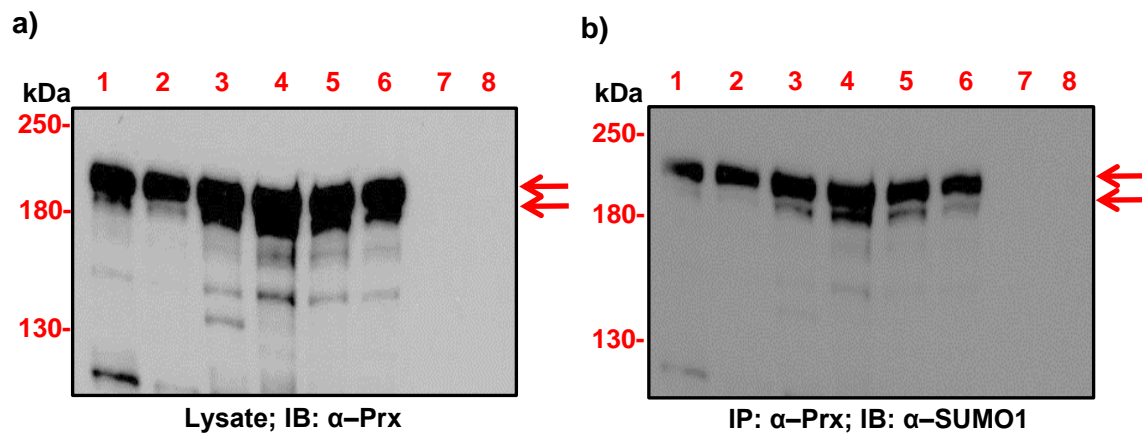


Figure 23. Identification of potential sumoylation sites in periaxin. a) Immunoblotting using anti-periaxin on lysates of wt periaxin or mutants. b) Immunoprecipitates of either wt or mutant periaxin proteins followed by immunoblotting using anti-SUMO1 antibody. **1** = Prx, **2** = K76A, **3** = K171A, **4** = K218A, **5** = K893A, **6** = K1174A, **7** = pEGFP, **8** = Hek. Arrows indicate sumoylated periaxin.

To further investigate the possibility of multiple sumoylation sites in predicted lysines, we generated constructs containing either two or three or all five predicted lysines and mutated them to arginine. The transfected HEK cells were lysed and immunoblotted with an anti-periaxin antibody. In the lysates from HEK cells transfected with periaxin mutants, we observed specific bands for periaxin, but not in the lysates from control-transfected HEK cells (Fig. 24a).

To identify the possible lysine residues as the target of sumoylation, we immunoprecipitated either wild type periaxin or different mutated periaxin using GFP-trap beads. The immunoprecipitated proteins were immunoblotted with SUMO1-antibody (Fig. 24b). We observed a protein band in the lane of periaxin wild type (Prx-WT) with a molecular weight of ~220 kDa (Fig. 24b, lane4), indicating that periaxin had been modified by sumoylation. However, we observed a band of lower molecular weight in the mutant constructs containing either two mutations or more (K893R-K1174R, Fig. 24b, lane2), indicating that periaxin had been partially desumoylated, but sumoylation is not completely abolished by mutating the predicted lysines. We expected that after mutating all five lysines (K76R-K171R-K218R-K893R-K1174R, lane 1), the protein band corresponding to periaxin would be observed at 175 kDa (theoretical size), but this was not the case.

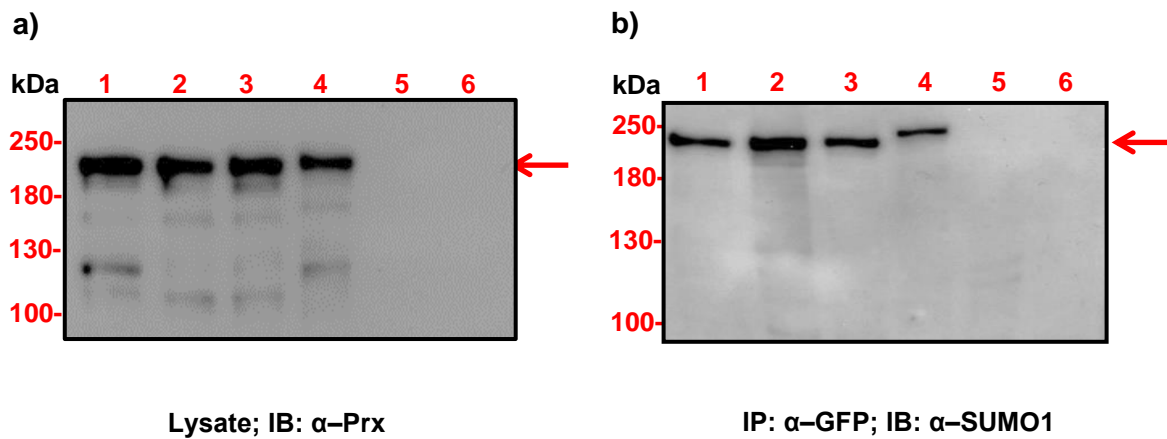


Figure 24. Identification of potential sumoylation sites in periaxin. Western blot analysis of periaxin mutants in (a) HEK cells lysates and (b) after precipitation using anti-GFP and immunoblotted with anti-Periaxin and SUMO1 antibody, respectively. **1** = Prx-K76R-K171R-K218R-K893R-K1174R, **2** = Prx-K893R-K1174R, **3** = Prx-K76R-K171R-K218R, **4** = Prx-WT, **5** = pEGFP, **6** = Untransfected HEK cells. Arrows indicate sumoylated periaxin.

Therefore, our preliminary results indicate that the five mutated lysines are not the unique sumoylation sites in periaxin and other target lysines still remain to be elucidated in future studies.

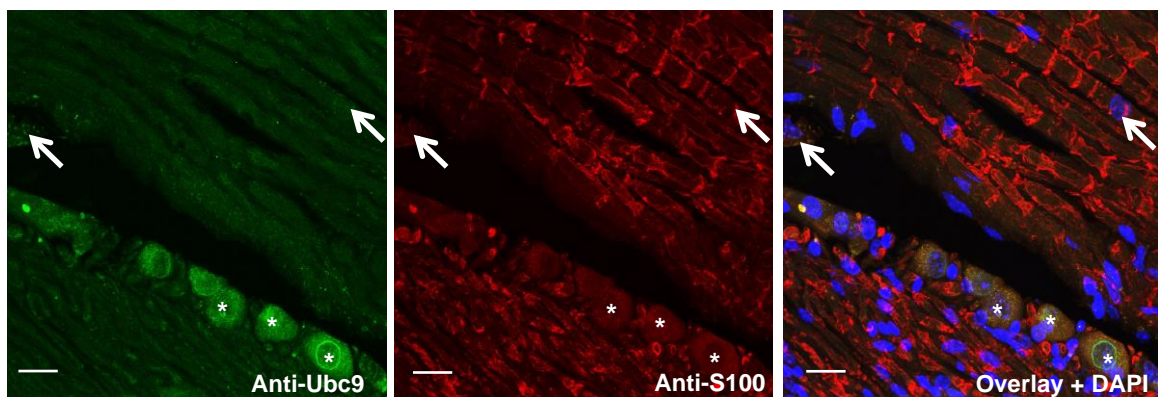
### 3.3.5 Conditional deletion of Ubc9 in Schwann cells

The generation of conditional mouse lines is a valuable approach to study genes and proteins in a physiological background. This is relevant specifically in analysing disease mechanisms of late-onset degenerative disorders and regeneration processes in mouse models. The approach using the Cre-recombinase for deleting DNA fragments between loxP sites to generate mutations in a temporally controlled manner has demonstrated to be effective (Lewandosky, 2001). Based on this, we designed an experiment to investigate the effect of SUMO modification on Schwann cells function *in vivo*, using a mouse model.

To address this, the mouse line PLP-Cre<sup>ERT2+/+</sup>Ubc9<sup>fl/fl</sup> was created in our laboratory as follows: mice carrying homozygous flox alleles of the Ubc9 gene (Ubc9<sup>fl/fl</sup>) were mated with mice in which, the Cre-recombinase is expressed upon tamoxifen injection, under the control of the proteolipid protein promoter (PLP-Cre<sup>ERT2</sup>) selectively in Schwann cells and oligodendrocytes (Leone *et al.*, 2003). In this mutant mouse line, Ubc9 (SUMO-conjugating enzyme) can be conditionally deleted upon tamoxifen injection.

For the characterization of the mouse line, we injected tamoxifen or vehicle into PLP-Cre<sup>ERT2+/+</sup>Ubc9<sup>fl/fl</sup> cre-positive mice. After 8 weeks, DRGs from PLPcreUbc9 vehicle-injected mice stained positively for S100 and Ubc9 (Fig. 25a), which are expressed mainly in cell nuclei. Conversely, though DRGs from PLPcreUbc9 tamoxifen-injected mice also stained positively for S100, there was an absence of Ubc9 expression after tamoxifen treatment. The absence of Ubc9 staining in S100 positive cells (marked by the arrowhead in Fig. 25b) as compared to DRGs from vehicle-injected mice (marked by the arrow in Fig. 25a) showed that upon tamoxifen injection, recombination occurs at Ubc9 gene locus in Schwann cells, which resulted in the deletion of Ubc9 protein in Schwann cells. Moreover, deletion of Ubc9 did not affect the survival of Schwann cells.

**a) PLP-Cre<sup>ERT2+/+</sup>Ubc9<sup>fl/fl</sup> + vehicle**



**b) PLP-Cre<sup>ERT2+/+</sup>Ubc9<sup>fl/fl</sup> + tamoxifen**

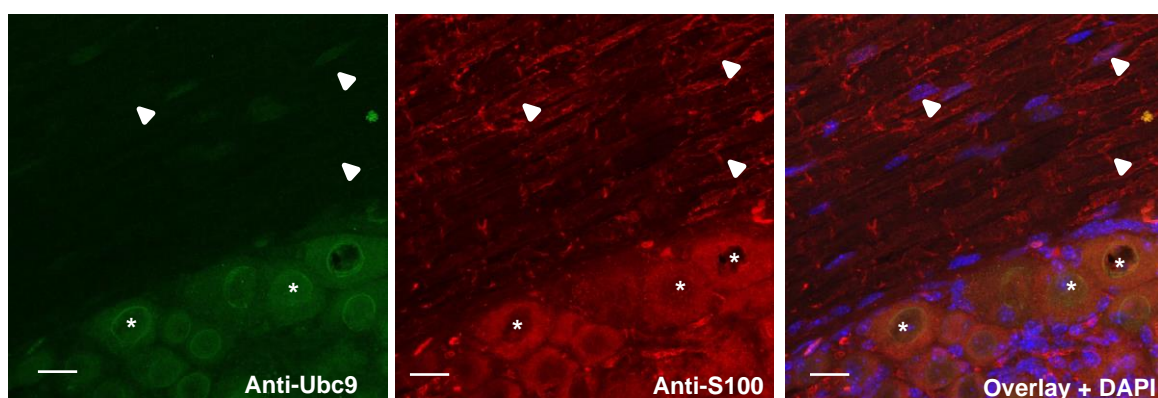
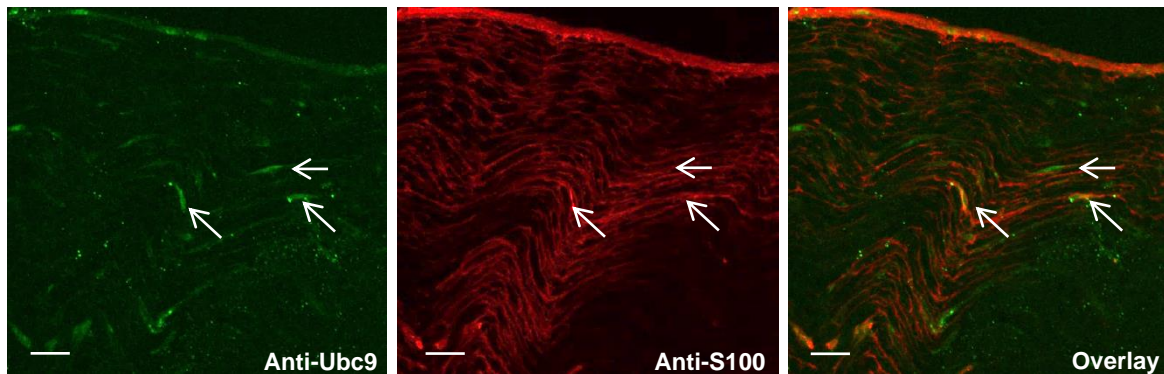


Figure 25. DRGs sections from PLPcre<sup>ERT2+/+</sup>Ubc9<sup>fl/fl</sup> mice injected with (a) vehicle or (b) tamoxifen were immunostained with anti-Ubc9, anti-S100 and counterstained with DAPI. Arrow indicates Schwann cells, arrowhead indicates Ubc9-deleted Schwann cells, asterisk indicates neuron cell. Scale bar represents 10  $\mu$ m.

However, DRG neurons showed comparable expression of Ubc9 in both the treated and untreated group (Fig. 25). Similarly, in the sciatic nerve, we could see the absence of Ubc9 staining in the tamoxifen-treated group (arrowhead in Fig. 26b), which remained intact in the untreated group (arrow in Fig. 26a).

**a) PLP-Cre<sup>ERT2+/+</sup>Ubc9<sup>fl/fl</sup> + vehicle**



**b) PLP-Cre<sup>ERT2+/+</sup>Ubc9<sup>fl/fl</sup> + tamoxifen**

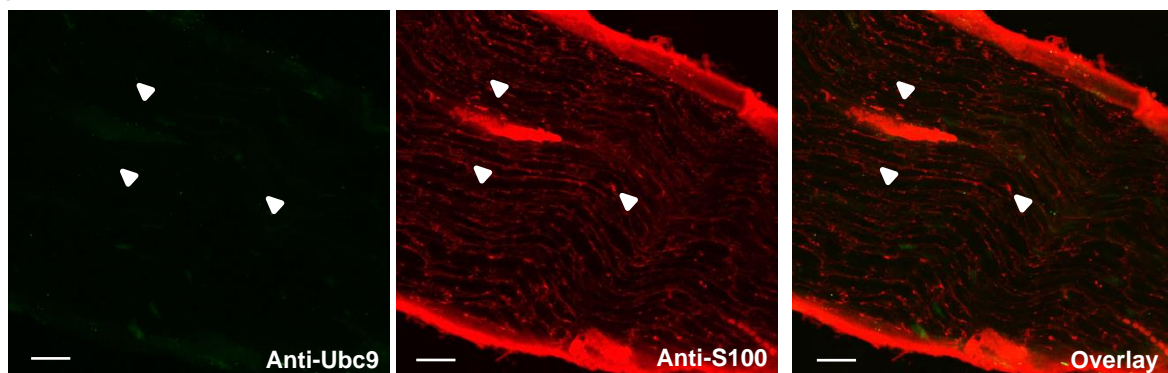
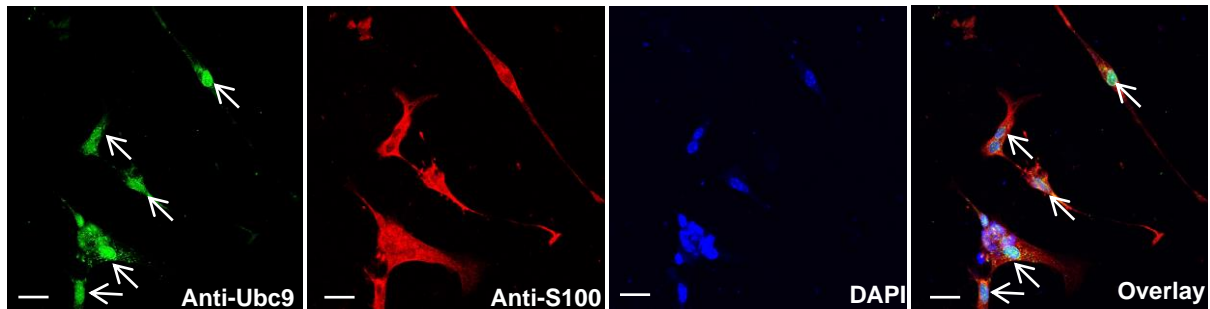


Figure 26. Sciatic nerve isolated from PLPcre<sup>ERT2+/+</sup>Ubc9<sup>fl/fl</sup> mice injected with (a) vehicle or (b) tamoxifen were immunostained with anti-Ubc9 and anti-S100. Arrow indicates Schwann cells and arrowhead indicates Ubc9-deficient Schwann cells. Scale bar represents 10  $\mu$ m.

To further validate the efficacy of recombination, we cultured Schwann cells from isolated sciatic nerve from PLP-Cre<sup>ERT2+/+</sup>Ubc9<sup>fl/fl</sup> mice without tamoxifen injection. Schwann cells were treated with 1  $\mu$ M 4-hydroxytamoxifen for 48 h and immunostained with anti-Ubc9 and anti-S100 antibodies (Fig. 27). The untreated group showed the nuclear staining of Ubc9 in S100-positive Schwann cells (Fig. 27a, arrow). The tamoxifen-treated group showed the deletion of Ubc9 staining in S100-positive Schwann cells (Fig. 27b, arrowhead). This indicated that tamoxifen treatment effectively induced the conditional deletion of Ubc9 expression in Schwann cells from PLP-Cre<sup>ERT2+/+</sup>Ubc9<sup>fl/fl</sup> mice.

**a) PLP-Cre<sup>ERT2+/+</sup>Ubc9<sup>fl/fl</sup> control**



**b) PLP-Cre<sup>ERT2+/+</sup>Ubc9<sup>fl/fl</sup> + tamoxifen**

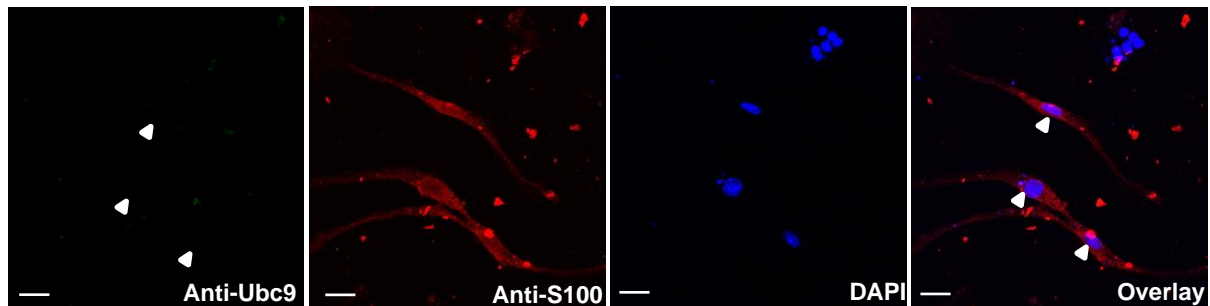


Figure 27. Schwann cells isolated from PLPcre<sup>ERT2+/+</sup>Ubc9<sup>fl/fl</sup> mice (a) vehicle treated and (b) treated with 4-hydroxytamoxifen. The cultures were immunostained with anti-Ubc9, anti-S100 and counterstained with DAPI. Arrow indicates Ubc9-expressing Schwann cells and arrowhead indicates Ubc9-deficient Schwann cells. Scale bar represents 10  $\mu$ m.

### 3.3.6 Behavioural experiments

#### 3.3.6.1 Hole-board test

The comparison of results between PLP-Cre<sup>ERT2+/+</sup>Ubc9<sup>fl/fl</sup> vehicle-injected and tamoxifen-injected mice did not show differences in the frequency of head-dipping into the hole-board apparatus during the analysed time frame (Fig. 28). The exploratory behaviour on this setup was decreased as the mice became less anxious and got habituated to this environment. Furthermore, at 16 weeks post-injection, the counts of head dips were considerably decreased in both groups of mice compared with baseline recordings, indicating less exploration of the apparatus. However, the hole-board test did not show significant differences between vehicle and tamoxifen-injected PLP-Cre<sup>ERT2+/+</sup>Ubc9<sup>fl/fl</sup> mice during this longitudinal study, which indicates that the deletion of sumoylation in Schwann cells did not induce an effect in exploratory behaviour of mice.

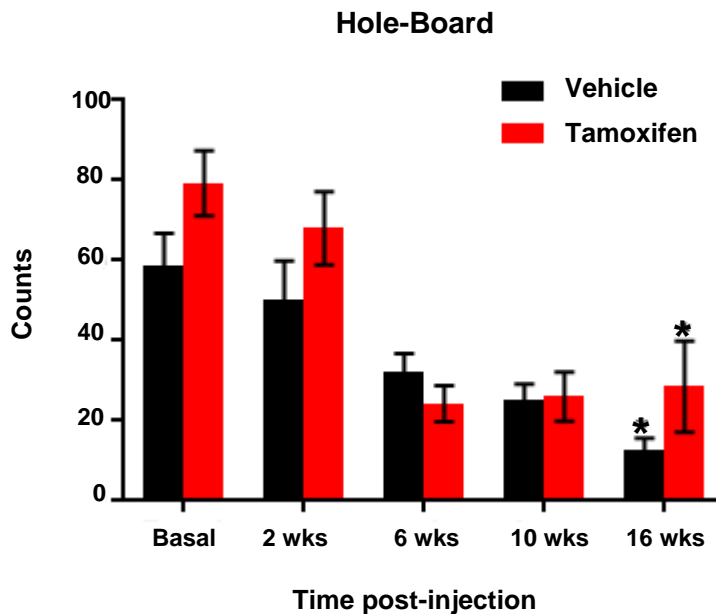


Figure 28. Change in frequency of head-dipping in PLP-Cre<sup>ERT2+/+</sup>Ubc9<sup>fl/fl</sup> mice during a 10 min period at different time points post-tamoxifen or vehicle injection.  $n = 8$  mice per group. Data are represented as mean  $\pm$  SEM. \* $p < 0.05$  compared to basal; two-way ANOVA for repeated measurements with Bonferroni multiple comparison test.

### 3.3.6.2 Elevated plus-maze test

In the elevated plus-maze test, the PLP-Cre<sup>ERT2+/+</sup>Ubc9<sup>fl/fl</sup> mice visited the open arms less than 30% of total counts at the different time points, but they visited the closed arms more than 60% of total counts (Fig. 29a). In addition, mice spent less than 16% of the time in open arms and more than 80% of the time in closed arms. Both groups of mice spent less time in the open arms and made fewer entries into the open arms than into the closed arms, without considerable differences between the groups (Fig. 29b). Thus, deletion of sumoylation in Schwann cells had no impact on anxiety-related behaviour.

These findings indicate that the mice preferred secure sections of the elevated maze, regardless of the treatment used. Therefore, we could claim there was not a meaningful difference in the anxiety behaviour between vehicle-injected and tamoxifen-injected PLP-Cre<sup>ERT2+/+</sup>Ubc9<sup>fl/fl</sup> mice.

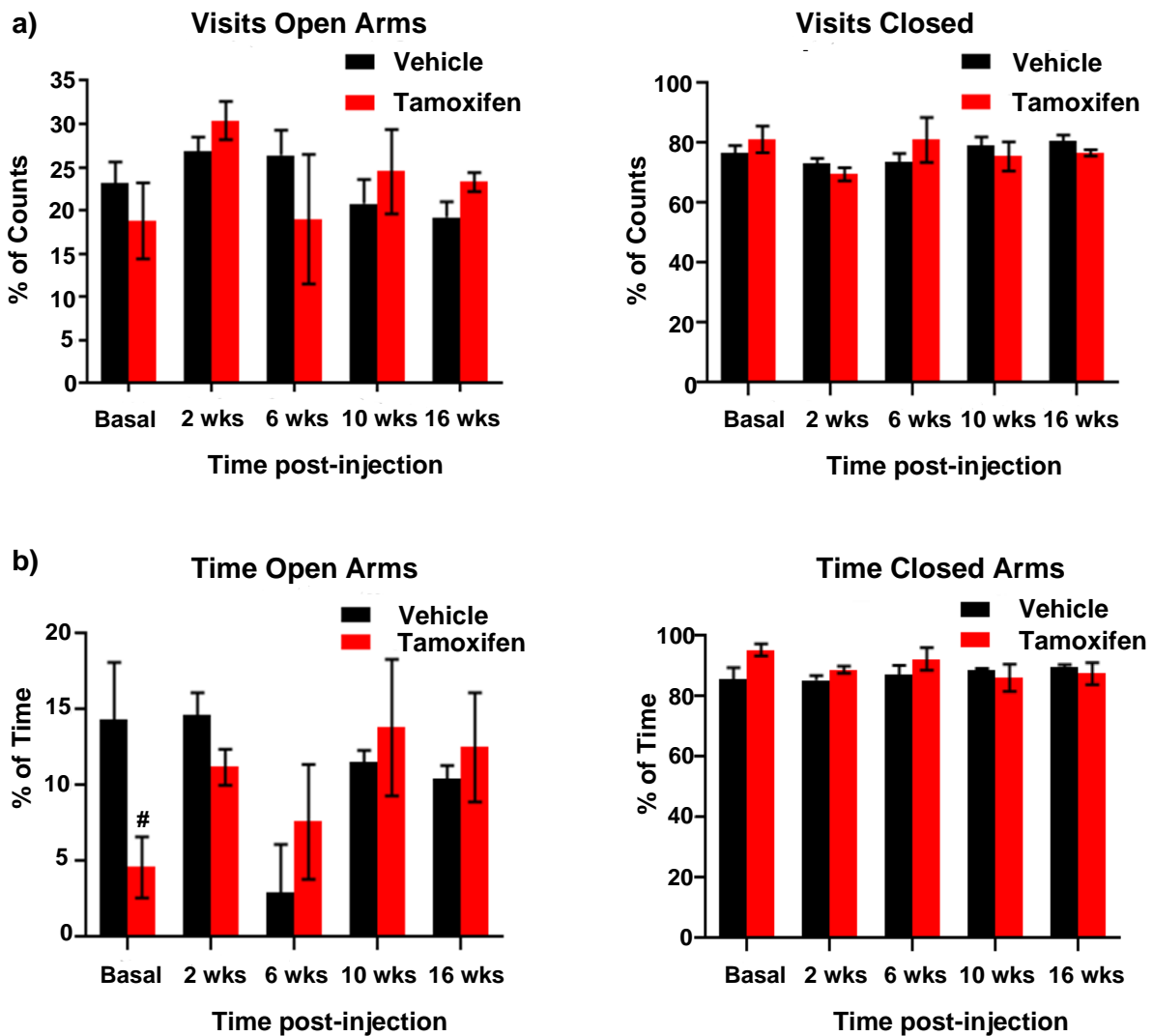


Figure 29. Percentage of (a) counts and (b) time spent by PLP-Cre<sup>ERT2+/+</sup>Ubc9<sup>fl/fl</sup> mice, in the open arms and the closed arms in the elevated plus-maze apparatus.  $n = 8$  mice per group. Data are represented as mean  $\pm$  SEM. #  $p < 0.05$  compared to control. Two-way ANOVA for repeated measurements with Bonferroni multiple comparison test.

### 3.3.6.3 Home cage monitoring

We observed that from week 10 onwards both groups of PLP-Cre<sup>ERT2+/+</sup>Ubc9<sup>fl/fl</sup> mice were less active and showed statistically significantly less counts over time. At 16 weeks both groups of mice reduced climbing activity. However, no significant differences were observed between the vehicle and Tamoxifen-treated groups (Fig. 30a).

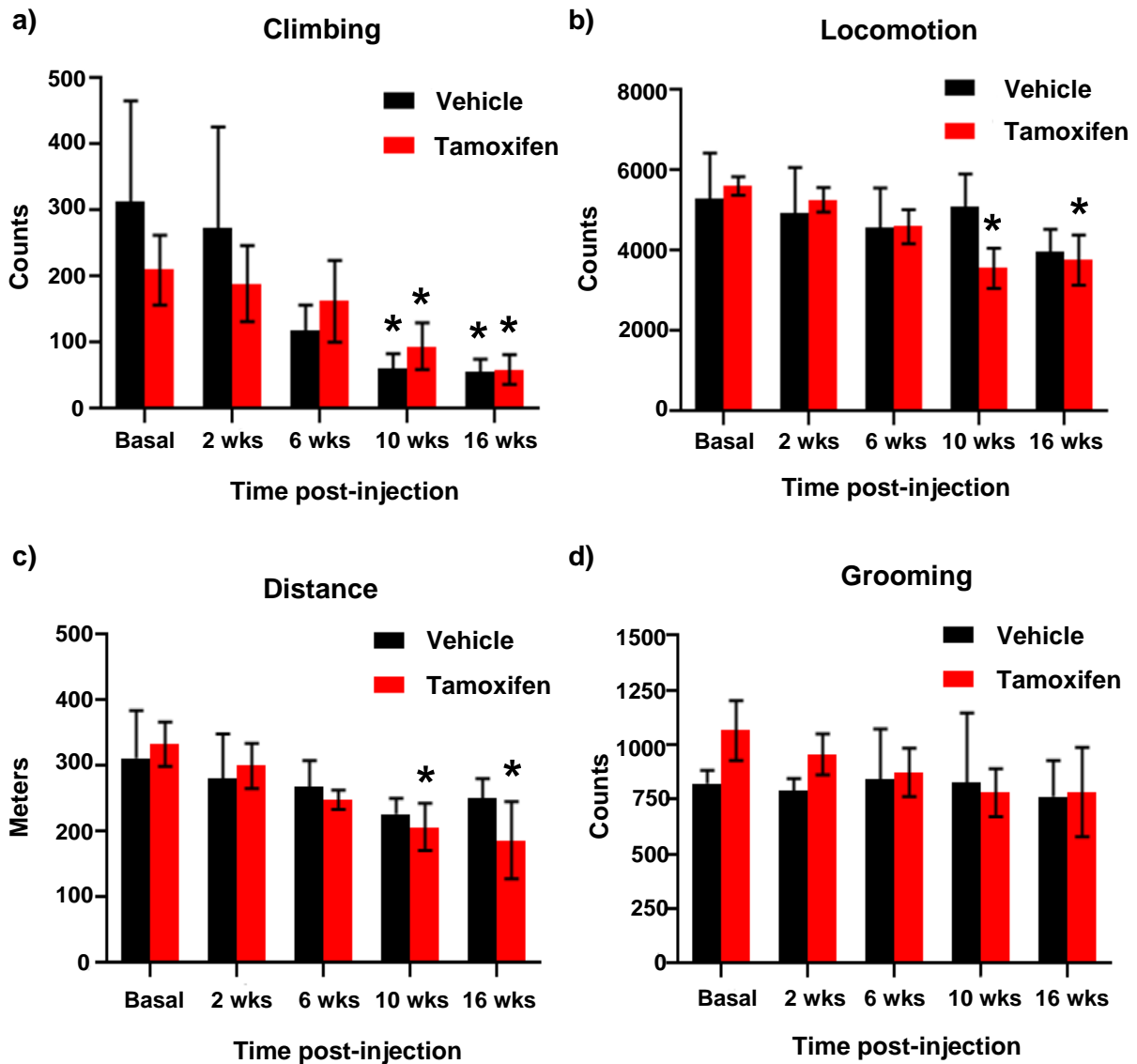


Figure 30. Home cage monitoring of PLP-Cre<sup>ERT2</sup>+/+Ubc9<sup>fl/fl</sup> mice after tamoxifen or vehicle injection. a) climbing counts, b) locomotion counts, c) moving distance and d) grooming counts, per 24 h period.  $n = 8$  mice per group. Data are represented as mean  $\pm$  SEM. \* $p < 0.05$  compared to basal. Two-way ANOVA for repeated measurements with Bonferroni multiple comparison test.

We observed a significant reduction in locomotion and distance at 10 and 16 weeks only in the Tamoxifen-treated group (Fig. 30b, c). Moreover, we did not find a difference in the grooming parameter neither between both groups of mice over time nor respect to basal (Fig. 30d). The results of this analysis showed that there were no significant differences between mice lacking Ubc9 in Schwann cells and oligodendrocytes and control mice for the parameters studied in the home cage monitoring.

### 3.3.6.4 Running wheel

We analysed the running behaviour of PLP-Cre<sup>ERT2+/+</sup>Ubc9<sup>fl/fl</sup> mice longitudinally up to 16 weeks post vehicle or tamoxifen injection. We found that the vehicle-injected mice presented a progressive increase in their running distance (Fig. 31a) during the evaluated time i.e., from 2000 m at baseline to 4300 m at 16 wks post-injection. This can be explained because of the training effect of the vehicle-injected group over time.

The tamoxifen-injected group also showed an increase in the running distance up to 6 weeks, after this moment, their running distance was reduced. Moreover, after 16 weeks we observed a significant difference in running distance between the vehicle and tamoxifen-injected PLP-Cre<sup>ERT2+/+</sup>Ubc9<sup>fl/fl</sup> mice (Fig. 31a).

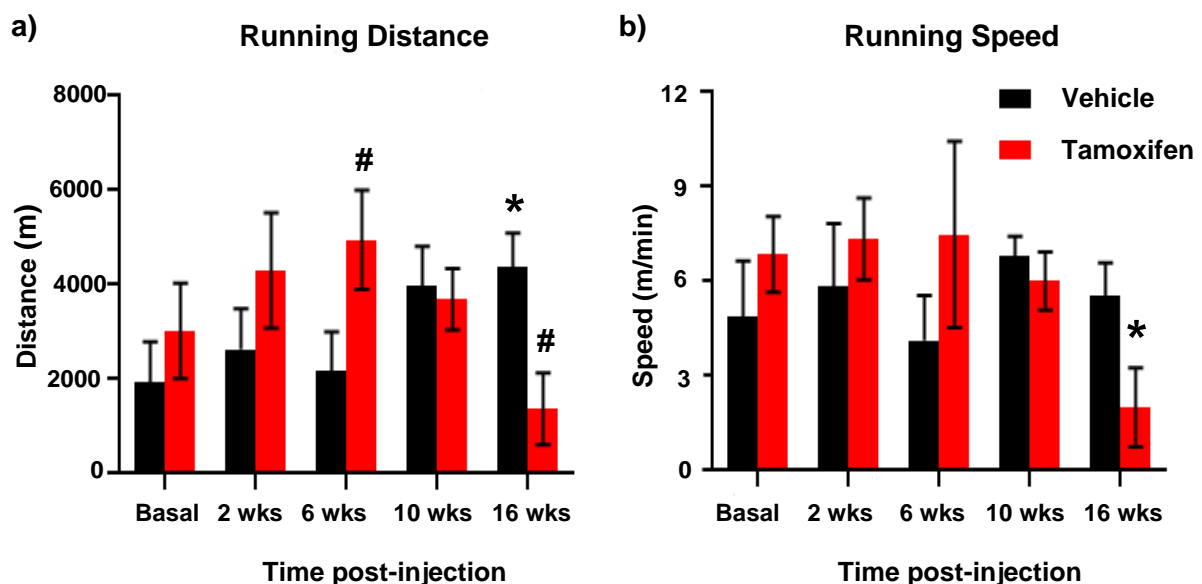


Figure 31. Voluntary running wheel behaviour of PLP-Cre<sup>ERT2+/+</sup>Ubc9<sup>fl/fl</sup> mice after tamoxifen or vehicle injection. a) Running distance (meters) and b) Speed (meter/min) per 24 h period.  $n = 8$  mice per group. Data are represented as mean  $\pm$  SEM. \* $p < 0.05$  compared to basal, # $p < 0.05$  compared to control. Two-way ANOVA for repeated measurements with Bonferroni multiple comparison test.

The running speed was also decreased in the mutant mice group after 16 weeks, but the vehicle-injected group did not demonstrate a specific trend changes in the running speed (Fig. 31b). In summary, deletion of sumoylation in Schwann cells and oligodendrocytes as compared to control mice, led to partial impairment in running behaviour, which could be due to onset of motor neuropathy.

### 3.3.6.5 Cat-walk

The analysis of dynamic gait parameters in PLP-Cre<sup>ERT2+/+</sup>Ubc9<sup>fl/fl</sup> mice showed that up to 16 weeks after injection, there was an increment in the average walking speed of vehicle-injected mice compared to baseline and compared to mutant mice (Fig. 32a).

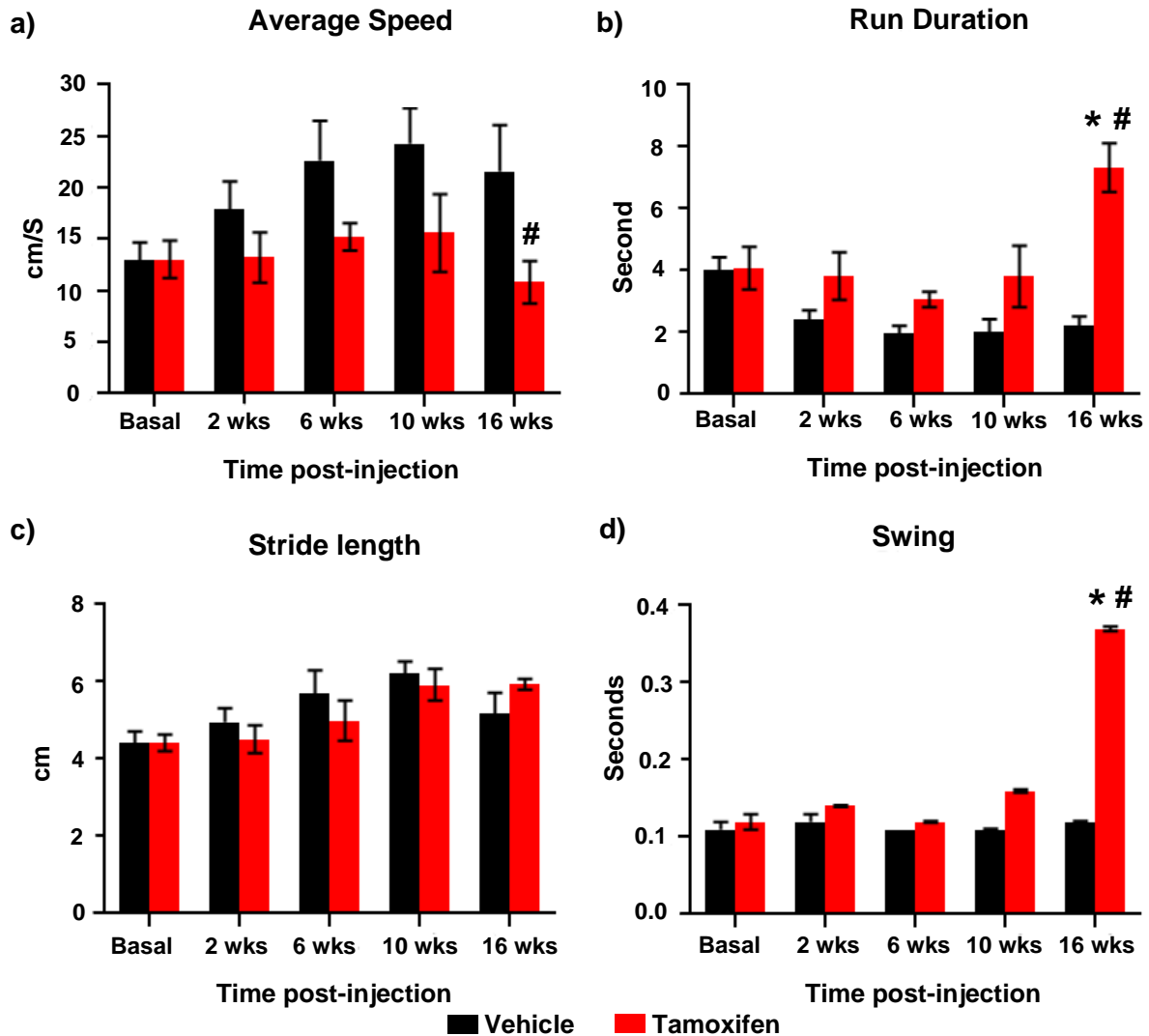


Figure 32. Dynamic gait parameters of PLP-Cre<sup>ERT2+/+</sup>Ubc9<sup>fl/fl</sup> mice after tamoxifen or vehicle injection. a) Average speed, b) run duration, c) stride length and d) swing phase.  $n = 8$  mice per group. Data are represented as mean  $\pm$  SEM. \* $p < 0.05$  compared to basal. # $p < 0.05$  compared to control. Effect of Tamoxifen on run duration ( $F(1,30)=26.98$ ,  $p < 0.0001$ ; two-way ANOVA for repeated measurements with Bonferroni multiple comparison test).

Besides, Ubc9 deficient mice presented a reduction in average speed at 16 weeks post-injection. Moreover, whereas control mice showed a decrease in run duration, we found an increase in the run duration of mutant mice at 16 weeks in comparison

to basal and control group (Fig. 32b). Moreover, no significant differences were observed in stride length parameter between mutant mice and controls (Fig. 32c). Furthermore, the swing phase, which indicates the time of no contact of a paw with the glass plate, increased substantially at 16 weeks post-injection in mutant mice as compared to controls (Fig 32d), indicating that mutant mice show sign of motor neuropathy starting at 16 weeks post-tamoxifen injection.

### 3.3.7 *In vitro* myelination assay

Periaxin is a relevant component of the myelination machinery (Sherman and Brophy, 2000). In order to elucidate the possible functional consequences of sumoylation on the periaxin function, we aimed to establish an *in vitro* myelination assay. The characterisation performed using Schwann cell-specific markers revealed that we could effectively isolate Schwann cells that were positive for the three tested markers, namely Prx, S100 and p75 (Fig. 33). Moreover, the cells presented an elongated and branched morphology, which is typical of Schwann cells (Honkanen *et al.*, 2007). These results indicate that the dissociation protocol used is suitable for the purification of Schwann cells from the mouse sciatic nerve.

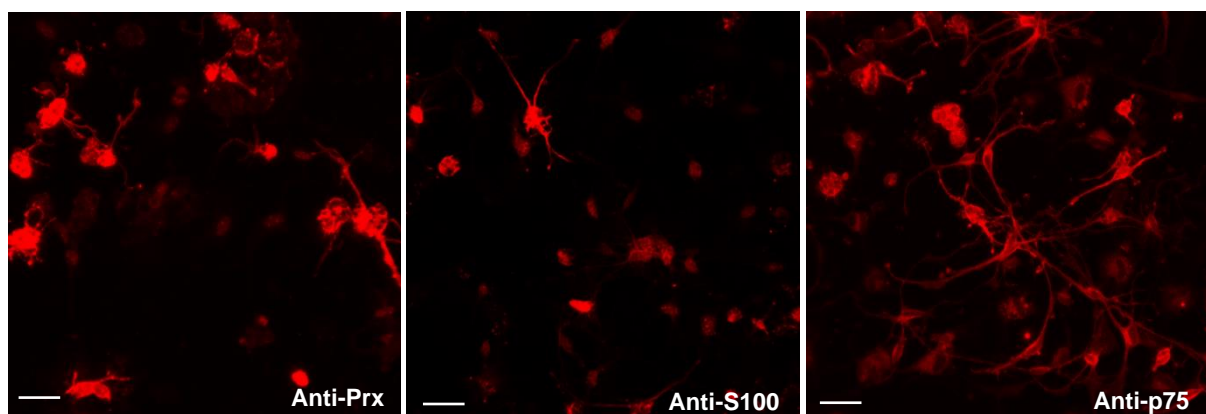


Figure 33. Schwann cells were cultured for 1 week, fixed and immunostained with anti-periaxin, anti-S100 and anti-p75. Scale bar represents 10  $\mu$ m.

Furthermore, we stained a DRG-Schwann cell co-culture with a late myelination marker (MBP) and a Schwann cell marker (S100). We found myelinated axons (shown by arrows, Fig. 34) as well as Schwann cells (shown by arrowheads, Fig. 34)

adhering to the growing axons of DRGs in culture, which demonstrated that the myelination process of wrapping axons had occurred.

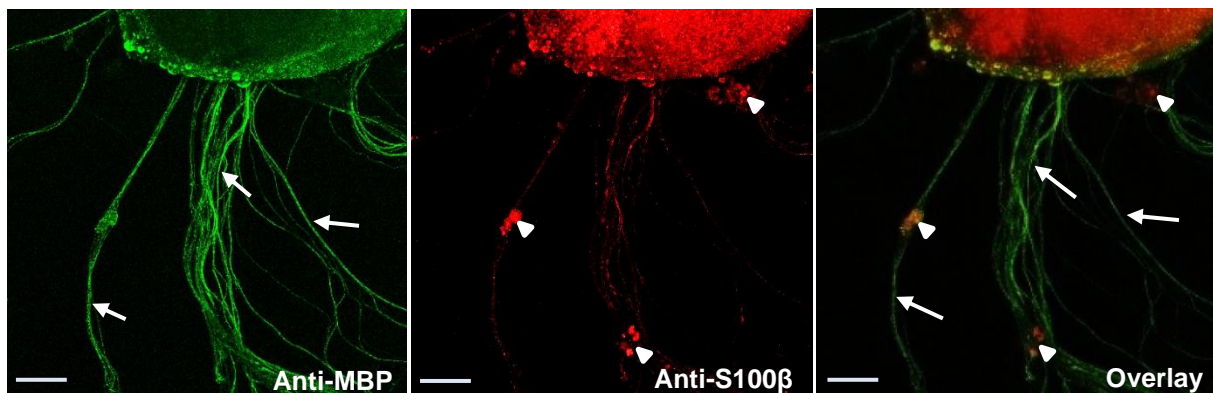


Figure 34. DRGs and Schwann cells were co-cultured for 3 weeks, fixed and immunostained with anti-myelin basic protein and anti-S100. Arrows indicate myelinated axons and arrowheads indicate Schwann cells. Scale bar represents 10  $\mu\text{m}$ .

Furthermore, we immunostained the Schwann cell-DRG cocultures with DAPI, anti- $\beta$ -tubulin III and anti-myelin-associated glycoprotein (MAG) (Fig. 35). Using this co-staining, we could specifically identify the presence of axons of the DRG, which was confirmed by the positive immunostaining against anti- $\beta$ -tubulin III (shown by arrows, Fig. 35).

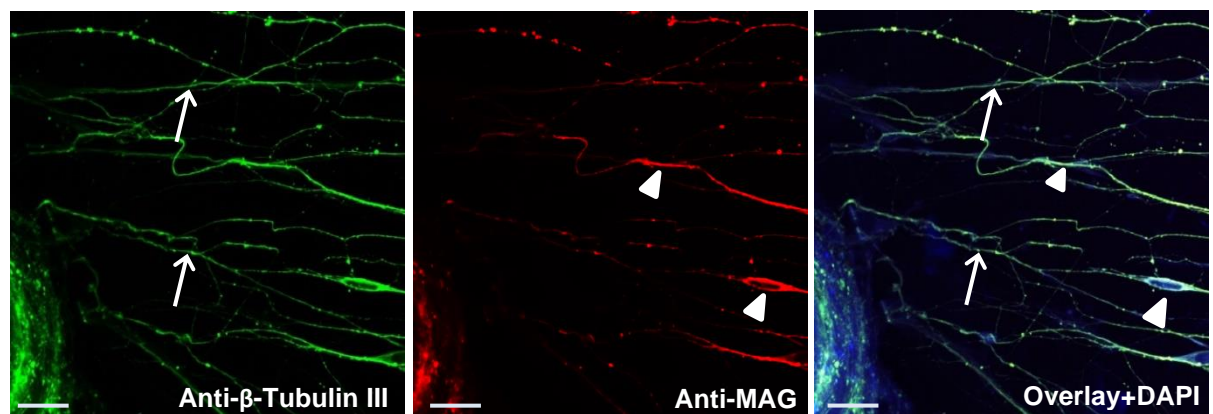


Figure 35. Whole mount DRGs and Schwann cells were co-cultured for 3 weeks, fixed and immunostained with anti- $\beta$ -Tubulin III, anti-myelin-associated glycoprotein and counterstained with DAPI. Arrows indicate axons and arrowheads indicate Schwann cells. Scale bar represents 10  $\mu\text{m}$ .

We identified the Schwann cells by the positive staining for MAG (in red), an early myelination indicator (shown by arrowheads, Fig. 35). The overlaid image of the staining with MAG and  $\beta$ -tubulin III corroborated the presence of Schwann cells adhered to the axons (in green) of the DRGs.

This confirms that Schwann cells myelinated the axons in DRG explants in the *in vitro* model we employed. These results lay a basis for performing qualitative and quantitative analyses in future experiments.

### **3.3.8 Summary:**

Altogether, the results obtained in this work can be summarised in three main points:

First, under prolonged diabetic conditions, we observed that the TCA cycle is inhibited in peripheral sensory neurons, which results in the switching of glycolytic flux to alternative pathways. It leads to the accumulation of toxic metabolites, which contribute to the loss of sensation and the progression of DPN in diabetic mice.

Second, during the onset and progression of DPN, the transcription factor HIF1 $\alpha$  possesses a protector function by limiting the augmentation of ROS levels and inhibiting injury of the peripheral sensory neurons.

Third, we found that periaxin protein is modified by sumoylation *in vitro* and *in vivo*. Moreover, the conditional suppression of sumoylation in Schwann cells and oligodendrocytes showed that mutant mice tend to develop symptoms of motor neuropathy in later stages of life.

## 4 DISCUSSION

### 4.1 Metabolomic screening in diabetes type I model

DPN is the most frequent burden among diabetic patients (Barret *et al.*, 2007). The disease-causing mechanisms responsible for the initiation and development of DPN still remain to be elucidated. The progression of DPN is not a stationary process; it is necessary to find metabolic markers through longitudinal studies, in which one can follow specific and transitory changes at the origin and through the progression of DPN. In this work, we attempted to delineate the metabolic alterations occurring in peripheral nerve tissue and serum and their contribution in the progression of DPN. The most relevant outcomes of this study are the following: (1) An early shift of metabolic flux in peripheral nerves from the oxidative pathway to alternative pathways occurs before perceptible symptoms of sensory loss and nerve damage appear and (2) elevated levels of BCAAs in serum lead to the modification of metabolic pathways in the sciatic nerve which could be a potential diagnostic marker to recognize the progression of DPN.

Former studies employing different diabetic mouse models revealed metabolic pathways dysfunction in type 1 and 2 diabetic models (Akude *et al.*, 2011; Hinder *et al.*, 2013, Ola *et al.*, 2006). Several manifestations including oxidative stress, protein and lipid oxidation, the arrest of metabolic enzymes, elevated BCAAs (Piccolo *et al.*, 2016) and downregulation of mitochondrial enzymes in nerves and DRGs have been reported in rodents after established DPN (Akude *et al.*, 2011). In this work, we wanted to understand the link between metabolic dysfunction and neuropathic symptoms. We showed that there is no perceptible nociceptive dysfunction at 12 weeks post-STZ injection between diabetic and non-diabetic mice. This was confirmed by the absence of noticeable alterations in IENFD in the epidermis marked by labelling either with CGRP or by PGP 9.5. Contrary to this, at 12 weeks post-STZ, we found decreased levels of citric acid and impaired TCA cycle. At 22 weeks post-STZ, the IENFD was considerably decreased and as well as levels of citric acid were reduced. Moreover TCA cycle was severely impaired.

To generate energy, the impaired TCA cycle can deviate metabolites to alternative metabolic pathways. We observed increased levels of L-lactate and sorbitol at early and late time points post-STZ injection. The deviation of glucose from the glycolysis pathway to the polyol pathway leads to elevated levels of sorbitol. Former studies have

also reported the increase and accumulation of sorbitol in response to hyperglycaemia and its association with DPN progression (Dvornik, 1987; Kador *et al.*, 1985). When the concentration of extracellular glucose rises, the enzyme aldose reductase converts glucose into sorbitol (Kador *et al.*, 1985). The accumulation of sorbitol induces an osmotic imbalance in cells and tissue which produces biochemical changes and modifies membrane permeability. When sorbitol accumulates in the sciatic nerves of diabetic rodents, it induces nerve swelling. This type of alteration is comparable to those that have been found to induce lens injury (Kador *et al.*, 1985). It is known that accumulation of sorbitol and nerve swelling are associated with reduced amino acid levels and nerve conduction velocity as well as diminished choline acetyltransferase (Tomlinson *et al.*, 1982; Yue *et al.*, 1982). We found higher levels of sorbitol at early time points and there were no evident neuropathic symptoms indicating that early molecular alterations in metabolic pathways are responsible for onset and progression of DPN. During sorbitol accumulation, other osmolytes including myo-inositol and adenosine are depleted in cytoplasm resulting in low production of ATP, decreased Na-K-ATPase activity and PKC activity (Greene *et al.*, 1987). Dyck *et al.* (1988) found that sorbitol levels in nerve of diabetic patients were inversely proportional to the number of myelinated fibres. Taken together, sorbitol levels manipulation could be potential target to manifest DPN progression.

At 22 weeks post-STZ, we detected increased levels of L-lactate in the sciatic nerve which suggests mitochondrial dysfunction and a switch from oxidative phosphorylation to anaerobic pathways (Dykens *et al.*, 2008; Regenold *et al.*, 2009; Pelicano *et al.*, 2014). Palm *et al.* (2004) found that diabetic rats presented an elevated lactate to pyruvate ratio in the medulla and renal cortex compared to non-diabetic rodents. The increased lactate to pyruvate ratio suggests hypoxia. It is known that over the course of hyperglycaemia, comparable changes occur due to elevated flow of metabolites into the polyol pathway. This flow results in a reduced rate of NAD<sup>+</sup> to NADH (Williamson *et al.*, 1993). Under hyperglycaemic conditions, a reduction in tissue oxygen tension occurs; one plausible explanation for this is an alteration in oxygen-haemoglobin dissociation which results from elevated lactate concentration and subsequent tissue pH reduction in diabetic animals (Palm *et al.*, 2003). The considerable increase in lactate and the lactate to pyruvate ratio in plasma of diabetic animals suggests that the major organs in the body are hypoxic. In the mouse model, it was found that the eventual increase in the anaerobic metabolism of lipids could be affected, thereby

contributing to hyperlipidemia (Mayrovitz and Larsen, 1996; Boulton and Malik 1999). Therefore, the increased lactate to pyruvate ratio suggests nerve injury and neuropathy onset.

Our results revealed that under diabetic conditions the decreased kinetics of the TCA cycle leads to a metabolic switch to substitutive pathways. When metabolites are fluxed over an extended period of time it results in onset and development of DPN. At 22 weeks post-STZ, mice demonstrate mechanical and thermal hypoalgesia, decreased IENFD and a complete reduction in the levels of TCA intermediates which are associated with established DPN.

Former studies in the sural nerve have reported that DPN is characterised by decreased expression of glycolytic enzymes and altered transport in axons (Figliomeni *et al.*, 1992). Our results indicate that these molecular changes in metabolic pathways in response to hyperglycaemia are the first effects to occur. These alterations may also result in oxidative stress and are partially responsible for the onset and progression of DPN.

To establish a non-invasive predictive marker, we associated the metabolic changes observed in the peripheral nerve to the alterations in amino acid levels in serum. It is known that in diabetic patients insulin resistance develops and the metabolic machinery of cells adapts to use glucogenic and ketogenic amino acids as an energy supply which then results in decreased levels of these amino acids throughout the course of DPN. Contrarily to this we observed higher levels of BCAAs at late time points post-STZ. BCAAs show structural characteristics and a standard catabolic route (Huang *et al.*, 2011). For instance, isoleucine displays hypoglycaemic effects in muscles and has an important function in the decrease of gluconeogenesis in the liver (Layman, 2003). BCAAs also support cellular metabolism, cell growth and the synthesis of proteins (Chotechuang *et al.*, 2009; Saha *et al.*, 2010). However, it has been shown that elevated levels of circulating BCAAs are associated with poor metabolic conditions. A former study (Yang *et al.*, 2014) presented evidence on a positive and relevant association between cardiovascular disease risk factors and the levels of BCAAs in plasma. Moreover, Newgard *et al.* (2009) reported that increased BCAA levels are associated with a higher probability of developing type 2 diabetes in both humans and animals.

Our longitudinal studies demonstrate that there is a trend of elevated levels of BCAAs at an early time point (5 weeks post-STZ), but this only becomes significant at 12 and

22 weeks post-STZ injection. The early increase of BCAAs in response to hyperglycaemia and its known contribution to metabolic dysfunction establish that the levels of BCAAs in plasma could be used as a predictor of future metabolic diseases (McCormack *et al.*, 2013). The levels of tyrosine were also elevated from 12 weeks post-STZ which in recent years has been investigated as a potential indicator for the regulation of insulin signalling under obese conditions (Hellmuth *et al.*, 2016). Wang *et al.* (2011) described that leucine, tyrosine and valine are considerably associated with the incidence of diabetes. Furthermore, tyrosine phosphatase was shown to be related to the negative modulation of insulin at *in vitro*, *ex vivo* and *in vivo* levels and also has been involved in diabetes and obesity in knock-out murine studies (Johnson *et al.*, 2002). In our study, at 12 weeks post-STZ, the levels of asparagine, histidine, alanine and proline were considerably increased, highlighting the development of diabetic complications. Feling (1973) observed that there is an increase in alanine levels following decreased circulating substrate under diabetic conditions and proposed a cycle in the periphery through which alanine is produced by transamination of pyruvate and carried to the liver where it is converted into glucose. Moreover, Newgard *et al.* (2009) showed that diabetic patients present elevated circulating proline levels and Liu *et al.* (2016) reported that high proline levels produce alterations in  $\beta$ -cell function and gene expression.

Wyse and Netto (2011) reported that elevated proline levels are related to the pathophysiology of some neurological disorders. In a hyperprolinemic mouse model, elevated proline levels in the peripheral and CNS were associated with neuronal dysfunction and learning deficit (Baxter *et al.*, 1985; Davis *et al.*, 1987). In addition, histidine has been found to induce toxicity in cell cultures (Hipkiss *et al.*, 1998) and Alhamdani *et al.* (2007) observed that histidine was toxic to cells even in absence of the stressing factor. Based on these previous findings, we postulate that elevated levels of alanine, proline, asparagine and histidine possibly contribute to nerve dysfunction and lead to progression of DPN.

We hypothesise that the inhibition of glycolytic enzymes in the sciatic nerve is an initiation event occurring before evident DPN symptoms. The inhibition of the TCA cycle switches the metabolism of glucose to alternative pathways which are characterised by elevated levels of L-lactate and sorbitol in peripheral nerves at an early stage. Simultaneously, alterations in BCAAs levels in serum occur at an early time point and likely hold prognostic value. These findings from our longitudinal studies

are useful to delineate the temporal sequence of abnormalities and may have novel therapeutic value in preventing and/or reversing the development of DPN.

#### **4.2 HIF1 $\alpha$ in Diabetic Neuropathy**

Under hyperglycaemic conditions mitochondrial dysfunction and ROS generation have gained attention as potential mechanisms for organ injury during DPN progression. The findings from wild type diabetic mice revealed that metabolic changes occur much earlier than any detectable phenotype changes. In order to understand these metabolic alterations, we analysed the regulation of transcription factor HIF1 $\alpha$  in response to prolonged hyperglycaemia.

The most important outcomes of this study are: (1) the HIF1 $\alpha$  transcription factor displays a protective function against peripheral sensory loss in DPN by promoting VEGF expression, (2) the deletion of HIF1 $\alpha$  in sensory neurons of diabetic mice accelerates the development of DPN-associated sensory loss and (3) suppression of HIF1 $\alpha$  leads to increased accumulation of ROS in sensory neurons.

In recent years, it has been proposed that HIF1 $\alpha$  regulates pain after direct mechanical damage to peripheral nerves (Kanngiesser *et al.*, 2014). Nevertheless, there have been no reports on the function of HIF1 $\alpha$  in nerve damage and pain induced by metabolic dysfunction. There are several mechanisms elucidated for pathological forms of pain but less is known about the progression of nerve injury under metabolic stress. We hypothesised that HIF1 $\alpha$  which is known to be regulated by hyperglycaemia in certain tissues, is one of the critical links between metabolic dysfunction and DPN. The SNS-HIF1  $\alpha^{-/-}$  mice demonstrate early onset of hypoalgesia as compared to controls mice. These findings indicate that HIF1 $\alpha$  has a protective function against DPN. Loss of HIF1 $\alpha$  in mutant mice leads to accelerated neuropathy.

The regulation of DPN by HIF1 $\alpha$  is of broad interest. Both destructive and protective roles of HIF1 $\alpha$  in the damage induced by hyperglycaemia or hypoxia have been reported (Xiao *et al.*, 2013; Bohuslavova *et al.*, 2017). In this work, we found a protective role for HIF1 $\alpha$  against nerve injury produced by metabolic dysfunction in the diabetic model type 1. DPN is characterised by elevated levels of ROS and oxidative stress. ROS, including H<sub>2</sub>O<sub>2</sub> and hydroxyl radicals, can alter the structure of proteins, membrane lipids and nucleic acids. All of these are crucial for maintaining neuronal health. We found elevated H<sub>2</sub>O<sub>2</sub> concentrations and levels of PKG1 $\alpha$  dimers in HIF1 $\alpha$  mutant mice as compared to controls which suggest a redox imbalance on loss of

HIF1 $\alpha$  transcription factor in sensory neurons. We showed that the deletion of HIF1 $\alpha$  produces an accumulation of ROS in sensory neurons during DPN development. This was unforeseen because, even though former studies conducted in other tissues showed that ROS regulates HIF1 $\alpha$  activity, there was scarce evidence that HIF1 $\alpha$  regulates ROS levels. Under diabetic conditions, ROS hinders HIF1 $\alpha$  activation and expression by inhibiting Rac1 and NO (Xiao *et al.*, 2013). In addition, ROS can increase ubiquitin-proteasome activity, thereby inhibiting HIF1 $\alpha$  activity (Botusan *et al.*, 2008). On the other hand, Bonello *et al.* (2007) reported that ROS induces the expression and activation of HIF1 $\alpha$  in a NF- $\kappa$ B-dependent manner in muscle cells of the pulmonary artery. We found an increase in HIF1 $\alpha$  expression in the sensory neurons of diabetic mice. Our results indicate that ROS is downstream of HIF1 $\alpha$ , suggesting that HIF1 $\alpha$  has a neuroprotective role by suppressing ROS production.

The precise mechanism by which HIF1 $\alpha$  modulates ROS levels need to be investigated. Nevertheless, we aimed to study the neuroprotective function of HIF1 $\alpha$  by examining alterations in the levels of VEGF, a known transcription target of HIF1 $\alpha$  (Dengler *et al.*, 2014). Clinical research has revealed elevated plasma levels of VEGF in diabetic patients (Zhang *et al.*, 2018). Studies in diabetic rodents have reported that nerve blood flow is restored by VEGF-induced angiogenesis in the peripheral nerves and can support the survival of the peripheral nerve (Schratzberger *et al.*, 2001). Our findings suggest that VEGF expression is diminished in diabetic SNS-HIF1 $\alpha$ <sup>-/-</sup> mice as compared to control mice which indicate that neuroprotection induced by VEGF is absent in SNS-HIF1  $\alpha$ <sup>-/-</sup> mice and results in the accelerated development of DPN. Several other previous studied mechanisms may contribute to this observed protective function of HIF1 $\alpha$ , for example the regulation of metabolic enzyme expression (Dengler *et al.*, 2014).

Several studies have hypothesised that ROS is involved in the regulation of acute pain (Kim *et al.*, 2004). It has been shown that injecting ROS scavengers peripherally or spinally produces antinociceptive effects in models of neuropathic and inflammatory pain (Yowtak *et al.*, 2011). It is known that the production of ROS via the mitochondrial chain constitutes a junction between hyperglycaemia and pathways associated with hyperglycaemia-induced tissue injury. Under diabetic conditions, an elevated flux of electrons in the respiratory chain occurs which drives an increase in the ATP/ADP ratio in the mitochondria. This is followed by the partial inhibition of complex II and eventually an accumulation of electrons that produce ROS (Brownlee, 2001; Murphy,

2009). It has been proposed that ROS accumulation may cause an energetic failure, thereby reducing antioxidants and neuroinflammation (Shah and Brownlee, 2016). These processes are likely responsible for the nerve damage and subsequent sensory loss that we observed in HIF1 $\alpha$  mutant mice under diabetic conditions.

In summary, this work demonstrates that HIF1 $\alpha$  is a critical signalling molecule involved in hyperglycaemia-induced nerve damage. Furthermore, we found that HIF1 $\alpha$  plays an important role in modulation of ROS levels in sensory neurons in diabetic conditions. These findings are relevant to chronic diabetic complications and serve as an important potential target for new therapeutic treatments, in which the protective role of HIF1 $\alpha$  in sensory neurons could be utilised to protect against these chronic complications.

### **4.3 Role of Sumoylation during the development of diabetic neuropathy**

One of the primary characteristics of DPN is an abnormal myelin membrane ensheathing axons (Vinik *et al.*, 2000). Moreover, DPN is related to harmful alterations in peripheral nerves, including myelin damage and decreased nerve conduction velocity (Malik *et al.*, 2005; Valls-Canals, 2002). Similar to the observation made in diabetic patients, diabetic rodents also show morphological changes in the sciatic nerve (Veiga *et al.*, 2006). Alterations in the myelin sheath can influence membrane function and fluidity, resulting in DPN pathology (Zuvic-Butorac *et al.*, 2001). However, how DPN specifically modifies the protein and myelin composition and the molecular mechanism resulting in these alterations remain to be elucidated.

Until now, the histological examination of myelinated and unmyelinated fibres in diabetic patients has been insufficient. Nerve conduction analysis is the most frequently used approach for the analysis of large fibres (Malik *et al.*, 2005). Among the chronic complications associated with DPN development, the demyelination of peripheral nerves and malfunction of Schwann cells are two of the most common complications. The sciatic nerve and Schwann cells express insulin receptor proteins that are affected by diabetes resulting in defective insulin signalling which then contributes to DPN development (Manu *et al.*, 2017). Rachana *et al.* (2016) demonstrated that insulin can drastically affect the capacity of Schwann cells to produce myelin-specific protein, while Schwann cells cultured without insulin were unable to express myelin proteins.

The developmental regulation of periaxin protein demonstrates the rearrangement of the Schwann cell membrane during myelination. It has been shown that in Schwann cell-axon cocultures, Schwann cells require interaction with axons to assemble a basal lamina (Clark and Bunge, 1989), properly myelinate axons and express MAG (Fernandez-Valle et al., 1993). Moreover, the relocation of periaxin from the adaxonal to the abaxonal Schwann cell membrane suggests the polarisation of these cells. Periaxin is a cytoskeleton-associated protein which can modulate Schwann cell shape and gene expression during axonal ensheathment by integrating extracellular signalling through the cytoskeleton (Fernandez-Valle et al., 1997; Tapon and Hall, 1997).

In this work, we investigated if periaxin is a sumoylation target and attempt to understand the functional modulation of periaxin by sumoylation. It has been reported that mutations in the *PRX* gene induce the development of heritable demyelinating neuropathies. It was also found that abnormalities in myelin and Schwann cell proteins are responsible for a phenotype marked by length distal axonal degeneration. Previous studies have revealed that periaxin induces autosomal Dejerine-Sottas neuropathy (DSN) and demyelinating Charcot-Marie-Tooth (CMT) disease (Boerkoel et al., 2001; Guilbot et al., 2001).

It is known that periaxin protein is modified by phosphorylation, acetylation (Uniprot), ubiquitylation (Vasiliou, 2001) and O-GlcNAc glycosylation (Kim et al., 2016). When O-GlcNAc glycosylation is disrupted, periaxin is mislocalised within the myelin sheath of mutant rats, suggesting that O-GlcNAc glycosylation is crucial for myelin maintenance, axonal integrity and peripheral nerve function.

In our studies we found and validated that periaxin is modified by sumoylation both *in vitro* as well as *in vivo*. We provided evidence that periaxin is sumoylated at multiple lysine residues. Though it was not possible to identify the exact lysine residues modified by SUMO1, due to large protein size and several possible target lysines.

Furthermore, it has been reported that periaxin interacts with DRP2 to form the myelination complex (Sherman et al., 2001). Later, it was found that DRP2 is modified by sumoylation (Hendriks et al., 2014). Based on our *in vitro* and *in vivo* findings, we hypothesise that periaxin sumoylation may have a crucial role in the stability of the myelin sheath through its interaction with other components of the myelination complex, such as dystroglycan, DRP2 and ezrin protein (Sherman et al., 2012; Guo

*et al.*, 2020). Therefore, we propose that periaxin desumoylation may lead to mislocalisation of periaxin in the myelin membrane and cause destabilisation of the myelination complex.

With an aim to develop a tool to investigate the role of sumoylation in myelination process, we attempt to develop an *in vitro* myelination assay. We co-cultured Schwann cells with DRG explants to investigate the extent of myelination using immunostaining methods. We could successfully establish the assay as evident from the results explained in section 3.3.7. Now we could take a benefit of using PLP-Cre<sup>ERT2+/+</sup>Ubc9<sup>fl/fl</sup> mice and can delete the sumoylation pathway specifically in Schwann cells either during or before myelination process in *in vitro* assay. This will assist us to investigate the role of sumoylation in Schwann cells in the process of myelination.

Several neurological disorders are related to dysfunction of the sumoylation process, including lateral sclerosis, Alzheimer's, Parkinson's and Huntington's diseases in which proteins have been identified as sumo targets (Steffan *et al.*, 2004; Dorval and Fraser, 2006; Shinbo, 2006; Andersen and Al-Chalabi, 2011), demonstrating the relevance of sumoylation to the development of neurological diseases (Liu *et al.*, 2016). In an *in vivo* stroke model injury-induced upregulation of sumoylation was observed (Cimarosti *et al.*, 2008). Also high levels of sumoylation in Ubc9 transgenic mice were protective against ischemic damage (Lee *et al.*, 2011).

In this work, we observed that there were no cognitive behavioural differences of PLP-Cre<sup>ERT2+/+</sup>Ubc9<sup>fl/fl</sup> mice after the conditional deletion of sumoylation, indicating that neophilia, exploration and anxiety were unaffected. However, mutant mice demonstrated considerable reductions in running performance and dynamic gait parameters, both of which are signs of neuropathy development suggesting that this phenotype is likely caused by the deletion of sumoylation in Schwann cells and oligodendrocytes. This led us to infer that sumoylation has an essential function in the maintenance of myelin complex stability and the ablation of sumoylation accelerates the development of peripheral neuropathy.

However, the molecular mechanisms which link the desumoylation of Periaxin to the onset of peripheral neuropathy observed in PLP-Cre<sup>ERT2+/+</sup>Ubc9<sup>fl/fl</sup> mice still need to be elucidated. Additional functional assessments of the sciatic nerve and Schwann cells of PLP-Cre<sup>ERT2+/+</sup>Ubc9<sup>fl/fl</sup> mice beyond the cat-walk and running wheel tests should be employed to further investigate potential causes of the observed phenotype in knock-out mice. Further studies using our PLP-Cre<sup>ERT2+/+</sup>Ubc9<sup>fl/fl</sup> mice are needed to resolve

the cell-specific role of sumoylation during the myelination process and development of peripheral neuropathies.

#### **4.4 Conclusion**

In this dissertation, we found that early previously undetected alterations in kinetic of metabolic pathways are associated with peripheral nerve damage and subsequent sensory loss. Impaired TCA cycle, flux of metabolites to harmful pathway such as polyol pathway and accumulation of toxic metabolites like sorbitol result in sensory loss and further DPN progression.

The findings of this work also demonstrate that during DPN progression, the transcription factor HIF1 $\alpha$  is an upstream regulator of ROS in peripheral sensory neurons and has a protective role which suppresses hyperglycaemia-induced nerve damage by limiting ROS levels and inducing VEGF expression, thereby promoting peripheral nerve survival. Therefore, HIF1 $\alpha$  stabilisation could be a new therapeutic target for limiting nerve injury and sensory loss.

Additionally, we analysed periaxin protein as a target of sumoylation. Deletion of sumoylation specifically in Schwann cells revealed that it is an essential process necessary for normal Schwann cell function. Further investigations are required to elucidate the role of sumoylation in Schwann cells and its contribution in peripheral neuropathy.

## 5 REFERENCES

- Agarwal, N., Offermanns, S., Kuner, R. 2004. Conditional gene deletion in primary nociceptive neurons of trigeminal ganglia and dorsal root ganglia. *Genesis* 38(3): 122-129.
- Agarwal, N., Taberner, F.J., Rangel Rojas, D., Moroni, M., Omberbasic, D., Njoo, C., Andrieux, A., Gupta, P., Bali, K.K., Herpel, E., Faghihi, F., Fleming, T., Dejean, A., Lechner, S.G., Nawroth, P.P., Lewin, G.R., Kuner, R. (in press). Sumoylation of metabolic enzymes and ion channels in sensory neurons protects against metabolic dysfunction, neuropathy and sensory loss in diabetes. *Neuron* In press.
- Akude, E., Zhrebetskaya, E., Chowdhury, S.K., Smith, D.R., Dobrowsky, R.T., Fernyhough, P. 2011. Diminished superoxide generation is associated with respiratory chain dysfunction and changes in the mitochondrial proteome of sensory neurons from diabetic rats. *Diabetes* 60(1): 288-297.
- Alhamdani, M., Al-Kassir, A., Abbas, F., Jaleel, N., Al-Tae, M. 2007. Antiglycation and antioxidant effect of carnosine against glucose degradation products in peritoneal mesothelial cells. *Nephron Clin Prac* 107(1): 26-34.
- Allen, M.D., Choi, I.H., Kimpinski, K., Doherty, T.J., Rice, C.L. 2013. Motor unit loss and weakness in association with diabetic neuropathy in humans. *Musc Nerv* 48(2): 298-300.
- Amici, S.A., Notterpek, L. 2005. Peripheral myelin protein 22 forms a complex with beta4 integrin in the Schwann cell membrane. *Am So Neurosci* 94(S1): 50.
- Andersen, P.M., Al-Chalabi, A. 2011. Clinical genetics of amyotrophic lateral sclerosis: what do we really know. *Nat Rev Neurol* 7: 603-615.
- Anderson, D.B., Wilkinson, K.A., Henley, J.M. 2009. Protein sumoylation in neuropathological conditions. *Drug News Perspect* 22:255-265.
- Andersson, D.A., Gentry, C., Light, E., Vastani, N., Vallortigara, J., Bierhaus, A., Fleming, T., Bevan, S. 2013. Methylglyoxal evokes pain by stimulating TRPA1. *PLoS One* 8(10):e77986.
- Arroyo, E.J., Scherer, S. 2007. The molecular organization of myelinating Schwann cells. *The Biology of Schwann cells*, Cambridge University Press, Cambridge, pp. 37-54.
- Ayrappetov, M.K., Xu, C., Sun. 2011. Activation of HIF1 $\alpha$  by the prolylhydroxylase inhibitor dimethylglyoxal decreases radiosensitivity. *PLoS One* 6: e26064.
- Bae, M.K., Ahn, M.Y., Jeong, J.W., Bae, M.H., Lee, Y. M., Bae, S.K., Park, J.W., Kim, K.R., Kim, K.W. 2002. Jab1 interacts directly with HIF-1 alpha and regulates its stability *J Biol Chem* 277:9-12.
- Bae, S.H., Jeong, J.W., Park, J.A., Kim, S.H., Bae, M.K., Choi, S.J., Kim, K.W. 2004. Sumoylation increases HIF-1 $\alpha$  stability and its transcriptional activity. *Biochem Biophys Res Commun* 324(1): 394-400.
- Bansal, V., Kalita, J., Misra, U. 2006. Diabetic neuropathy. *Post Medic J* 82: 95-100.
- Barret, A.M., Lucero, M.A., Le, T., Robinson, R.L., Dworkin, R.H., Chappell, A.S. 2007. Epidemiology, public health burden, and treatment of diabetic peripheral neuropathic pain: a review. *Pain Med* 2: S50-S62.
- Baxter, C.F., Baldwin, R.A., Davis, J.L., Flood, J.F. 1985. High proline levels in the brains of mice as related to specific learning deficits. *Pharmacol Biochem Behav* 22(6): 1053-1059.
- Beiswenger, K.K., Calcutt, N.A., Mizisin, A.P. 2008. Epidermal nerve fiber quantification in the assessment of diabetic neuropathy. *Acta Histochem* 110(5): 351-362.

- Beisswenger, P.J., Howell, S.K., Smith, K., Szwergold, B.S. 2003. Glyceraldehyde-3-phosphate dehydrogenase activity as an independent modifier of methylglyoxal levels in diabetes. *Biochim Biophys Acta* 1637: 98-106.
- Ben Othmane, K., Hentati, F., Lennon, F., Ben Hamida, C., Blel, S., Roses, A.D., Pericak-Vance, M.A., Ben Hamida, M., Vance, J.M. 1993. Linkage of a locus (CMT4A) for autosomal recessive Charcot-Marie-Tooth disease to chromosome 8q. *Hum Mol Genet* 2: 1625-1628.
- Berger, J.R., Choi, D., Kamiski, H.J., Gordon, M.F., Hurko, O., D´Cruz, O., Pleasure, S.J., Feldman, E.L. 2013. Importance and hurdles to drug discovery for neurological disease. *Ann Neurol* 74: 441-446.
- Blatnik, M., Thorpe, S.R., Baynes, J.W. 2008. Succination of proteins by fumarate: mechanism of inactivation of glyceraldehyde-3-phosphate dehydrogenase in diabetes. *Annals New York Acad Sci* 1126:272-275.
- Boerkoel, C.F., Takashima, H., Stankiewicz, P., Garcia, C.A., Leber, S.M., Rhee-Morris, L., Lupski, J.R. 2001. Periaxin mutations cause recessive Dejerine-Sottas neuropathy. *Am J Hum Genet* (68):325-333.
- Boerkoel, C.F., Takashima, H., Garcia, C.A., Olney, R.K., Johnson, J., Berry, K., Russo, P., Kennedy, S. 2002. Charcot-Marie-Tooth disease and related neuropathies: Mutation distribution and genotype-phenotype correlation. *Neurol* 51(2): 190-201.
- Bohuslavova, R., Cerychova, R., Nepomucka, K., Pavlinkova, G. 2017. Renal injury is accelerated by global hypoxia-inducible factor 1 alpha deficiency in a mouse model of STZ-induced diabetes. *BMC Endocr Disord* 17(1):48.
- Bonello, S., Zähringer, C., BelAiba, R.S., Djordjevic, T., Hess, J., Michiels, C. 2007. Reactive oxygen species activate the HIF-1alpha promoter via a functional NFkappaB site. *Arterioscler Throm Vasc Biol* 27(4): 755-761.
- Borhini, I., Ania-Lahuerta, A., Regazzi, R. 1994.  $\alpha$ ,  $\beta$ I,  $\beta$ II,  $\delta$ , and  $\epsilon$  protein kinase C isoforms and compound activity in the sciatic nerve of normal and diabetic rats. *J Neurochem* 62: 686-696.
- Botusan, I., Sunkari, V.G., Savu, O., Catrina, A.I., Grünler, J., Lindberg, S. 2008. Stabilization of HIF-1alpha is critical to improve wound healing in diabetic mice. *Proc Natl Acad Sci USA* 105(49):19426-19431.
- Boulton, A.J., Malik, R.A. 1999. Organ specific vascular changes. *Diabetic Angiopathy*, Oxford University Press, New York, 267-275.
- Bourquin, A.F., Süveges, M., Pertin, M., Gilliard, N., Sardy, S., Davison, A.C., Spahn, D.R., Decosterd, I. 2006. Assessment and analysis of mechanical allodynia-like behaviour induced by spared nerve injury (SNI) in the mouse. *Pain* 122(1-2): 14.e1-14.e14.
- Brennan, K.M., Bai, Y., Pisciotta, C., Wang, S., Feely, S.M., Hoegger, M., Gutmann, L., Moore, S.A., Gonzalez, M., Sherman, D.L., Brophy, P.J., Züchner, S., Shy, M.E. 2015. Absence of dystrophin related protein-2 disrupts Cajal bands in a patient with Charcot-Marie-Tooth disease. *Neuro Disord* 25(10): 786-793.
- Brockes, J.P., Fields, K.L., Raff, M.C. 1979. Studies on cultured rat Schwann cells I. Establishment of purified populations from cultures of peripheral nerve. *Brain Res* 165: 105-118.
- Brown, G., Nemes, C. 2008. The exploratory behaviour of rats in the hole-board apparatus: Is head-dipping a valid measure of neophilia? *Behav Procc* 78: 442-448.
- Brownlee, M. 2001. Biochemistry and molecular cell biology of diabetic complications. *Nature* 414(6865): 813-820.
- Brownlee, M., Giacco, F. 2012. Mechanisms of hyperglycemic damage in diabetes. *Atl Diab* 217-231.

- Bugger, H., Chen, D., Riehle, C., Soto, J., Theobald, H.A., Hu, X.X., Ganesan, B., Weimer, B.C., Abel, E.D. 2009. Tissue-specific remodeling of the mitochondrial proteome in type 1 diabetic akita mice. *Diabetes* 58:1986-1997.
- Bullock, J.J., Mehta, S.L., Lin, Y., Lolla, P., Li, P.A. 2009. Hyperglacemia-enhanced ischemic brain damage in mutant manganese SOD mice is associated with suppression of HIF- $\alpha$ . *Neurosci Lett* 456(2): 89-92.
- Burghardt, P.R., Fulk, L.J., Hand, G.A., Wilson, M.A. 2004. The effects of chronic treadmill and wheel running on behaviour in rats. *Brain Res* 1019:84-96.
- Brügger, V., Duman, M., Bochud, M., Münger, E., Heller, M., Ruff, S., Jacob, C. 2017. Delaying histone deacetylase response to injury accelerates conversion into repair Schwann cells and nerve regeneration. *Nat Commun* 8 (14272).
- Cai, Z., Yan, L.J. 2013. Protein oxidative modifications: beneficial roles in disease and health. *Journal of Biochemical and Pharmacological Research* 1(1):15–26.
- Callaghan, B.C., Cheng, H.T., Stables, C.L., Smith, A.L., Feldman, E.L. 2012. Diabetic neuropathy: clinical manifestations and current treatments. *Lancet Neurol* 11(6):521-534.
- Cameron, N.E., Cotter, M.A. 1994. The relationship of vascular changes to metabolic factors in diabetes mellitus and their role in the development of peripheral nerve complications. *Diabetes Metab Rev* 10: 189-224.
- Catrina, S.B., Okamoto, K., Pereira, T., Brismar, K., Poellinger, L. 2004. Hyperglycemia regulates hypoxia-inducible factor-1 $\alpha$  protein stability and function. *Diabetes* 53(12):3226-3232.
- Cereghetti, G.M., Stangherlin, A., Martins de Brito, O., Chang, C.R., Blackstone, C., Bernardi, P., Scorrano, L. 2008. Dephosphorylation by calcineurin regulates translocation of Drp1 to mitochondria. *Proc Natl Acad Sci USA* 105: 15803-15808.
- Chakravarti, B., Chakravarti, D.N. 2007. Oxidative modification of proteins: age-related changes. *Gerontology*. 53(3):128–139.
- Chan, J.R., Phillips, L.J., Glaser, M. 1998. Glucocorticoids and progestins signal the initiation and enhance the rate of myelin formation. *Proc Natl Acad Sci USA* 95: 10459-10464.
- Chan, J.R., Cosgaya, J.M., Wu, Y.J., Shooter, E.M. 2001. Neurotrophins are key mediators of the myelination program in the peripheral nervous system. *Proc Natl Aca Sci USA* 98: 14661-14668.
- Cheah, M., Fawcett, J.W., Andrews, M.R. 2017. Assessment of thermal pain sensation in rats and mice using the Hargreaves test. *Bio Protoc* 7(16): e2506.
- Chen, Y.C., Shiau, S.Y., Lin, J.K. 1998. Involvement of reactive oxygen species and caspase 3 activation in arsenite-induced apoptosis. *J Cell Phys* 177(2): 324-333.
- Chen, A., Mannen, H., Li, S.S. 1998. Characterization of mouse ubiquitin-like SMT3A and SMT3B cDNAs and gene/pseudogenes. *Biochem Mol Biol Int* 46:1161-1174.
- Chen, Z.L., Strickland, S. 2003. Laminin  $\gamma$ 1 is critical for Schwann cell differentiation, axon myelination, and regeneration in the peripheral nerve. *J Cell Biol* 163: 889-899.
- Cheng, J., Bawa, T., Lee, P., Gong, L., Yeh, E.T. 2006. Role of desumoylation in the development of prostate cancer. *Neoplasia* 8(8): 667-676.
- Chen, C.H., Chang, C.C., Lee, T.H., Luo, M., Huang, P., Liao, P.H., Wei, S., Li, F.A., Chen, R.H., Zhou, X.Z., Shih, H.M., Lu, K.P. 2013. SENP1 deSUMOylates and regulates Pin1 protein activity and cellular function. *Mol and Cell Pathol* 73(13): 3951-3962.

- Cho, D.H., Nakamura, T., Fang, J., Cieplak, P., Godzik, A., Gu, Z., Lipton, S.A. 2009. S-nitrosylation of Drp1 mediates beta-amyloid related mitochondrial fission and neuronal injury. *Science* 324: 102-105.
- Chotechuan, N., Azzout-Marniche, D., Bos, C., Chaumontet, C., Gausseres, N. 2009. mTOR, AMPK and GCN2 coordinate the adaptation of hepatic energy metabolic pathways in response to protein intake in the rat. *Am J Physiol Endocrinol Metab* 297: E1313-1323.
- Choi, C.S., Kim, Y.B., Lee, F.N., Zabolotny, J.M., Kahn, B.B., Youn, J.H. 2002. Lactate induces insulin resistance in skeletal muscle by suppressing glycolysis and impairing insulin signaling. *Am J Physiol Endocrinol Metab* 283: E233-E240.
- Chung, S.S., Ho, E.C., Lam, K.S., Chung, S.K. 2003. Contribution of polyol pathway to diabetes-induced oxidative stress. *J Am Soc Nephrol* 14(3): 233-236.
- Cimarosti, H., Lindberg, C., Bomholt, S.F., Ronn, L.C., Henley, J.M. 2008. Increased protein sumoylation following focal cerebral ischemia. *Neuropharm* 54: 280-289.
- Clark, M.B., Bunge, M.B. 1989. Cultured Schwann cells assemble normal-appearing basal laminae only when they ensheath axons. *Dev Biol* 133: 393-404.
- Cohen, R.D., Campbell, K.P. 2000. Molecular basis of muscular dystrophies. *Muscle Nerve* 23:1456-1471.
- Colloca, L., Ludman, T., Bouhassira, D., Baron, R., Dickenson, A.H., Yarnitsky, D., Freeman, R., Truini, A., Attal, N., Finnerup, N.B., Eccleston, C., Kalso, E., Bennett, D.L., Dworkin, R.H., Raja, S.N. 2017. Neuropathic pain. *Nat Rev Dis Primers* 3:17002.
- Corfas, G., Velardez, M.O., Ko, C.P., Ratner, N., Peles, E. 2004. Mechanisms and roles of axon-Schwann cell interactions. *J Neurosci* 24: 9250-9260.
- Cottet-Rouselle, C., Ronot, X., Leverve, X., Mayol, J.F. 2011. Cytometric assessment of mitochondria using fluorescent probes. *Cytometry A* 79(6): 405-425.
- Court, F.A., Sherman, D.L., Pratt, T., Garry, E.M., Ribchester, R.R., Cottrell, D.F., Fletwood-Walker, S.M., Brophy, P.J. 2004. Restricted growth of Schwann cells lacking Cajal bands slows conduction in myelinated nerves. *Nature* (431):191-195.
- Court, F.A., Brophy, P.J., Ribchester, R.R. 2008. Remodelling of motor nerve terminals in demyelinating axons of periaxin-null mice. *Glia* 56(4): 471-479.
- Craig, T.J., Henley, J.M. 2012. Protein sumoylation in spine structure and function. *Curr Opin Neurobiol* 22: 480-487.
- Davis, J.L., Pico, R.M., Flood, J.F. 1987. Differences in learning between hyperprolinemic mice and their congenic controls. *Behav Neural Biol* 48(1): 128-137.
- Decker, L., Desmarquet-Trin-Dinh, C., Taillebourg, E., Ghislain, J., Vallat, J.M., Charnay, P. 2006. Peripheral myelin maintenance is a dynamic process requiring constant Krox20 expression. *J Neurosci* 26(38): 9771-9779.c
- Delague, V., Bareil, C., Tuffery, S., Bouvagnet, P., Chouery, E., Koussa, S., Maisonobe, T., Loiselet, J., Megarbane, A., Claustres, M. 2000. Mapping of a new locus for autosomal recessive demyelinating Charcot-Marie-Tooth disease to 19q13.1-13.3 in a large consanguineous Lebanese family: exclusion of MAG as a candidate gene. *Am J Hum Genet* 67: 236-243.
- De Morrée, A., Droog, M., Grand Moursel, L., Bisschop, I.J., Impagliazzo, A., Frants, R.R., Klooster, R., van der Maarel, S.M. 2012. Self-regulated alternative splicing at the AHNAK locus. *FASEB J* 26:93-103.

- Dengler, V.L., Galbraith, M., Espinosa, J.M. 2014. Transcriptional regulation by hypoxia inducible factors. *Crit Rev Biochem Mol Biol* 49(1): 1-15.
- Desterro, J.M., Thomson, J., Hay, R.T. 1997. Ubch9 conjugates SUMO but not ubiquitin. *FEBS Lett* 417:297-300.
- Desterro, J.M., Rodriguez, M.S., Hay, R.T. 1998. SUMO-1 modification of I $\kappa$ B $\alpha$  inhibits NF- $\kappa$ B activation. *Mol Cell* 2:233-239.
- Digiacomio, V., Gando, I.A., Venticinqu, L., Hurtado, A., Meruelo, D. 2015. The transition of the 37-kDa laminin receptor (RPSA) to higher molecular weight species: Sumoylation or artifact? *Cell Mol Biol Letters* 20(4): 571-585.
- Dmitriev, L.F., Dugin, S.F. 2007. Aldehydes and disturbance of carbohydrate metabolism: some consequences and possible approaches to its normalization. *Arch Physiol Biochem* 113(2):87–95.
- Dong, Z., Sinanan, A., Parkinson, D., Parmantier, E., Mirsky, R., Jessen, K.R. 1999. Schwann cell development in embryonic mouse nerves. *J. Neurosci Res* 56: 334– 348.
- Dorval, V., Fraser, P.E. 2006. Small ubiquitin-like modifier (SUMO) modification of natively unfolded proteins tau and  $\alpha$ -synuclein. *J Biol Chem* 281: 9919-9924.
- Drews, G., Krippeit, P., Düfer, M. 2010. Oxidative stress and beta-cell dysfunction. *Eur J Physiol* 460: 703-718.
- Du, X.L., Edelstein, D., Rossetti, L., Fantus, I.G., Goldberg, H., Ziyadeh, F. 2000. Hyperglycemia-induced mitochondrial superoxide overproduction activates the hexosamine pathway and induces plasminogen activator inhibitor-1 expression by increasing Sp1 glycosylation. *Proc Natl Acad Sci USA* 97(22):12222-12226.
- Dubby, J.J., Campbell, R.K., Setter, S.M., White, J.R., Rasmussen, K.A. 2004. Diabetic neuropathy: an intensive review. *Am J Health Syst Pharm* 61:160-173.
- Duprez, E., Saurin, A.J., Desterro, J.M., Lallman-Breitenbach, V., Howe, K., Boddy, M.N., Solomon, E., de The, H., Hay, R.T., Fremont, P.S. 1999. SUMO-1 modification of the acute promyelocytic leukaemia protein: PML implications for nuclear localization. *J Cell Sci* 112: 381-393.
- Dvornik, D. 1987. Aldose reductase inhibition: an approach to the prevention of diabetic complications. McGraw-Hill, Inc. New York.
- Dyck, P.J., Zimmerman, B.R., Vilen, T.H., Minnerath, S.R., Karnes, J.L., Yao, J.K., Poduslo, J.F. 1988. Nerve glucose, fructose, sorbitol, myo-inositol and fiber degeneration and regeneration in diabetic neuropathy. *N Engl J Med* 319: 542-548.
- Dyck, P.J., Thomas, P.K. 2005. *Peripheral Neuropathy*. Elsevier Saunders.
- Dyken, J.A., Jamieson, J., Marroquin, L., Nadanaciva, S., Billis, P.A., Will, Y. 2008. Biguanide-induced mitochondrial dysfunction yields increased lactate production and cytotoxicity of aerobically-poised HepG2 cells and human hepatocytes *in vitro*. *Toxic Appl Pharm* 233(2): 203-210.
- Dytrych, L., Sherman, D.L., Gillespie, C.S., Brophy, P.J. 1998. Two PDZ domain proteins encoded by the murine periaxin gene are the result of alternative intron retention and are differentially targeted in Schwann cells. *J Biol Chem* 273:5794-5800.
- Edwards, J.L., Vincent, A.M., Cheng, H.T., Feldman, E.L. 2008. Diabetic neuropathy: Mechanisms to management. *Pharm Therap* 120(1): 1-34.
- Eichberg, J. 2002. Protein kinase C changes in diabetes: is the concept relevant to neuropathy? *Int Rev Neurobiol* 50:61-82.

- Espejo, E.F. 1997. Structure of the mouse behaviour on the elevated plus-maze test of anxiety. *Behav Brain Res* 86: 105-112.7
- Espinosa de los Monteros, A., Kumar, S., Zhao, P., Huang, C.J., Nazarian, R., Pan, T., Scully, S., Chang, R., de Vellis, J. 1999. Transferrin is an essential factor for myelination. *Neurochem Res* 24: 235-248.
- Fan, J., Ren, H., Fei, E., Jia, N., Ying, Z., Jiang, P., Wu, M., Wang, G. 2008. Sumoylation is critical for DJ-1 to repress p53 transcriptional activity. *FEBS Letters* 582(7): 1151-1156.
- Feldman, E.L., Nave, K.A., Jensen, T.S., Bennett, D.L.H. 2017. New horizons in diabetic neuropathy: mechanisms, bioenergetics, and pain. *Neuron* 93(6):1296-1313.
- Felig, P. 1973. The glucose-alanine cycle. *Metabolism* 22(2): 179-207.
- Feligioni, M., Nistico, R. SUMO: a (oxidative) stressed protein. 2013. *Neuromol Med* 15(4):707-719.
- Feltri, M.L., Graus, P.D., Previtali, S.C. 2002. Conditional disruption of beta 1 integrin in Schwann cells impedes interactions with axons. *J Cell Biol* 156:199-209.
- Feltri, M.L., Wrabetz, L. 2005. Laminins and their receptors in Schwann cells and hereditary neuropathies. *J Peripher Nerv Syst* 10:128-143.
- Fernandez-Valle, C., Fregein, N., Wood, P.M., Bunge, M.B. 1993. Expression of the protein zero myelin gene in axon-related Schwann cells is linked to basal lamina formation. *Development* 119: 867-880.
- Fernandez-Valle, C., Gorman, D., Gomez, A.M., Bunge, M.B. 1997. Actin plays a role in both changes in cell shape and gene-expression associated with Schwann cell myelination. *J Neurosci* 17: 241-250.
- Figliomeni, B., Bacci, B., Panozzo, C., Fogarolo, F., Triban, C., Fiori, M.G. 1992. Experimental diabetic neuropathy. Effect of ganglioside treatment on axonal transport of cytoskeletal proteins. *Diabetes* 41(7): 866-871.
- Fiorentino, T.V., Prioleta, A., Zuo, P., Folli, F. 2013. Hyperglycemia-induced oxidative stress and its role in diabetes mellitus related cardiovascular diseases. *Curr Pharm Des* 19(32): 5695-5703.
- Firth, J.D., Ebert, B.L., Pugh, C.W., Ratcliffe, P.J. 1994. Oxygen-regulated control elements in the phosphoglycerate kinase 1 and lactate dehydrogenase A genes: similarities with the erythropoietin 3'enhancer. *Proc Natl Acad Sci USA* 91: 6496-6500.
- Fredriksson, A., Stigsdotter, I.M., Hurtig, A., Kvist, B.E., Archer, T. 2011. Running wheel activity restores MPTP-induced functional deficits. *J Neur Transm* 118: 407-420.
- Friede, R.L. 1972. Control of myelin formation by axon calibre (with a model of the control mechanism). *J Comp Neurol* 144: 233.252.
- Gabriel, A.F., Marcus, M.A., Honig, W. M., Walenkamp, G.H., Joosten, E.A. 2007. The CatWalk method: A detailed analysis of behavioural changes after acute inflammatory pain in the rat. *J Neuro Meth* 163: 9-16.
- Gabriely, I., Yang X.M., Cases, J.A., Ma, X.H., Rossetti, L., Barzilai, N. 2002. Hyperglycemia induces PAI-1 gene expression in adipose tissue by activation of the hexosamine biosynthetic pathway. *Athero* 160(1): 115-122.
- Galer, B.S., Gianas, A., Jensen, M.P. 2000. Painful diabetic polyneuropathy: epidemiology, pain description, and quality of life. *Diabet Res Clin Pract* 47(2): 123-128.
- Garbay, B., Heape, A. M., Sargueil, F., Cassagne, C. 2000. Myelin synthesis in the peripheral nervous system. *Prog Neurobiol* 61: 267-304.

- Geiss-Friedlander, R., Melchior, F. 2007. Concepts in sumoylation: a decade on. *Nat Rev Mol Cell Biol* 8: 947-956.
- Giacco, F., Brownlee, M. 2010. Oxidative stress and diabetic complications. *Circ Res* 107(9):1058–1070.
- Gillespie, C.S., Sherman, D.L., Blair, G.E., Brophy, P.J. 1994. Periaxin, a novel protein of myelinating Schwann cells with a possible role in axonal ensheathment. *Neuron* 12:497-508.
- Gillespie, C.S., Lee, M., Fantes, J.F., Brophy, P.J. 1997. The gene encoding the Schwann cell protein periaxin localizes on mouse chromosome 7 (Prx). *Genomics* 41: 297-298.
- Gillespie, C.S., Sherman, D.L., Fleetwood-Walker, S.M., Cotrell, D.F., Tait, S., Garry, E.M., Wallace, V.C., Ure J., Griffiths, I.R., Smith, A., Brophy, P.J. 2000. Peripheral demyelination and neuropathic pain behavior in Periaxin-deficient mice. *Neuron* 26(2):523-531.
- Girard, M., Goossens, M. 2006. Sumoylation of the SOX10 transcription factor regulates its transcriptional activity. *FEBS Letters* 580(6): 1635-1641.
- Gordois, A., Scuffham, P., Shearer, A., Oglesby, A., Tobian, J.A. 2003. The health care costs of diabetic peripheral neuropathy in the US. *Diabetes Care* 26:1790-1795.
- Gough, D.R., Cotter, T.G. 2011. Hydrogen peroxide: a Jekyll and Hyde signalling molecule. *Cell Death Dis* 6(2):e213.
- Greene, D.A., Lattimer, S.A., Sima, A.A. 1987. Sorbitol, phosphoinositides and sodium-potassium-ATPase in the pathogenesis of diabetic complications. *N Engl J Med* 316: 599-606.
- Greene, D.A., Sima, A.A., Stevens, M.J., Feldman, E.L., Lattimer, S.A. 1992. Complications: neuropathy, pathogenetic considerations. *Diabetes Care* 15: 1902-1925.
- Gu, J., Royland, J.E., Wiggins, R.C., Konat, G.W. 1997. Selenium is required for normal upregulation of myelin genes in differentiating oligodendrocytes. *J Neurosci Res* 47: 626-635.
- Guilbot, A., Williams, A., Ravise, N., Verny, C., Brice, A., Sherman, D.L., Brophy, P.J., LeGuern, E., Delague, V., Bareil, C., Megarbane, A., Claustres, M. 2001. A mutation in periaxin is responsible for CMT4F, an autosomal recessive form of Charcot-Marie-Tooth disease. *Hum Mol Genet* (10):415-421.
- Guo, T., Zhang, L., Xiao, H., Yang, Y., Shi, Y. 2020. Ezrin interacts with L-periaxin by the head to head and tail to tail mode and influences the location of L-periaxin in Schwann cell RSC96. *Biochim Biophys Acta Gen Subj* 1864(4): 1-14.
- Gupta, M.K., McLendon, P.M., Gulick, J., James, J., Khalili, K., Robbins, J. 2016. Ubc9-mediated sumoylation favorably impacts cardiac function in compromised hearts. *Circ Res* 118(12): 1894-1905.
- Ha, H., Hwang, I.A., Park, J.H., Lee, H.B. 2008. Role of reactive oxygen species in the pathogenesis of diabetic nephropathy. *Diabet Res Clin Pract* 82(1): S42-S45.
- Han, X.J., Lu, Y.F., Li, S.A., Kaitsuka, T., Sato, Y., Tomizawa, K., Nairn, A. C., Takei, K., Matsui, H., Matsushita, M. 2008. CaM kinase I alpha-induced phosphorylation of Drp1 regulates mitochondrial morphology. *J Cell Biol* 182: 573-585.

- Han, H., Kursula, P. 2014. Periaxin and Ahnak nucleoprotein 2 form intertwined homodimers through domain swapping. *J Biol Chem* 289:14121-14131.
- Hanson, P., Schumacker, P., Debugne, T., Clerin, M. 1992. Evaluation of somatic and autonomic small fibers neuropathy in diabetes. *Am J Phys Med Rehabil* 71: 44-47.
- Harding, A.E., Thomas, P.K. 1980. The clinical features of hereditary motor and sensory neuropathy types I and II. *Brain* 103: 259-280.
- Hay, R.T. 2007. SUMO-specific proteases: a twist in the tail. *Trends Cell Biol* 17: 370-376.
- Hayashi, N., Shirakura, H., Uehara, T., Nomura, Y. 2006. Relationship between SUMO-1 modification of caspase-7 and its nuclear localization in human neuronal cells. *Neurosci Lett* 397: 5-9.
- He, X., Lai, Q., Chen, C., Li, N., Sun, F., Huang, W., Zhang, S., Yu, Q., Yang, P., Xiong, F., Chen, Z., Gong, Q., Ren, B., Wenig, J., Eizirik, D.L., Zhou, Z., Wang, C.Y. 2018. Both conditional ablation and overexpression of E2 SUMO-conjugating enzyme (UBC9) in mouse pancreatic beta cells result in impaired beta cell function. *Diabetol* 61: 881.895.
- Hellmuth, C., Kirchberg, F.F., Lass, N., Harder, U., Peissner, W., Koletzko, B., Reinehr, T. 2016. Tyrosine is associated with insulin resistance in longitudinal metabolomic profiling of obese children. *J Diabetes Res* 2016:2108909.
- Hendriks, I.A., Souza, R.C., Yang, B., Vries, M.V., Mann, M., Vertegaal, A.C. 2014. Uncovering global sumoylation signaling networks in a site-specific manner. *Nat Struct Mol Biol* 21: 927-936.
- Henley, J.M., Craig, T.J., Wilkinson, K.A. 2014. Neuronal sumoylation: mechanisms, physiology, and roles in neuronal dysfunction. *Physiol Rev* 94: 1249-1285.
- Herrmann, D.N., Griffin, J.W., Hauer, P., Cornblath, D.R., McArthur, J.C. 1999. Epidermal nerve fiber density and sural nerve morphometry in peripheral neuropathies. *Neurol* 53: 1634-1640.
- Hinder, L.M., Vivekanandan-Giri, A., McLean, L.L., Pennathur, S., Feldman, E.L. 2013. Decreased glycolytic and tricarboxylic acid cycle intermediates coincide with peripheral nervous system oxidative stress in a murine model of type 2 diabetes. *J Endocrinol* 216(1):1-11.
- Hipkiss, A., Preston, J., Himsworth, D., Worthington, V., Keown, M., Abbott, N. 1998. Pluripotent protective effects of carnosine, a naturally-occurring dipeptide. *Ann New York Acad Sci* 854(1): 37-53.
- Hirota, K., Semenza, G.L. 2001. Rac1 activity is required for the activation of hypoxia-inducible factor 1. *J Biol Chem* 276(24): 21166-21172.
- Hochstrasser, M. 2001. SP-RING for SUMO: new functions bloom for a ubiquitin-like protein. *Cell* 107:5-8.
- Honkanen H., Lahti, O., Nissinen, M., Myllyla, R.M., Kangas, S., Paivalainen, S., Alanne, M.H., Peltonen S., Peltonen, J., Heape A.M. 2007. Isolation, purification and expansion of myelination-competent, neonatal mouse Schwann cells. *Eur. J. Neurosci.* 26: 953-964.
- Hsiao, G., Chapman, J., Ofrecio, J.M., Wilkes, J., Resnik, J.L., Thapar, D. 2011. Multi-tissue, selective PPAR $\gamma$  modulation of insulin sensitivity and metabolic pathways in obese rats. *Am J Physiol Endocrinol Metab* 300:E164-E174.
- Huang, T.J., Price, S.A., Chilton, L., Calcutt, N.A., Tomlinson, D.R., Verkhatsky, A., Fernyhough, P. 2003. Insulin prevents depolarization of the mitochondrial inner membrane in sensory neurons to type 1 diabetic rats in the presence of sustained hyperglycemia. *Diabetes* 52:2129-2136.
- Huang, Y., Zhou, M., Sun, H., Wang, Y. 2011. Branched-chain amino acid metabolism in heart disease: an epiphenomenon or a real culprit? *Cardiovasc Res* 90: 220-223.

- Imwalle, D.B., Gustafsson, J.A., Rissmann, E.F. 2005. Lack of functional estrogen receptor beta influences anxiety behaviour and serotonin content in female mice. *Physiol Behav* 84: 157-163.
- Iommarini, L., Porcelli, A.M., Gasparre, G., Kurelac, I., 2017. Non-canonical mechanisms regulating hypoxia-inducible factor 1 alpha in cancer. *Front Oncol* 7:286.
- Itani, S., Ruderman, N., Schmieder, F., Boden, G. 2002. Lipid-induced insulin resistance in human muscle is associated with changes in diacylglycerol, protein kinase C, and I $\kappa$ B- $\alpha$ . *Diabetes* 51: 2005-2011.
- Iwai, K., Yamanaka, K., Kamura, T., Minato, N., Conaway, R.C., Conaway, J.W., Klausner, R.D., Pause, A. 1999. Identification of the von Hippel-Lindau tumor-suppressor protein as part of an active E3 ubiquitin ligase complex. *Proc Natl Acad Sci USA* 96(22):12436-12441.
- Janssen, K., Hofmann, T.G., Jans, D.A., Hay, R.T., Schulze-Osthoff, K., Fischer, U. 2006. Apoptin is modified by SUMO conjugation and targeted to promyelocytic leukemia protein nuclear bodies. *Oncogene* 26: 1557-1566.
- Jentsch, S., Pyrowolakis, G. 2000. Ubiquitin and its kin: how close are the family ties? *Trends Cell Biol* 10:335-342.
- Jessen, K.R., Mirsky, R. 2005. The origin and development of glial cells in peripheral nerves. *Nat. Rev. Neurosci.* 6:671-682.
- Johnson, E.S., Blobel, G. 1997. Ubc9p is the conjugating enzyme for the ubiquitin-like protein Smt3p. *J Biol Chem* 272:26799-26802.
- Johnson, E.S., Schweinhorst, I., Dohmen, R.J., Blobel, G. 1997. The ubiquitin-like protein Smt3p is activated for conjugation to other proteins by an Aos1p/Uba2p heterodimer. *EMBO J* 16:5509-5519.
- Johnson, T.O., Ermolieff, J., Jirousek, M.R. 2002. Protein tyrosine phosphatase 1B inhibitors for diabetes *Nature Rev Drug Discov* 1: 696-709.
- Johnson, E. S. 2004. Protein modification by SUMO. *Annu Rev Biochem* 73: 355-382.
- Johnstone, M., Gearing, A.J., Miller, K.M. 1999. A central role for astrocytes in the inflammatory response to  $\beta$ -amyloid; chemokines, cytokines and reactive oxygen species are produced. *J Neuroimm* 93(1-2): 182-193.
- Judzewitsch, R.J., Jaspan, J.B., Polonsky, K.S., Weinberg, C.R., Halter, J.B., Halar, E., Pfeifer, M.A., Vukadinovic, C., Bernstein, L., Schneider, M. 1983. Aldose reductase inhibition improves motor nerve conduction velocity in diabetic patients *N Engl J Med* 308: 119-125.
- Kabzinska, D., Drac, H., Sherman, D.L., Kostera-Pruszczyk, A., Brophy, P.J., Kochanski, A., Hausmanowa-Petrusewicz. 2006. Charcot-Marie-Tooth type 4F disease caused by S399fsx410 mutation in the PRX gene. *Neurol* 66: 745-747.
- Kador, P. F., Sharpless, N.E., Kinoshita, J.H. 1985. Perspective series: aldose reductase inhibitors: a potential new class of agents for the pharmacological control of certain diabetic complications. *J Med Chem* 28: 841-849.
- Kagey, M.H., Melhuish, T.A., Wotton, D. 2003. The polycomb protein Pc2 is a SUMO E3. *Cell* 113:127-137.
- Kamitani, T., Kito, K., Nguyen, H.P., Fukuda-Kamitani, T., Yeh, E.T. 1998 Characterization of a second member of the Sentrin family of Ubiquitin-like proteins. *J Biol Chem* 273:11349-11353.
- Kanngiesser, M., Mair, N., Lim, H.Y. Zschiebsch, K., Blees, J., Häussler, A., Brüne, B., Ferreiros, N., Kress, M., Tegeder, I. 2014. Hypoxia-inducible factor 1 regulates heat and cold pain sensitivity and persistence. *Antioxid Redox Signal* 20(16):2555-2571.

- Kawanashi, K., Ueda, H., Moriyasu, M. 2003. Aldose reductase inhibitors from the nature. *Curr Med Chem* 10(15): 1353-1374.
- Keij, J. F., Prince, C.B., Steinkamp, J.A. 2000. Staining of mitochondrial membranes with 10-nonyl acridine orange MitoFluor Green, and Mito Tracker Green is affected by mitochondrial membrane potential altering drugs. *Cytometry* 39: 203-210.
- Kelley, D.E., He, J., Menshikova, E.V., Ritov, V.B. 2002. Dysfunction of mitochondria in human skeletal muscle in type 2 diabetes. *Diabetes* 51(10): 2944-2950.
- Kennedy, W.R., Wendelschafer-Crabb, G., Johnson, T. 1996. Quantitation of epidermal nerves in diabetic neuropathy. *Neurol* 47: 1042-1048.
- Kijima, K., Numakura, C., Shirahata, E., Sawaishi, Y., Shimohata, M., Igarashi, S., Tanaka, T., Hayasaka, K. 2004. Mutation causes early-onset but slow-progressive Charcot-Marie-Tooth disease. *J Hum Genet* 49:376-379.
- Kim, J.K. 2006. Fat uses a TOLL-road to connect inflammation and diabetes. *Cell Metab* 4: 417-419.
- Kim, H.K., Par, S.K., Zhou, J.L., Tagliatela, G., Chung, K., Coggeshall, R.E. 2004. Reactive oxygen species (ROS) play an important role in a rat model of neuropathic pain. *Pain* 111(1-2):116-124.
- Kim, H.A., Mindos, T., Parkinson, D.B. 2013. Plastic fantastic: Schwann cells and repair of the peripheral nervous system. *Stem Cells Transl Med* 2(8): 553-557.
- Kim, S, Maynard, J.C., Sasaki, Y., Strickland, A., Sherman, D.L., Brophy, P.J., Burlingame, A.L., Milbrandt, J. 2016. Schwann Cell O-GlcNAc Glycosylation is required for myelin maintenance and axon integrity. *J Neurosci* 36(37): 9633-9646.
- Kioussi, C., Gross, M.K., Gruss, P. 1995. Pax3: a paired domain gene as a regulator in PNS myelination. *Neuron* 15: 553-562.
- Kleitman, N., Wood, P.M., Bunge, R.P. 1997. Tissue culture methods for the study of myelination. W.M. Cowan, T.M. Jessell, S.L. Zipursky (Eds.), *Molecular and cellular approaches to neural development*, Oxford University Press, New York Oxford, 337-377.
- Koeck, T., Corbett, J.A., Crabb, J.W., Stuehr, D.J., Aulak, K.S. 2009. Glucose-modulated tyrosine nitration in beta cells: targets and consequences. *Archiv Biochem and Biophys* 484(2):221-231.
- Koenig, H.L., Schumacher, M., Ferzaz, B., Thi, A.N., Ressouches, A., Guennoun, R., Jung-Testas, I., Robel, P., Akwa, Y., Baulieu, E.E. 1995. Progesterone synthesis and myelin formation by Schwann cells. *Science* 268: 1500-1503.
- Komgut, L., Ma, C.H., Martinez, J.A., Toth, C.C., Guo, G.F., Singh, V. 2012. Overexpression of human HSP27 protects sensory neurons from diabetes. *Neurobiol Dis* 47(3): 436-443.
- Koulmanda, M., Qipo, A., Chebrolu, S., O'Neil, J., Auchincloss, H., Smith, R.N. 2003. The effect of low versus high dose of streptozotocin in cynomolgus monkeys (*Macaca fascicularis*). *Am J Transplant* 3: 267-272.
- Kromer, L.F., Cornbrooks, C.J. 1985. Transplants of Schwann cell cultures promote axonal regeneration in the adult mammalian brain. *Proc Natl Aca Sci USA* 82: 6330-6334.
- Kumar, A., Zhang, K.Y. 2015. Advances in the development of SUMO specific protease (SENPs) inhibitors. *Comp Struct Biotech J* 13: 204-211.
- Kursula, P. 2008. Structural properties of proteins specific to the myelin sheath. *Amino Acids* 34:175-185.

- Kurosaka, M., Naito, H., Ogura, Y., Kojima, A., Goto, K., Katamoto, S. 2009. Effects of voluntary wheel running on satellite cells in the rat plantaris muscle. *J Sports Sci Med* 8(1): 51-57.
- Kushnareva, Y., Murphy, A.N., Andreyev, A. 2002. Complex I-mediated reactive oxygen species generation: modulation by cytochrome c and NAD(P)<sup>+</sup> oxidation-reduction state. *Biochem J* 368(2): 545-553.
- Lacomis, D. 2002. Small-fiber neuropathy. *Muscle Nerve* 26: 173-188.
- Lashin, O.M., Szweda, P.A., Szweda, L.I., Romani, A.M. 2006. Decreased complex II respiration and HNE-modified SDH subunit in diabetic heart. *Free Radic Biol Med* 40(5): 886-896.
- Layman, D.K. 2003. The role of leucine in weight loss diets and glucose homeostasis. *J Nutr* 133: 261S-267S.
- Lee, Y.J., Mou, Y., Maric, D., Klimanis, D., Auh, S., Hallenbeck, J.M. 2011. Elevated global sumoylation in Ubc9 transgenic mice protects their brains against focal cerebral ischemic damage. *PLoS ONE* 6(10): e25852.
- Lee, C.C., Perkins, B.A., Kayaniyil, S., Harris, S.B., Retnakaran, R., Gerstein, H.C., Zinman, B., Hanley, A.J. 2015. Peripheral neuropathy and nerve dysfunction in individuals at high risk for type 2 diabetes: The Promise cohort. *Diabetes Care* 38: 793-800.
- Leiter, E.H. 1982. Multiple low-dose streptozotocin-induced hyperglycemia and insulinitis in C57BL mice: influence of inbred background, sex, and thymus. *Proc Natl Acad Sci USA* 79(2): 630-634.
- Lenzen, S. 2008. The mechanisms of alloxan- and streptozotocin-induced diabetes. *Diabetol* 51: 216-226.
- Leone, D., Genoud, S., Atanasoski, S., Grausenburger, R., Berger, P., Metzger, D., Macklin, W.B., Chambon, P., Suter, U. 2003. Tamoxifen-inducible glia-specific Cre mice for somatic mutagenesis in oligodendrocytes and Schwann cells. *Mol Cell Neurosci* 22: 430-440.
- Lepore, G., Zedda, M., Gadau, S., Farina, V. 2003. Purified Schwann cell primary cultures from mouse and rat sciatic nerve. *Arch Ital Biol* 141: 207-210.
- Lewandoski, M. 2001. Conditional control of gene expression in the mouse. *Nat Rev Genet* 2:743-755.
- Li, M., Guo, D., Isales, C.M., Elzirik, D.L., Atkinson, M., She, J.X., Wang, C.Y. 2005. SUMO wrestling with type 1 diabetes. *J Mol Med* 83: 504-513.
- Li, X., Lee, Y.K., Jeng, J.C., Yen, Y., Schultz, D.C., Shih, H.M., Ann, D.K. 2007. Role for KAP1 Serine 824 phosphorylation and sumoylation/desumoylation switch in regulating KAP1-mediated transcriptional repression. *J Biol Chem* 282: 36177-36189.
- Li, X., Luo, Y., Yu, L., Lin, Y., Luo, D., Zhang, H., He, Y., Kim, Y.O., Kim, Y., Tang, S., Min, W. 2008. SENP1 mediates TNF-induced desumoylation and cytoplasmic translocation of HIPK1 to enhance ASK1-dependent apoptosis. *Cell Death Differ* 15: 739-750.
- Lin, X., Liang, M., Liang, Y.Y., Brunicardi, F.C., Feng, X.H. 2003. SUMO-1/Ubc9 promotes nuclear accumulation and metabolic stability of tumor suppressor Smad4. *J Biol Chem* 278:31043-31048.
- Liu, Z., Jeppesen, P.B., Gregersen, S., Larsen, L.B., Hermansen, K. 2016. Chronic exposure to proline causes aminoacidotoxicity and impaired beta-cell function: Studies in vitro. *Rev Diabet Stud* 13(1): 66-78.
- Liu, F.Y., Liu, Y.F., Yang, Y., Luo, Z.W., Xiang, J.W., Cheng, Z.G., Qi, R.L., Yang, T.H., Xiao, Y., Qing, W.J., Li, D.W. 2016. Sumoylation in neurological diseases. *Curr Mol Med* 16: 893-899.

- Luciani, A., Vilella, V.R., Vasaturo, A., Giardino, I., Raia, V., Mantovani, M.P., D'Apolito, M., Guido, S., Leal T., Quarantino, S., Maiuri, L. 2009. Sumoylation of tissue transglutaminase as link between oxidative stress and inflammation. *J Immunol* 183(4): 2775-2784.
- Lund, T.D., Rovis, T., Chung, W.C., Handa, R.J. 2005. Novel actions of estrogen receptor-beta on anxiety-related behaviours. *Endocrinol* 146: 797-807.
- Lupski, J.R., Garcia, C.A. 2001. Charcot-Marie-Tooth peripheral neuropathies and related disorders. The metabolic and molecular bases of inherited disease. McGraw-Hill, New York: 5759-5788.
- Ma, Q., Battelli, L., Hubbs, A.F. 2006. Multiorgan autoimmune inflammation, enhanced lymphoproliferation, and impaired homeostasis of reactive oxygen species in mice lacking the antioxidant-activated transcription factor Nrf2. *Amer J Pathol* 168(6): 1960-1974.
- Maclsaac, R.J., Jerums, G., Ekinci, E. 2017. Effects of glycaemic management on diabetic kidney disease. *World J Diabet* 8(5): 172-186.
- Malik, R.A., Tesfaye, S., Newrick, P.G., Walker, D., Rajbhandari, S.M., Siddique, I., Sharm, A.K., Boulton, A.J., King, R. H., Thomas, P.K. 2005. Sural nerve pathology in diabetic patients with minimal but progressive neuropathy. *Diabetol* 48: 578-585.
- Manent, J., Oguievetskaia, K., Bayer, J., Ratner, N., Giovannini, M. 2003. Magnetic cell sorting for enriching Schwann cells from adult mouse peripheral nerves. *J Neurosci Meth* 123: 167– 173.
- Manu, M.S., Rachana, K.S., Advirao, G.M. 2017. Altered expression of IRS2 and GRB2 in demyelination of peripheral neurons: Implications in diabetic neuropathy. *Neuropeptides* 62: 71-79.
- Marcinek, D.J. 2004. Mitochondrial dysfunction measured *in vivo*. *Act Phys Scand* 182(4): 343-352.
- Margolis, D., Malay, D.S., Hoffstad, O.J. 2011. Incidence of diabetic foot ulcer and lower extremity amputation among Medicare beneficiaries, 2006 to 2008. Data Poits #2, Agency for Healthcare Research and Quality, Rockville.
- Marshall, S., Bacote, V., Traxinger, R.R. 1991. Discovery of a metabolic pathway mediating glucose-induced desensitization of the glucose transport system. Role of hexosamine biosynthesis in the induction of insulin resistnace. *J Biol Chem* 5: 4706-4712.
- Martini, R. 2001. The effect of myelinating Schwann cells on axons. *Muscle Nerve* 24:456-466.
- Masaki, T., Matsumura, K. 2010. Biological role of Dystroglycan in Schwann cell function and its implications in peripheral nervous system diseases. *J Biomed Biotech* 2010:1-17.
- Masoud, G.N., Li, W. 2015. HIF-1 $\alpha$  pathway: role, regulation and intervention for cancer therapy. *Acta Pharm Sin B* 5(5):378-389.
- Martin, S., Wilkinson, K.A., Nishimune, A., Henley, J.M. 2007. Emerging extranuclear roles of protein SUMOylation in neuronal function and dysfunction. *Nat Rev Neurosci* 8: 948-959.
- Mathers, C.D., Loncar, D . 2006. Projections of global mortality and burden of disease from 2002 to 2030. *PLoS Med* 3(11):e442.
- Matsakas, A., Macharia, R., Otto, A., Elashry, M.I., Mouisel, E., Romanello, V. 2012. Exercise training attenuates the hypermuscular phenotype and restores skeletal muscle function in the myostatin null mouse. *Exp Physiol* 97(1): 125-140.
- Matunis, M.J., Coutavas, E., Blobel, G. 1996. A novel ubiquitin-like modification modulates the portioning of the Ran-GTPase-activating protein RanGAP1 between the cytosol and the nuclear pore complex. *J Cell Biol* 135:1457-1470.
- Mayrovitz, H.N., Larsen, P.B. 1996. Functional microcirculatory impairment: A possible source of reduced skin oxygen tension in human diabetes mellitus. *Microvasc Res* 52: 115-126.

- McArthur, J.C., Stocks, E.A., Hauer, P., Cornblath, D.R., Griffin, J.W. 1998. Epidermal nerve fiber density: normative reference range and diagnostic efficiency. *Arch Neuro* 55: 1513-1520.
- McCormack, S.E., Shaham, O., McCarthy, M.A., Deik, A.A., Wang, T.J. 2013. Circulating branched-chain amino acid concentrations are associated with obesity and future insulin resistance in children and adolescents. *Pediatr Obes* 8: 52-61.
- McDoniels-Silvers, A.L., Nimri, C.F., Stoner, G.D., Lubet, R.A., You, M. 2002. Differential gene expression in human lung adenocarcinomas and squamous cell carcinomas. *Clin Cancer Res* 8:1127-1138.
- Melchior, F. 2000. SUMO-Nonclassical Ubiquitin. *Annu.Rev, Cell Dev. Biol.* 16:591-626.
- Melchior, F., Schergaut, M., Pichler, A. 2003. SUMO: ligases, isopeptidases and nuclear pores. *Trends Biochem Sci* 28: 612-618.
- Meluh, P.B., Koshland, D. 1995. Evidence that the MIF2 gene of *Saccharomyces cerevisiae* encodes a centromere protein with homology to the mammalian centromere protein CENP-C. *Mol Biol Cell* 6: 793-807.
- Meulmeester, E., Melchior, F. 2008. SUMO. *Nature Cell Biol* 452:709-711.
- Mirsky, R., Jessen, K.R. 1996. Schwann cell development, differentiation and myelination. *Curr Opin Neurobiol* 6: 89-96.
- Mirsky, R., Woodhoo, A., Parkinson, D.B., Arthur-Farraj, P., Bhaskaran, A., Jessen, K.R. 2008. Novel signals controlling embryonic Schwann cell development, myelination and dedifferentiation. *J. Peripher. Nerv. Syst.* 13:122-135.
- Misur, I, Zarkovic, K., Barada, A., Batelja, L., Milicevic, Z., Turk, Z. 2004. Advanced glycation end products in peripheral nerve in type 2 diabetes with neuropathy. *Acta Diabetol* 41(4):158-166.
- Miyauchi, Y., Shikama, H., Takasu, T., Okamiya, H., Umeda, M., Hirasaki, E., Ohhata, I., Nakayama, H., Nakagawa, S. 1996. Slowing of peripheral motor nerve conduction was ameliorated by aminoguanidine in streptozocin-induced diabetic rats. *Eur J Endocrinol* 134(4):467-473.
- Mittal, M., Siddiqui, M.R., Tran, K., Reddy, S.P., Malik, A.B. 2014. Reactive oxygen species in inflammation and tissue injury. *Antiox Red Signal* 20(7): 1126-1167.
- Mizukami, Y., Kohgo, Y., Chung, D.C. 2007. Hypoxia inducible factor-1-Independent pathways in tumor angiogenesis. *Clin Cancer Res* 13(19): 5670-5674.
- Mogensen, M., Sahlin, K., Fernström, M., Glinborg, D., Vind, B.F., Beck-Nielsen, H. 2007. Mitochondrial respiration is decrease in skeletal muscle of patients with type 2 diabetes. *Diabetes* 56(6):1592-1599.
- Monk, K.R., Feltri, M.L., Taveggia, C. 2015. New insights on Schwann cell development. *Glia* 63: 1376-1393.
- Montanari, A., Simoni, I., Vallisa, D., Trifiro, A., Colla, R., Abbiati. 1998. Free amino acids in plasma and skeletal muscle of patients with liver cirrhosis. *Hepatology* 8: 1034-1039.
- Montell, C. 2000. A PDZ protein ushers in new links. *Nat Genet* 26: 6-7.
- Morgan, L., Jessen, K.R., Mirsky, R. 1991. The effects of cAMP on differentiation of cultured Schwann cells: Progression from an early phenotype (04+) to a myelin phenotype (P0+, GFAP-, N-CAM-, NGF-receptor-) depends on growth inhibition. *J Cell Biol* 112: 457-467.

- Moutal, A., Dustrude, E.T., Larnet-Milnes, T.M., Vanderah, T.W., Khanna, M., Khanna, R. 2018. Blocking CRMP2 sumoylation reverses neuropathic pain. *Mol Psych* 23: 2119-2121.
- Mukhopadhyah, D., Dasso, M. 2007. Modification in reverse: the SUMO proteases. *Trends Biochem Sci* 32: 286-295.
- Muller, S., Matunis, M.J., Dejean, A. 1998. Conjugation with the ubiquitin-related modifier SUMO-1 regulates the partitioning of PML within the nucleus. *EMBO J* 17: 61-70.
- Muller, S., Hoege, C., Pyrowolakis, G., Jentsch, S. 2001. SUMO, ubiquitin's mysterious cousin. *Nat Rev Mol Cell Biol* 2: 202-210.
- Munasamy, S., Saba H., Mitchell, T., Megyesi, J.K., Brock, R.W., MacMillan-Crow, L.A. 2009. Alteration of renal respiratory complex-III during experimental type-1 diabetes. *BMC Endoc Disord* 9:2.
- Murakami, T., Iwanaga, T., Ogawa, Y., Fujita, Y., Sato, E., Yoshitomi, H., Sunada, Y., Nakamura, A. 2013. Development of sensory neuropathy in streptozotocin-induced diabetic mice. *Brain Behav* 3: 35-41.
- Murphy, M.P. 2009. How mitochondria produce reactive oxygen species. *Biochem J* 417(1):1-13.
- Naccerdine, K., Lehembre, F., Bhaumik, M., Artus, J., Cohen-Tannoudji, M., Babinet, C., Pandolfi, P.P., Dejean, A. 2005. The SUMO pathway is essential for nuclear integrity and chromosome segregation in mice. *Develop Cell* 9(6): 769-779.
- Nave, K.A., Trapp, B.D. 2008. Axon-glia signaling and the glial support of axon function *Annu Rev Neurosci* 31: 535-561.
- Nave, K.A. 2010. Myelination and the trophic support of long axons. *Nat Rev Neurosci* 11: 275-283.
- Newgard, C.B., An, J., Brain, J.R., Muehlbauer, M.J., Stevens, R.D. 2009. A branched-chain amino acid-related metabolic signature that differentiates obese and lean humans and contributes to insulin resistance. *Cell Metab* 9: 311-326.
- Newsholme, P., Haber, E.P., Hirabara, S.M., Rebelato, E.L., Procopio, J., Morgan, D., Oliveira, H.C., Carpinelli, A.R., Curi, R. 2007. Diabetes associated cell stress and dysfunction: role of mitochondrial and non-mitochondrial ROS production and activity. *J Physiol* 583(1): 9-24.
- Nicholson, S.M., Gomes, D., De Nechaud, B., Bruzzone, R. 2001. Altered gene expression in Schwann cells of connexin32 knockout animals. *J Neurosci Res* 66: 23-36.
- Nishikawa, T., Edelstein, D., Du, X.L., Yamagishi, S., Matsumura, T., Kaneda, Y., Yorek, M.A., Beebe, D., Oates, P.J., Hammes, H.P., Giardino, I., Brownlee, M. 2000. Normalizing mitochondrial superoxide production blocks three pathways of hyperglucemic damage. *Nature* 404: 787-790.
- Niskanen, E.A., Palvimo, J.J. 2017. Chromatin sumoylation in heat stress: to protect, pause and organise? *Bioessays* 39(6): 1-10.
- Oates, P.J. 2002. Polyol pathway and diabetic peripheral neuropathy. *Int Rev Neurobiol* 50:325-392.
- Obrosova, I.G., Pacher, P., Szabó, C., Zsengeller, Z., Hirooka, H., Stevens, M.J., Yorek, M.A. 2005. Aldose reductase inhibition counteracts oxidative-nitrosative stress and poly(ADP-ribose) polymerase activation in tissue sites for diabetes complications. *Diabetes*.54(1):234-242.
- Okuma, T., Honda, R., Ichikawa, G., Tsumagari, N., Yasuda, H. 1999. In vitro SUMO-1 modification requires two enzymatic steps, E1 and E2. *Biochem Biophys Res Commun* 254:693-698.
- Ola, M.S., Berkich, D.A., Xu, Y., King, M.T., Gardner, T.W., Simpson, I. 2006. Analysis of glucose metabolism in diabetic rat retinas. *Am J Physiol Endocrinol Metab* 290(6): E1057-E1067.

- Pabbidi, R.M., Yu, S.Q., Peng, S., Khardori, R., Pauza, M.E., Premkumar, L.S. 2008. Influence of TRPV1 on diabetes-induced alterations in thermal pain sensitivity. *Mol Pain* 1(4):9.
- Palm, F., Cederberg, J., Hansell, P., Liss, P., Carlsson, P.O. 2003. Reactive oxygen species cause diabetes-induced decrease in renal oxygen tension. *Diabetol* 46: 1153-1160.
- Palm, F., Hansell, P., Ronquist, G., Waldenström, A., Liss, P., Carlsson, P.O. 2004. Polyol-pathway-dependent disturbances in renal medullary metabolism in experimental insulin-deficient diabetes mellitus in rats. *Diabetol* 47: 1223-1231.
- Pannunzio, M.E., Jou, I.M., Long, A., Wind, T.C., Beck, G., Balian, G. 2005. A new method of selecting Schwann cells from adult mouse sciatic nerve. *J Neurosci Meth* 149: 74–81.
- Pantaleon, M., Tan, H.Y., Kafer, G.R., Kaye, P.L. 2010. Toxic effects of hyperglycemia are mediated by the hexosamine signaling pathway and O-linked glycosylation in early mouse embryos. *Biol Reprod* 82(4): 751-758.
- Parkinson, D.B., Bhaskaran, A., Arthur-Farraj, P., Noon, L.A., Woodhoo, A., Lloyd, A.C., Feltri, M.L., Wrabetz, L., Behrens, A., Mirsky, R., Jessen, K.R. 2008. C-Jun is a negative regulator of myelination. *J Cell Biol* 181(4): 625-637.
- Pelicano, H., Zhang, W., Liu, J., Hammoudi, N., Dai, J., Xu, R.H., Pusztai, L., Huang, P. 2014. Mitochondrial dysfunction in some triple-negative breast cancer cell lines: role of mTOR pathway and therapeutic potential. *Breast Cancer Res* 16: 434.
- Pereira, A. P., Dias, C.E., Souza, L.O., Bitencourt, F., Mazzola, P.N., Coelho, J.G., Mescka, C.P., Dutra, C.S. 2015. Neonatal hyperglycemia induces oxidative stress in the rat brain: the role of pentose phosphate pathway enzymes and NADPH oxidase. *Mol Cell Biochem* 403: 159-167.
- Periquet, M.I., Novak, V., Collins, M.P., Nagaraja, H.N., Erdem, S., Nash, S.M., Freimer, M.L., Sahenk, Z., Kissel, J.T., Mendell, J.R. 1999. Painful sensory neuropathy: prospective evaluation using skin biopsy. *Neurol* 53: 1641-1647.
- Pichler, A., Gast, A., Seeler, J.S., Dejean, A., Melchior, F. 2002. The nucleoporin RanBP2 has SUMO1 E3 ligase activity. *Cell* 108:109-120.
- Piccolo, B.D., Graham, J.L., Stanhope, K.L., Fiehn, O., Havel, P.J., Adams, S.H. 2016. Plasma amino acid and metabolite signatures tracking diabetes progression in the UCD-T2DM rat model. *Am J Physiol Endocrinol Metab* 310(11): E958-E969.
- Poitelon, Y., Bogni, S., Matafora, V., Nunes, G.D., Hurley, E., Ghidinelli, M., Katzenellenbogen, B.S., Taveggia, C., Silvestri, N., Bachi, A., Sannino, A., Wrabetz, L., Feltri, M.L. 2015. Spatial mapping of juxtacrine axo-glial interactions identifies novel molecules in peripheral myelination. *Nature Commun* 6(8303): 1-13.
- Pollard J.D., Armati, P.J. 2011. CIDP-The relevance of recent advances in Schwann cell/axonal neurobiology. *J Peripher Nerv Syst.* 16(1): 15-23.
- Pop-Busui, R., Boulton, A.J., Feldman, E.L., Bril, V., Freeman, R., Malik, R.A., Sosenko, J.M., Ziegler, D. 2017. Diabetic neuropathy: A position statement by the American Diabetes Association. *Diabetes Care* 40: 136-154.
- Poot, M., Zhang, Y.Z., Krämer, J.A., Wells, K.S., Jones, L.J., Hanzel, D.K., Lugade, A.G., Singer, V.L., Haugland, R.P. 1996. Analysis of mitochondrial morphology and function with novel fixable fluorescent stains. *J Histochem Cytochem* 44(12): 1363-1372.
- Price, S.A., Agthong, S., Middlemas, A.B., Tomlinson, D.R. 2004. Mitogen-activated protein kinase p38 mediates reduced nerve conduction velocity in experimental diabetic neuropathy: interactions with aldose reductase. *Diabetes* 53: 1851-1856.

- Pugh, C.W., Ratcliffe, P.J. 2003. Regulation of angiogenesis by hypoxia: role of the HIF system. *Nature Medicine* 9: 677-684.
- Quinn, L.P., Stean, T.O., Trail, B., Duxon, M.S., Stratton, S.C., Billinton, A., Upton, N. 2003. Laboras™: Initial pharmacological validation of a system allowing continuous monitoring of laboratory rodent behaviour. *J Neuro Meth* 130(1): 83-92.
- Raasakka, A., Linxweiler, H., Brophy, P.J., Sherman, D.L., Kursula, P. 2019. Direct binding of the flexible C-terminal segment of Periaxin to beta4 integrin suggests a molecular basis for CMT4F. *Front Mol Neurosci* 12: 84.
- Rabbani, Z.N., Mi, J., Zhang, Y. 2010. Hypoxia inducible factor 1  $\alpha$  signalling in fractionated radiation induced lung injury: Role of oxidative stress and tissue hypoxia. *Radiat Res* 173:165-174.
- Rachana, K.S., Manu, M.S., Advirao, G.M. 2016. Insulin influenced expression of myelin proteins in diabetic peripheral neuropathy. *Neurosci Lett* 629: 110-115.
- Rains, J.L., Jain, S.K. 2011. Oxidative stress, insulin signalling, and diabetes. *Free radical biology and medicine* 50(5): 567-575.
- Rajashree, R., Kholkute, S.D., Goudar, S.S. 2011. Effects of duration of diabetes on behavioral and cognitive parameters in streptozotocin-induced juvenile diabetic rats. *Malays J Med Sci* 18(4): 26-31.
- Ray, P.D., Huang, B.W., Tsuji, Y. 2012. Reactive oxygen species (ROS) homeostasis and redox regulation in cellular signalling. *Cell Signal* 24(5): 981-990.
- Regenold, W.T., Phatak, P., Marano, C.M., Sassan, A., Conley, R.R., Kling, M.A. 2009. Elevated cerebrospinal fluid lactate concentrations in patients with bipolar disorder and schizophrenia: Implications for the mitochondrial dysfunction hypothesis. *Biol Psych* 65(6): 489-494.
- Renner, F., Moreno, R., Schmitz, M.L. 2010. Sumoylation-dependent localization of IKK $\epsilon$  in PML nuclear bodies is essential for protection against DNA-damage-triggered cell death. *Mol Cell* 37(4): 503-515.
- Rogers, T., Chandler, D., Angelicheva, D., Thomas, P.K., Youl, B., Tournev, I., Gergelcheva, V., Kalaydjieva, L. 2000. A novel locus for autosomal recessive peripheral neuropathy in the EGR2 region on 10q23. *Am J Hum Genet* 67:664-671.
- Rolo, A.P., Palmeira, C.M. 2006. Diabetes and mitochondrial function: role of hyperglycemia and oxidative stress. *Toxicol Appl Pharmacol* 212(2):167-178.
- Rossetti, L., Hawkins, M., Chen, W., Gindi, J., Barzilai, N. 1995. *In vivo* glucosamine infusion induces insulin resistance in normoglycemic but not in hyperglycemic conscious rats. *J Clin Invest* 96: 132-140.
- Rösen, P., Nawroth, P.P., King, G., Möller, W., Tritschler, H.J., Packer, L. 2001. The role of oxidative stress in the onset and progression of diabetes and its complications: a summary of a congress series sponsored by UNESCO-MCBN, the American Diabetes Association and the German Diabetes Society. *Diabetes/Metabolism Research and Reviews* 17: 189-212.
- Russell, J.W., Cheng, H.L., Feldman, E.L. 1998. Insulin-like growth factor-I (IGF-I) promotes neuronal myelination in peripheral sensory neurons (PSN). *Neurol* 50: A28-A29.
- Sacher, M., Pfander, B., Jentsch, S. 2005. Identification of SUMO-protein conjugates. *Methods Enzym* 399: 392-404.
- Saha, A.K., Xu, X.J., Lawson, E., Deoliveira, R., Brandon, A.E. 2010. Downregulation of AMPK accompanies leucine- and glucose- induced increases in protein synthesis and insulin resistance in rat skeletal muscle. *Diabetes* 59: 2426-2434.

- Sahin, U., The, H., Breitenbach, V.L. 2014. PML nuclear bodies: Assembly and oxidative stress-sensitive sumoylation. *Nucleus* 5(6): 499-507.
- Said, G., Goulon-Goeau, C., Slama, G., Tchobroutsky, G. 1992. Severe early-onset polyneuropathy in insulin-dependent diabetes mellitus: a clinical and pathological study. *The New England Journal of Medicine* 326:1257-1263.
- Salam, J.N., Fox, J.H., Detroy, E.M., Guignon, M.H., Wohl, D.F., Falls, W.A. 2009. Voluntary exercise in C57 mice is anxiolytic across several measures of anxiety. *Behav Brain Res* 197: 31-40.
- Salceda, S., Caro, J. 1997. Hypoxia-inducible factor 1 alpha (HIF-1alpha) protein is rapidly degraded by the ubiquitin-proteasome system under normoxic conditions. Its stabilization by hypoxia depends on redox-induced changes. *J Biol Chem* 272(36):22642-22647.
- Salzer, J.L. & Bunge, R.P. 1980. Studies of Schwann cell proliferation. I. An analysis in tissue culture of proliferation during development, wallerian degeneration, and direct injury. *J Cell Biol* 84:739-752.
- Sambrook, J., Russell, D.W. 2000. *Molecular cloning: A laboratory manual*. Cold Spring Harbor, NY Cold Spring Harbor Laboratory Press.
- Scherer, S.S., Xu, Y.T., Bannerman, P.G., Sherman, D.L., Brophy, P.J. 1995. Periaxin expression in myelinating Schwann cells: modulation by axon-glia interactions and polarized localization during development. *Development* (121):4265-4273.
- Scheschonka, A., Tang, Z., Betz, H. 2007. Sumoylation in neurons: nuclear and synaptic roles? *Trends Neurosci* 30: 85-91.
- Schmidt, D., Müller, S. 2002. Members of the PIAS family act as SUMO ligases for c-Jun and p53 and repress p53 activity. *Proc Natl Acad Sci USA* 99:2872-2877.
- Schratzberger, P., Walter, D.H., Rittig, K., Bahlmann, F.H., Pola, R., Curry, C., Silver, M., Krainin, J.G., Weinberg, D.H., Ropper, A.H., Isner, J.M. 2001. Reversal of experimental diabetic neuropathy by VEGF gene transfer. *J Clin Invest* 107(9):1083-1092.
- Schumacher, M., Guennoun, R., Mercier, G., Desarnaud, F., Lacor, P., Benavides, J., Ferzaz, B., Robert, F., Baulieu, E.E. 2001. Progesterone synthesis and myelin formation in peripheral nerves. *Bran Res Rev* 37: 343-359.
- Seeler, J.S., Dejean, A. 2003. Nuclear and unclear functions of SUMO. *Nat. Rev. Mol. Cell Biol.* 4:690-699.
- Seilheimer, B., Persohn, E., Schachner, M. 1989. Antibodies to the L1 adhesion molecule inhibit Schwann cell ensheathment of neurons in vitro. *J Cell Biol* 109:3095-3103.
- Semenza, G.L. 1998. Hypoxia-inducible factor 1: master regulator of O<sub>2</sub> homeostasis. *Curr Opin Genet Dev* 8:588-594.
- Shah, M.S., Brownlee, M. 2016. Molecular and cellular mechanisms of cardiovascular disorders in diabetes. *Circ Res* 118(11): 1808-1829.
- She, P., Reid, T.M., Bronson, S.K., Vary, T.C., Hajnal, A., Lynch, C.J. 2007. Disruption of BCATm in mice leads to increased energy expenditure associated with the activation of a futile protein turnover cycle. *Cell Metab* 6: 181-194.
- She, P., Van Horn, C., Reid, T., Hutson, S.M., Cooney, R.N., Lynch, C.J. 2007. Obesity-related elevations in plasma leucine are associated with alterations in enzymes involved in branched-chain amino acid metabolism. *Am J Physiol Endocrinol Metab* 293: E1552-E1563.
- Shen, Z., Pardington-Purtymun, P.E. Comeaux, J.C., Moyzis, R.K., Chen, D.J. 1996. UBL1, a Human Ubiquitin-like protein associating with human RAD51/RAD52 proteins. *Genomics* 36:11249-11353.

- Sherman, D.L. 1998. Regulation and developmental expression of periaxin in the peripheral nervous system. University of Edinburgh.
- Sherman, D.L., Brophy, P.J. 2000. A tripartite nuclear localization signal in the PDZ-domain protein L-periaxin. *J Biol Chem* 275(7):4537-4540.
- Sherman, D.L., Brophy, P.J. 2005. Mechanisms of axon ensheathment and myelin growth. *Nature Neurosci* 6:683-690.
- Sherman, D.L., Fabrizi, C., Gillespie, C.S., Brophy, P.J. 2001. Specific disruption of a Schwann cell dystrophin-related protein complex in a demyelinating neuropathy. *Neuron* (30):677-687.
- Sherman, D.L. 2008. Regulation and developmental expression of periaxin in the peripheral nervous system. University of Edinburgh, Preclinical Veterinary Sciences.
- Sherman, D.L., Wu, L.M.N., Grove, M., Gillespie, C.S., Brophy, P.J. 2012. Drp2 and Periaxin form cajal bands with dystroglycan but have distinct roles in Schwann cell growth. *J Neurosci* 32: 9419-9428.
- Shi, Y., Zhang, L., Yang, T. 2014. Nuclear export of L-periaxin, mediated by its nuclear export signal in the PDZ domain. *PLoS One* 9(3): e9153.
- Shiba, T., Inoguchi, T., Sportsman, J.R., Heath, W.F., Bursell, S., King, G.L. 1993. Correlation of diacylglycerol level and protein kinase C activity in rat retina to retinal circulation. *Am J Physiol* 265(5): E783-E793.
- Shinbo, Y. 2006. Proper SUMO-1 conjugation is essential to DJ-1 to exert its full activities. *Cell Death Differ* 13: 96-108.
- Shinomura, T., Asaoka, Y., Oka, M., Yoshida, K., Nishizuka, Y. 1991. Synergistic action of diacylglycerol and unsaturated fatty acid for protein kinase C activation: its possible implications. *PNAS* 88(12): 5149-5153.
- Sima, A.A., Nathaniel, V., Bril, V., McEwen, T.A., Greene, D.A. 1988. Histopathological heterogeneity of neuropathy in insulin-dependent and non-insulin-dependent diabetes, and demonstration of axo-glial dysjunction in human diabetic neuropathy. *J Clin Invest* 81: 349-364.
- Sima, A.A., Sugimoto, K. 1999. Experimental diabetic neuropathy: an update. *Diabetol* 42: 773-788.
- Singh, V.P., Bali, A., Singh, N., Jaggi, A. S. 2014. Advanced glycation end products and diabetic complications. *Korean J Physiol Pharmacol* 18(1): 1-14.
- Song, F., Jia, W., Yao, Y., Hu, X., Lei, L., Lin, J., Sun, X., Liu, L. 2007. Oxidative stress, antioxidant status and DNA damage in patients with impaired glucose regulation and newly diagnosed type 2 diabetes. *Clin Sci* 112(12): 599-606.
- Srinivasan, S., Stevens, M., Wiley, J.W. 2000. Diabetic peripheral neuropathy: evidence for apoptosis and associated mitochondrial dysfunction. *Diabetes* 49: 1932-1938.
- Stadtman, E.R. 2001. Protein oxidation in aging and age-related diseases. *Annals of the New York Academy of Sciences* 928:22-38.
- Steffan, J.S., Agarwal, N., Pallos, J., Rockabrand, E., Trotman, L.C., Slepko, N., Illes, K., Lukacsovich, T., Zhu, Y.Z., Cattaneo, E., Pandolfi, P.P., Thompson, L.M., Marsh, J.L. *Science* 304(5667): 100-104.
- Sternsdorf, T., Jensen, K., Will, H. 1997. Evidence for covalent modification of the nuclear dot-associated proteins PML and Sp100 by PIC1/SUMO-1. *J Cell Biol* 139: 1621-1634.
- Stewart, H.J., Bradke, F., Taberner, A., Morrell, D., Jessen, K.R., Mirsky, R. 1996. Regulation of rat Schwann cell P0 expression and DNA synthesis by insulin-like growth factors in vitro. *Eur J Neurosci* 8: 553-564.

Stewart, W.F., Ricci, J.A., Chee, E., Hirsch, A.G., Brandenburg, N.A. 2007. Lost productive time and costs due to diabetes and diabetic neuropathic pain in the US workforce. *J Occup Environ Med* 49: 672-679.

Su, X., Han, X., Mancuso, D.J., Abendschein, D.R., Gross, R.W. 2005. Accumulation of long-chain acylcarnitine and 3-hydroxy acylcarnitine molecular species in diabetic myocardium: identification of alterations in mitochondrial fatty acid processing in diabetic myocardium by shotgun lipidomics. *Biochem* 44: 5234-5245.

Sun, X.X., Chen, Y., Su, Y., Wang, X., Chauhan, K.M., Liang, J., Colin, J.D., Sears, R.C., Dai, M.S. 2018. SUMO protease SENP1 desumoylates and stabilizes c-Myc. *Proc Natl Acad Sci USA* 115(43): 10983-10988.

Suter, U., Scherer, S.S. 2003. Disease mechanisms in inherited neuropathies. *Nat. Rev. Neurosci.* 4:714-726.

Sveen, K.A., Karimé, B., Jorum, E., Mellgren, S.I., Fagerland, M.W., Monnier, V.M. 2013. Small-and large fibre neuropathy after 40 years of type 1 diabetes: associations with glycemic control and advanced protein glycation: the Oslo Study. *Diabetes Care* 36(11): 3712-3717.

Takashima, H., Boerkoel, C.F., De Jonghe, P. 2002. Periaxin mutations cause a broad spectrum of demyelinating neuropathies. *Ann Neurol* 51:709-715.

Tangvarasittichai, S. 2015. Oxidative stress, insulin resistance, dyslipidemia and type 2 diabetes mellitus. *World J Diabetes* 6(3): 456-480.

Tapon, N., Hall, A. 1997. Rho, Rac and Cdc42 GTPases regulate the organization of the actin cytoskeleton. *Curr Opin Cell Biol* 9: 86-92.

Themistocleous AC, Ramirez, J.D., Serra, J., Bennett, D.L. 2014. The clinical approach to small fibre neuropathy and painful channelopathy. *Pract Neurol* 14(6): 368-379.

Thomas, P.K., Tonlinson, D.R. 1997. Diabetic and hypoglycemic neuropathy. In: *Peripheral Neuropathy*. Dyck, P.J., Thomas, P.K., Griffin, J.W., Low, P.A., Poduslo, J.F. (Eds). W.B. Saunders Company, Philadelphia, 1219-1250.

Tomlinson, D.R., Holmes, P.R., Mayer, J.H. 1982. Reversal by treatment with an aldose reductase inhibitor of impaired axonal transport and motor nerve conduction velocity in experimental diabetes mellitus. *Neurosci Lett* 31: 189-193.

Tomlinson, D.R., Gardiner, N.J. 2008. Glucose neurotoxicity. *Nat Rev Neurosci* 9: 36-45.

Tong, H., Hateboer, G., Perrakis, A., Bernards, R., Sixma, T.K. 1997. Crystal structure of murine/human Ubc9 provides insight into the variability of the ubiquitin-conjugating system. *J Biol Chem* 272:21381-21387.

Tretter, L., Adam-Vizi, V. 2000. Inhibition of Krebs cycle enzymes by hydrogen peroxide: a key role of (alpha)-ketoglutarate dehydrogenase in limiting NADH production under oxidative stress. *J Neurosci* 20(24): 8972-8979.

Valls-Canals, J., Povedano, M., Montero, J., Pradas, J. 2002. Diabetic polyneuropathy. Axonal or demyelinating. *Electromyogr Clin Neurophysiol* 42: 3-6.

Van Acker, K., Bouhassira, D., De Bacquer, D. 2009. Prevalence and impact on quality of life of peripheral neuropathy with or without neuropathic pain in type 1 and type 2 diabetic patients attending hospital outpatients clinics. *Diabetes Metab* 35:206-213.

Van der Vlies, D., Makkinje, M., Jansens, A., Braakman, Braakman, I, Verkleij, A. J., Wirtz, K.W. 2003. Oxidation of ER resident proteins upon oxidative stress: effects of altering cellular redox/antioxidant status and implications for protein maturation. *Antioxid Redox Signal* 5(4):381-387.

- Van Niekerk, E.A., Willis, D.E., Chang, J.H., Reumann, K., Heise, T., Twiss, J.L. 2007. Sumoylation in axons triggers retrograde transport of the RNA-binding protein La. *Proc Natl Acad Sci USA* 104(31): 12913-12918.
- Vas, P.R., Edmonds, M.E., 2016. Early recognition of diabetic peripheral neuropathy and the need for one-stop microvascular assessment. *Lancet Diabetes Endocrinol* 4: 723-725.
- Vasiliou, A.S. 2001. Regulation of L-periaxin by the Ubiquitin/Proteasome pathway. University of Edinburgh. Pp.160.
- Veiga, S., Leonelli, E., Beelke, M., Garcia-Segura, L.M., Melcangi, R.C. 2006. Neuroactive steroids prevent peripheral myelin alterations induced by diabetes. *Neurosci Lett* 402:150-153.
- Vincent, A.M., Callaghan, B.C., Smith, A.L., Feldman, E.L. 2011. Diabetic neuropathy: cellular mechanisms as therapeutic targets. *Nat Rev Neurol* 7(10):573-583.
- Vinik, A. I., Park, T.S., Stansberry, K.B., Pittenger, G.L., 2000. Diabetic neuropathies. *Diabetol* 43:957-973.
- Vogt, M.A., Chourbaji, S., Brandwein, C., Dormann, C., Sprengel, R., Gass, P. 2008. Suitability of tamoxifen-induced mutagenesis for behavioural phenotyping. *Experim Neurol* 211(1): 25-33.
- Voyvodic, J.T. 1989. Target size regulates calibre and myelination of sympathetic axons. *Nature* 342: 430-433.
- Walf, A.A., Frye, C.A. 2005. ERbeta-selective estrogen receptor modulators produce antianxiety behaviour when administered systemically to ovariectomized rats. *Neuropsych* 30: 1598-1609.
- Wang, G.L., Jiang, B.H., Rue, E.A., Semenza, G.L. 1995. Hypoxia-inducible factor 1 is a basic-helix-loop-helix-PAS heterodimer regulated by cellular O<sub>2</sub> tension. *Proc Natl Acad Sci USA* 92(12):5510-5514.
- Wang, T.J., Larson, M.G., Vasan, R.S., Cheng, S., Rhee, E.P., McCabe, E. 2011. Metabolite profiles and the risk of developing diabetes. *Nat Med* 17: 448-453.
- Wang, A, Ding, X., Demarque, M., Liu, X., Pan, D., Xin, H., Zhong, B., Wang, X., Dejean, A., Jin, W., Dong, C. 2017. Ubc9 is required for positive selection and late-stage maturation of Thymocytes. *J Immunol* 198(9): 3461-3470.
- Wasiak, S., Zunino, R., McBride, H.M. 2007. Bax/Bak promote sumoylation of Drp1 and its stable association with mitochondria during apoptotic cell death. *J Cell Biol* 177: 439-450.
- Waters, R.E., Rotevatn, S., Li, P., Annex, B.H., Yan, Z. 2004. Voluntary running induces fibre-type specific angiogenesis in mouse skeletal muscle. *Am J Physiol Cell Physiol* 287(5): C1342-C1348.
- Webster, H.D. 1971. The geometry of peripheral myelin sheaths during their formation and growth in rat sciatic nerves. *J Cell Biol* 48: 348-367.
- Wei, F., Schöler, H.R., Atchison, M.L. 2007. Sumoylation of Oct4 enhances its stability, DNA binding, and transactivation. *J Biol Chem* 282: 21551-21560.
- West, I. 2000. Radicals and oxidative stress in diabetes. *Diabet Med* 17: 171-180.
- Wijekoon, E.P., Skinner, C., Brosnan, M.E., Brosnan, J.T. 2004. Amino acid metabolism in the Zucker diabetic fatty rat: effects of insulin resistance and of type 2 diabetes. *Can J Phys Pharm* 82(7): 506-514.
- Wilkinson, K.A., Nakamura, Y., Henley, J.M. 2010. Targets and consequences of protein sumoylation in neurons. *Brain Res Rev* 64: 195-212.

- Williamson, J.R., Chang, K., Frangos, M. 1993. Hyperglycemic pseudohypoxia and diabetic complications. *Diabetes* 42: 801-813.
- Woeller, C.F., Anderson, D.D., Szebenyi, D.M, Stover, P.J. 2007. Evidence for small ubiquitin-like modifier-dependent nuclear import of the thymidylate biosynthesis pathway. *J Biol Chem* 282: 17623-17631.
- Wolfe, R.R. 2017. Branched-chain amino acids and muscle protein synthesis in humans: myth or reality? *J Int Soc Sports Nutr* 22(14): 30.
- Wood, P.M. 1976. Separation of functional Schwann cells and neurons from normal peripheral nerve tissue. *Brain Res* 115: 361–375.
- Wood, P., Moya, F., Eldridge, C., Owens, G., Ranscht, B., Schachner, M., Bunge, M., Bunge, R. 1990. Studies of the initiation of myelination by Schwann cells. *Ann NY Acad Sci* 605: 1-14.
- Wu, J., Jin, Z., Zheng, H., Yan, L.J. 2016. Sources and implications of NADH/NAD<sup>+</sup> redox imbalance in diabetes and its complications. *Diabetes Metab Syndr Obes* 9: 145-153.
- Wyse, A.T., Netto, C.A. 2011. Behavioral and neurochemical effects of proline. *Metab Brain Disea* 26: 9246
- Xiao, H., Gu, Z., Wang, G., Zhao, T. 2013. The possible mechanisms underlying the impairment of HIF1 $\alpha$  pathway signaling in hyperglycemia and the beneficial effects of certain therapies. *Int J Med Sci* 10(10):1412-1421.
- Xu, Z., Chau, S.F., Lam, K.H., Chan, H.Y., Ng, T.B., Au, S.W.N. 2006. Crystal structure of the SENP1 mutant C603S-SUMO complex reveals the hydrolytic mechanism of SUMO-specific protease. *Biochem J* 398:345-352.
- Yagihashi, S. 1995. Pathology and pathogenetic mechanisms of diabetic neuropathy. *Diabetes Metab Rev* 11: 193-225.
- Yagihashi, S., Mizukami, H., Sugimoto, K. 2011. Mechanism of diabetic neuropathy: where are we now and where to go? *J Diabetes Investig* 2(1): 18-32.
- Yamada, H., Komiyama, A., Suzuki, K. 1995. Schwann cell responses to forskolin and cyclic AMP analogues: Comparative study of mouse and rat Schwann cells. *Brain Res* 681:97–104.
- Yan, L.J. 2014. Pathogenesis of chronic hyperglycemia: From reductive stress to oxidative stress. *J Diab Res* ID 137919.
- Yang, J.Y., Yeh, H.Y, Lin, K., Wang, P.H. 2009. Insulin stimulates Akt translocation to mitochondria: implications on dysregulation of mitochondrial oxidative phosphorylation in diabetic myocardium. *J Mol Cell Cardiol* 46(6):919-926.
- Yang, R., Dong, J., Zhao, H., Li, H., Guo, H. 2014. Association of branched-chain amino acids with carotid intima-media thickness and coronary artery disease risk factors. *PLoS One* 9: e99598.
- Yang, Y., Shi, Y. 2015. L-periaxin interacts with S-periaxin through its PDZ domain. *Neuro Lett* 609:23-29.
- Yang, Y., Shi, Y. 2015. Spectrin-like domain 2 of DRP2 serves as a novel binding region for the NLS2 and 3 sub-domains of L-periaxin. *RSC Adv* 5: 84356-84366.
- Yang, Y., Min, L., Shi, Y. 2017. Self-association of L-periaxin occurs via its acidic domain and NLS2/NLS3, and affects its trafficking in RSC96 cells. *RSC Adv* 7: 44112-44123.
- Yorek, M.A. 2016. Alternatives to the streptozotocin-diabetic rodent. *Int Rev Neurobiol* 127:89-112.

- Yowtak, J., Lee, K.Y., Kim, H.Y., Wang, J., Kim, H.K., Chung, K., Chung, J.M. 2011. Reactive oxygen species contribute to neuropathic pain by reducing spinal GABA release. *Pain* 152(4):844-852.
- Yu, W.M., Feltri, M.L., Wrabetz, L., Strickland, S., Chen, Z.L. 2005. Schwann cell-specific ablation of laminin gamma1 causes apoptosis and prevents proliferation. *J Neurosci* 25: 4463-4472.
- Yu, L., Ji, W, Zhang, H., Renda, M.J., He, Y., Lin, S., Cheng, E.C., Chen, H., Krause, D.S., Min, W. 2010. SENP1-mediated GATA1 desumoylation is critical for definitive erythropoiesis. *J Exp Med* 207(6): 1183-1195.
- Zalc, B., Goujet, D., Colman, D. 2008. The origin of the myelination program in vertebrates. *Curr Biol* 18:511-512.
- Zhang, Q., Fang, W., Ma, L., Wang, Z.D., Yang, Y.M., Lu, Y.Q. 2018. VEGF levels in plasma in relation to metabolic control, inflammation, and microvascular complications in type-2 diabetes: a cohort study. *Medicine (Baltimore)* 97(15):e0415.
- Zhao, J. 2007. Sumoylation regulates diverse biological processes. *Cellular and Molecular Life Sciences* 64(23):3017–3033.
- Zhayo, T., Zhang, H., Guo, Y., Fan, Z. 2007. Granzyme K directly processes bid to release cytochrome c and endonuclease G leading to mitochondria-dependent cell death. *J Biol Chem* 282: 12104-12111.
- Zhou, M., Diwu, Z., Voloshina, N.P., Haugland, R.P. 1997. A stable nonfluorescent derivative of resorufin for the fluorometric determination of trace hydrogen peroxide: Applications in detecting the activity of phagocyte NADPH oxidase and other oxidases. *Anal Biochem* 253(2): 162-168.
- Zhou, X. Ferraris, J.D., Cai, Q., Agarwal, A., Burg, M.B. 2005. Increased reactive oxygen species contribute to high NaCl-induced activation of the osmoregulatory transcription factor TonEBP/OREBP. *Amer J Physiol* 289(2): F377-F385.
- Zochodne, D.W. 2014. Mechanisms of diabetic neuron damage: Molecular pathways. *Handb Clin Neurol* 126: 379-399.
- Zuvic-Butorac, M., Kriz, J., Simonic, A., Schara, M. 2001. Fluidity of the myelin sheath in the peripheral nerves of diabetic rats. *Biochim Biophys Acta* 1537: 110-116.
- Zwick, M., Davis, B.M., Woodbury, C.J., Burkett, J.N., Koerber, H.R., Simpson, J.F., Albers, K.M. 2002. Glial cell line-derived neurotrophic factor is a survival factor for isolectin B4-positive, but not vanilloid receptor 1-positive, neurons in the mouse. *J Neurosci* 22: 4057-4065.

## 6 PUBLICATIONS

**Rangel Rojas**, D., Tegeder, I., Kuner, R., Agarwal, N. 2018. Hypoxia-inducible factor 1 $\alpha$  protects peripheral sensory neurons from diabetic peripheral neuropathy by suppressing accumulation of reactive oxygen species. *J Mol Medic* 96:1395-1405.

**Rangel Rojas**, D., Kuner, R., Agarwal, N. 2019. Metabolomic signature of type 1 diabetes-induced sensory loss and nerve damage in diabetic neuropathy. *J Mol Medic* 97:845-854.

Agarwal, N., Helmstädter, J., **Rangel Rojas**, D., Bali, K.K., Gangadharan, V., Kuner, R. 2018. Evoked hypoalgesia is accompanied by tonic pain and immune cell infiltration in the dorsal root ganglia at late stages of diabetic neuropathy in mice. *Mol Pain* 14:1-11.